THESIS

INFLUENCE OF THE MADDEN-JULIAN OSCILLATION AND CARIBBEAN LOW-LEVEL

JET ON EAST PACIFIC EASTERLY WAVES

Submitted by

Justin W. Whitaker

Department of Atmospheric Science

In partial fulfillment of the requirements

For the Degree of Master of Science

Colorado State University

Fort Collins, Colorado

Spring 2018

Master's Committee:

    Advisor: Eric Maloney

    Michael Bell
    Jeffrey Niemann

ABSTRACT

INFLUENCE OF THE MADDEN-JULIAN OSCILLATION AND CARIBBEAN LOW-LEVEL

JET ON EAST PACIFIC EASTERLY WAVES

The east Pacific warm pool exhibits basic state variability associated with the Madden-Julian Oscillation (MJO) and Caribbean Low-Level Jet (CLLJ), which affects the development of easterly waves (EWs). This study compares and contrasts composite changes in the background environment, eddy kinetic energy (EKE) budgets, moisture budgets, and EW tracks during MJO and CLLJ events. While previous studies have shown that the MJO influences jet activity in the east Pacific, the influence of the MJO and CLLJ on EWs is not synonymous. The CLLJ is a stronger modulator of the ITCZ than the MJO, while the MJO has a more expansive influence on the northeastern portion of the basin. Anomalous low-level westerly MJO and CLLJ periods are associated with favorable conditions for EW development paralleling the Central American coast, contrary to previous findings about the relationship of the CLLJ to EWs. Easterly MJO and CLLJ periods support enhanced ITCZ EW development, although the CLLJ is a greater modulator of EW tracks in this region, which is likely associated with stronger moisture and convection variations and their subsequent influence on the EKE budget. ITCZ EW growth during easterly MJO periods is more reliant on barotropic conversion than in strong CLLJ periods, when EAPE to EKE conversion associated with ITCZ convection is more important. Enhanced background state moisture anomalies during strong CLLJ periods lead to stronger diluted CAPE anomalies in the mean state and EWs that support convection. Thus, the influence of these phenomena on east Pacific EWs should be considered distinct. [1]

---

[1]This abstract is adapted from the abstract of: Whitaker, J. W., and E. D. Maloney, 2018: Influence of the Madden-Julian Oscillation and Caribbean Low-Level Jet on East Pacific Easterly Wave Dynamics. *J. Atmos. Sci.*, in press. ©American Meteorological Society. Used with permission.

ACKNOWLEDGEMENTS

instrumental you have been to my progression not only as a scientist, but also as a person. Thank you for always being there for me every step of the way and for helping me navigate all of life's twists and turns—you truly are special.

TABLE OF CONTENTS

LIST OF FIGURES

Chapter 1

Introduction

1.1   Purpose

Easterly waves (EWs) are a leading source of tropical variability on synoptic timescales (e.g., Wheeler and Kiladis 1999; Kiladis et al. 2006) and can act as precursor disturbances to tropical cyclones during boreal summer (Avila and Pasch 1992; Landsea 1993; Avila et al. 2003; Russell et al. 2017). Understanding how EWs and the environment they propagate in are modulated by local and remote phenomena may aid in our ability to forecast tropical cyclogenesis (e.g., Slade and Maloney 2013), and allow us to determine which processes are most important for EW intensification and maintenance (Rydbeck and Maloney 2014, 2015). In the east Pacific basin, where this study focuses, the Madden-Julian Oscillation (MJO) and Caribbean low-level jet (CLLJ) have been cited as key modulators of the basic state conditions (Maloney and Hartmann 2000; Maloney and Kiehl 2002; Maloney and Esbensen 2003; Wang 2007; Cook and Vizy 2010; Martin and Schumacher 2011) that subsequently affect EWs and tropical cyclones (Molinari et al. 1997; Maloney and Hartmann 2000, 2001; Serra et al. 2010; Rydbeck and Maloney 2014, 2015). In addition, the MJO has been shown to influence the CLLJ (Maloney and Esbensen 2007), with MJO easterly anomalies being associated with stronger jet activity. In the east Pacific EW literature, there seems to be some disagreement about which modulated low-level wind regimes provide more favorable conditions for EW development. MJO studies (e.g., Maloney and Hartmann 2001) conclude that the anomalous low-level westerly wind periods associated with the MJO produce more suitable conditions for EW activity, while studies involving the CLLJ conclude that enhanced EW activity results from the anomalous easterly winds entering the basin (e.g., Serra et al. 2010). In an attempt to resolve some of these apparent discrepancies, this study directly compares the influences of the MJO and CLLJ on east Pacific easterly waves. Eddy kinetic energy and moisture budgets are used to highlight how important EW processes are altered during MJO and CLLJ low-level wind peri-

1

ods. Overall, this study hopes to improve our understanding of the variability of the east Pacific mean state and to identify any differences between how the basin is modulated by the MJO and by the CLLJ. Additional insight into the roles the MJO and CLLJ play in the east Pacific could be used to improve global climate model simulations. Finally, as east Pacific EWs can transition into landfalling tropical cyclones, which can be devastating to Central American coastal communities, we hope that this study could be included in operations to better inform the public in advance of potential threats and in hurricane forecasting models to provide additional context for developing EWs.

1.2   East Pacific boreal summer background state

The eastern tropical Pacific basin (defined from the equator to 25°N and from 140°W to the Americas in this study) is characterized by unique atmospheric and oceanic conditions that are associated with the surrounding complex topography on its eastern boundary. First, the mountainous Central American isthmus separates the Caribbean Sea from the east Pacific. Gaps in the Sierra Madre mountains that stretch through this area can help produce strong wind jets into the Pacific due to pressure gradients between the basins and blocked low-level easterly trade wind flow (Chelton et al. 2000a). In the second part of their study, Chelton et al. (2000b) found that while the Tehuantepec jet in southern Mexico is most closely associated with pressure changes in the Gulf of Mexico, the Papagayo jet in Nicaragua and Panama jet are linked to variations in the Caribbean trade winds that approach the eastern Pacific, and that these jets affect the mean wind field of the east Pacific. In addition, the Papagayo jet is associated with the upwelling of cooler water and reduced boreal summer precipitation in the Costa Rica dome region off the Pacific coast of Central America (Xie et al. 2005). The Andes mountains also play a role in affecting the weather and climate of the east Pacific. Mapes et al. (2003b) found that the elevated terrain of the Andes helps to initiate convection on diurnal timescales, which then propagates offshore into the Panama Bight region. Mapes et al. (2003a) found that as the convection reaches the Panama Bight, it tends to be organized into larger mesoscale convective systems, which they suggest may be due to the concave

topography of northwest South America. Mapes et al. (2003a) also indicate that this mechanism for convective initiation is consistent with the climatological rainfall pattern, highlighting the importance and regularity of these systems to an area with very high annual rainfall.

The east Pacific background state is associated with a moist atmosphere that is favorable for convective development. Maloney and Esbensen (2007, the top panel of Figure 11 in their paper) and Rydbeck and Maloney (2015, the bottom panel of Figure 7 in their paper) show total column water vapor during mean boreal summer conditions, and are given in this thesis as Figure 1.1. These plots highlight that mean moisture is enhanced over most of the east Pacific basin relative to the western Caribbean and Gulf of Mexico. A maximum of moisture occurs in and extends northwestward from the Panama Bight, with Rydbeck and Maloney (2015) indicating values over 56 mm there. In addition, the boreal summer position of the Intertropical Convergence Zone (ITCZ) is evident in the low-level moisture fields shown in Figure 3.6. The ITCZ is an area of active convection that is located where the tropical trade winds converge (Back and Bretherton 2009), and during boreal summer it begins in the eastern portion of the basin and extends zonally westward, located around 10°N with a mean meridional width of approximately 5°-10°. Serra et al. (2010, the top panel of Figure 1 in their paper and given as Figure 1.2 in this thesis) highlight that mean boreal summer outgoing longwave radiation (OLR, used as proxy for deep convection) is fairly low across the eastern portion of the basin, and is minimized in the Panama Bight and ITCZ with values near 200 W m^{-2}. This result emphasizes that most of the basin is convectively active in boreal summer and that east Pacific deep convection is most prevalent in locations with the highest tropospheric moisture content. As a strong connection has been found between tropospheric water vapor, convection, and precipitation (e.g., Bretherton et al. 2004; Holloway and Neelin 2009), the ITCZ and Panama Bight also experience elevated rain rates relative to the rest of the basin (Mapes et al. 2003a; Maloney and Esbensen 2007). One notable exception to this relationship between high water vapor, convection, and precipitation is the Costa Rica Dome near the Central American coast (Xie et al. 2005, the bottom panel of Figure 8 in their paper and given as Figure 1.3 in this thesis). Another interesting area to mention is the equatorial east Pacific. Figures 1.1 and 1.2

show that the equatorial portion of the basin is relatively dry, with total column water vapor values below 42 mm (Rydbeck and Maloney 2015), and is associated with decreased convective activity compared to other portions of the basin (Serra et al. 2010).

In addition to the moisture distribution, the boreal summer low-level winds are important contributors to the mean state conditions of the east Pacific. Toma and Webster (2010a) argue that the strength of the southerly low-level cross-equatorial flow in the southern portion of the basin, which stems from a strong meridional sea surface temperature (SST) gradient and cross-equatorial pressure gradient, can be used to determine the latitude of the east Pacific ITCZ. Serra et al. (2010, Figure 2 of their paper and given as Figure 1.4 in this thesis) show that while the low-level winds entering the basin from the Caribbean are easterly, (and can interact with the Central American topography as discussed above), the southerly cross-equatorial flow begins to curve eastward as it moves north of the equator. As a result, the mean state winds in the southern portion of the basin have a westerly zonal component northward to the ITCZ. Figure 1.4 also shows that due to the easterly winds associated with the Papagayo jet and the westerly winds located to the south of the jet, a region of strong mean positive vorticity occurs that extends westward into the basin along the latitude of the ITCZ (Serra et al. 2010). Further, Molinari et al. (1997) found that this region is associated with a mean state sign change in the meridional potential vorticity gradient, which meets the Charney-Stern necessary condition for instability of the mean flow, and suggests that the easterly flow entering the basin can potentially support the growth of transient tropical disturbances. On the other hand, Figure 1.4 also shows that there are areas of mean negative vorticity in the basin with a broad area occurring south of the ITCZ (where the winds transition from southerly to westerly) and localized regions near northern and western sides of the Papagayo and Tehuantepec jets, respectively (Serra et al. 2010).

Boreal summer SSTs also have an interesting structure in the basin (Maloney et al. 2008, Figure 1 of their paper and given as Figure 1.5 in this thesis) and generally align with the mean moisture field discussed above; warm SSTs are coincident with areas of high moisture content. The equatorial cold tongue, which describes the cooler waters extending from the South American coast

along the equator, is produced through wind-induced upwelling (e.g., Wyrtki 1981) and serves as the lower boundary of the basin with SSTs ranging between 22°C-24°C (Maloney et al. 2008). This region of cooler water is associated with higher atmospheric pressure, and helps establish a cross-equatorial pressure gradient in the region (Toma and Webster 2010a). Figure 1.5 also shows that in a relatively short distance to the north, the waters of the east Pacific warm significantly and reach temperatures over 29°C near the Central American coast (Maloney et al. 2008).

Along with its impacts on local phenomena, the mean state conditions of the east Pacific play a role in global climate and circulation. The deep convection along the ITCZ can be thought of as the rising branch of the Hadley cell, which is a meridional overturning atmospheric circulation characterized by vertical motion near the equator and sinking motion in the subtropics (e.g., Dima and Wallace 2003). Global subtropical deserts are linked to the large scale subsidence on the poleward branch of the Hadley cell, and in a warmer climate, the sinking branch of the Hadley cell may extend further poleward (Lu et al. 2007). The equatorial portion of the east Pacific, characterized by the SST cold tongue and suppressed convection, is associated with the Walker circulation, which is a zonal overturning atmospheric circulation linking subsidence over the equatorial east Pacific with strong vertical motion and convection in the west Pacific (e.g., Bjerknes 1969; McPhaden et al. 1998). McPhaden et al. (1998) also explain that the mean surface easterly flow associated with the Walker circulation causes a warmer thermocline in the west Pacific that produces warmer surface waters by minimizing the colling effect of upwelling.

1.3 The Madden-Julian Oscillation and Caribbean Low-Level Jet and their modulation of the east Pacific

1.3.1 Madden-Julian Oscillation

The Madden-Julian Oscillation (MJO) is a large-scale equatorial convective disturbance that is a prominent source of tropical intraseasonal variability, with a time scale of 30 to 90 days and an eastward phase speed of approximately 5 m s^{-1} (Zhang 2005). The MJO initiates in the western In-

5

dian Ocean and travels eastward across the basin into the Pacific Ocean (Madden and Julian 1994). However, it is not well described by equatorial wave theory, as Wheeler and Kiladis (1999) show that MJO OLR variance, used as a proxy for deep convection, does not align with theoretical equatorial wave dispersion curves. Hence, an active and unresolved area of research is the development of theories based on physical mechanisms that describe the spatial and temporal characteristics of the MJO. One leading theory is the description of the MJO as a moisture mode (e.g., Sobel and Maloney 2012, 2013; Adames and Kim 2016). In moisture mode theory, column integrated water vapor is used as a prognostic variable to describe the evolution of convection and subsequently the propagation of the MJO (Sobel and Maloney 2012). Simulations from a moisture mode model by Adames and Kim (2016) reveal that the moisture mode framework produces a reasonable MJO that is comparable to observations in wavenumber-frequency space, and that moisture advection plays an important role in its eastward propagation. In addition to investigating the propagation of the MJO, other studies focus on the teleconnections, or connections at a distance, that result from MJO convection. For example, the MJO have been shown to modulate Northern Hemisphere mid-latitude blocking (Henderson et al. 2016) and atmospheric river activity (Mundhenk et al. 2016), as well as convective activity in eastern Africa (Alaka and Maloney 2012). In terms of the east Pacific, much work has been done in the last two decades to highlight and quantify the influence of the MJO on the basic state conditions and to emphasize its role in modulating local weather phenomena.

East Pacific convective activity has been shown to be modulated by the MJO (e.g., Maloney and Esbensen 2003). One of the first studies to link the MJO to changes in east Pacific convection was Maloney and Hartmann (1998). In this study the authors composited the life cycle of the MJO over all seasons based on the leading empirical orthogonal functions of 20-80 day bandpass filtered 850 hPa equatorially averaged zonal wind. Although the study was not focused on the boreal summer east Pacific specifically, the authors note that positive anomalies of precipitation, moisture and cyclonic shear occur near the Central American coast during anomalous 850 hPa westerly wind periods, and that negative anomalies of these fields occur during anomalous easterly

6

periods. The authors also briefly mention that the enhanced convective activity during westerly periods may play a role in influencing tropical cyclone activity in the basin, as will be discussed further in the next section on easterly waves. Ultimately, the findings of Maloney and Hartmann (1998) spurred additional research on the connection between the MJO and tropical variability in the east Pacific basin.

In a study on tropical cyclogenesis, Maloney and Hartmann (2000) found that in MJO low-level westerly wind periods, anomalous positive low-level relative vorticity was coincident with enhanced precipitation anomalies near the Central American coast. They further note that the anomalous vorticity may help promote convergence and upward motion. Maloney and Hartmann (2001) show that negative MJO OLR anomalies and positive low-level convergence anomalies do in fact occur in this region, while anomalous easterly periods are associated with a decreased convective response and anomalous low-level divergence. Results by Raymond et al. (2006); Maloney and Esbensen (2007); Aiyyer and Molinari (2008); Jiang and Waliser (2008); Crosbie and Serra (2014) have reaffirmed the view that MJO westerly wind periods are associated with enhanced convection in the east Pacific, while Maloney and Esbensen (2007) reiterate that easterly periods are associated with suppressed convection and precipitation. Further, Maloney and Esbensen (2003) find that positive MJO diabatic heating anomalies occur during the convectively active westerly periods, and that these diabatic heating anomalies are positively correlated with MJO temperature anomalies near 250 hPa, which leads to the generation of perturbation available potential energy at upper levels. The authors then show that this generated perturbation available potential energy is almost completely converted to perturbation kinetic energy at the same levels. Ultimately, this energy conversion allows for the intensification of the MJO circulation through geopotential flux convergence. With a resulting increased MJO circulation, stronger convection can continue to be produced through a positive feedback loop involving enhanced convergence and surface latent heat flux anomalies (Maloney and Esbensen 2003).

Recent work on the influence of the MJO on east Pacific convection has suggested a more complicated interaction. A modeling study by Small et al. (2011) suggests that the MJO influences the

east Pacific remotely through eastward Kelvin wave propagation, and that east Pacific convection can be generated through frictional convergence and other local processes due to the arrival of the Kelvin wave. As a result of this, east Pacific intraseasonal convective anomalies have similar phasing to the MJO. Rydbeck et al. (2013) show through simulations of the NCAR CAM model that the east Pacific can independently produce local intraseasonal variability similar to what has been typically attributed to the MJO. In their experiment, the authors damped eastward propagating Kelvin waves in the Central Pacific to isolate the east Pacific from MJO-like signals and found comparable intraseasonal anomalies to those in the control simulation. However, Rydbeck et al. (2013) still suggest that the MJO and east Pacific intraseasonal activity may be phase-locked on similar time scales, leading to the strong statistical relationship of local intraseasonal anomalies to remote MJO indices. One example of a local source of intraseasonal variability in the east Pacific is the Central American midsummer drought, which is characterized by a minimum of rainfall in July and August that occurs in-between months where rainfall is maximized in the region (e.g., Magana et al. 1999). The midsummer drought and its relationship to the Caribbean low-level jet will be discussed in a subsequent section.

Finally, variability associated with MJO has been shown to be a strong modulator of SSTs in the east Pacific, with temperature variations of 0.5°C (Maloney and Kiehl 2002) to 1°C (Maloney et al. 2008) occurring over an MJO life cycle, with differences in these values arising based on the SST product used (Maloney et al. 2008). Also, Maloney et al. (2008) found that during boreal summer the MJO explained 30%-40% of intraseasonal SST anomalies in the basin. Maloney and Kiehl (2002) suggest that MJO SST anomalies are highly correlated with surface latent heat and shortwave fluxes in the east Pacific due to the shallow mixed layer depths in the basin. While convection is maximized during westerly MJO periods, positive SST anomalies occur in the transition from easterly to westerly periods; SST anomalies are in quadrature with MJO precipitation and lag easterly period suppressed precipitation by 7-10 days (Maloney and Kiehl 2002; Maloney et al. 2008). Finally, Maloney and Kiehl (2002) used a diagnostic primitive equation model to show that MJO positive SST anomalies can also modulate the surface wind field. The study suggests positive

SST anomalies can produce surface convergence in the region and may provide a more favorable environment for later convection.

1.3.2   Caribbean Low-Level Jet

In comparison to the MJO, the Caribbean low-level jet (CLLJ; Amador 2008, refered to as the Intra-Americas Sea low-level jet in their paper) has received less attention in the literature. An important early study describing the CLLJ was performed by Amador (1998). In this study, monthly mean NCEP/NCAR reanalysis data were used to document the vertical and spatial structure of the jet during boreal summer. Amador (1998) found that the CLLJ is a region of strong easterly winds over the Caribbean with wind speeds maximizing around 925 hPa. During the month of July, easterly wind speeds at this level reach up 14 m s^{-1}. Wang (2007) reaffirm these results and show that the CLLJ has two annual maxima (in January and July) and minima (in May and October), and associate changes in jet strength to variations in the north Atlantic subtropical high. The authors suggest that during strong (enhanced easterly) CLLJ periods, the subtropical high is strengthened and extends further west, which allows for enhanced meridional pressure gradients and a subsequent geostrophically balanced response in the Caribbean. However, Serra et al. (2014) emphasize that further work must be done to elucidate mechanisms that govern the maintenance of the CLLJ. Interestingly, Amador (2008), Munoz et al. (2008), and Cook and Vizy (2010) highlight that the CLLJ structure differs between boreal summer and winter. These studies mention that during boreal winter the flow tends to travel westward across Central America from the Caribbean, while in summer months, the CLLJ divides into two branches, with the southern branch continuing westward into the Pacific, while the northern branch curves and becomes southerly flow into the Gulf of Mexico. In addition, Maloney and Esbensen (2007) show that the MJO can modulate the CLLJ and the regional mountain jets, with strengthening occurring during easterly MJO periods. Finally, other studies have investigated the effects of the CLLJ interacting with Central American topography (e.g., Zehnder 1991; Chelton et al. 2000a; Xie et al. 2005). For example, Zehnder (1991)

model the interactions between easterly flow and an idealized representation of the Sierra Madre mountains and show that Rossby wave-like structures form on the leeward side of the topography.

The variation in strength of the CLLJ is associated with changes in precipitation across the Caribbean and east Pacific. Both Wang (2007) and Cook and Vizy (2010) use a CLLJ index based on monthly mean zonal wind in the jet core to note that a stronger jet is associated with reduced rainfall over the central Caribbean and on the Pacific coast of Central America, while a weaker jet is associated with increased rainfall in these areas. Further, strong easterly flow associated with the Papagayo jet is linked to the forcing of the Costa Rica Dome and suppressed boreal summer convection in its vicinity (Xie et al. 2005). Munoz et al. (2008) highlights that easterly moisture fluxes in the Caribbean associated with the CLLJ increase when the jet increases in strength in July and January, and that a greater flux of moisture away from the Caribbean during strong jet periods may be associated with decreased rainfall in the region. Amador (2008) also shows that when the jet is strong, there is a region of lower-level divergence over the central and eastern Caribbean. Using a suite of IPCC AR4 models, Martin and Schumacher (2011) highlight that the models were generally able to simulate the relationship between the CLLJ and rainfall in the region. In addition to being correlated to rainfall, the CLLJ has also been linked to changes in SST. Wang (2007) and Amador (2008) mention that a strong (weak) CLLJ is related to negative (positive) SST anomalies across the Caribbean. Wang (2007) also found boreal summer positive SST anomalies in the east Pacific are positively correlated to a strong monthly CLLJ index and suggests a possible seasonal relationship between ENSO and the CLLJ, which is discussed further in Krishnamurthy et al. (2015). However, Magana et al. (1999) find that SSTs in the east Pacific decrease with an increase in the low-level easterlies at the onset of the midsummer drought.

The CLLJ is also related to the Central American midsummer drought. The midsummer drought is an annual precipitation feature that is characterized by a local minimum in rainfall in July and August that occurs in the middle of the summer rainy season along the Pacific coast of Central America (e.g., Magana et al. 1999). In their work, Magana et al. (1999) document that changes in the low-level wind flow associated with the CLLJ occur at the beginning and end of

the midsummer drought, with a shift to anomalous easterly (westerly) winds occurring at the onset (conclusion) of the drought. Further, using models and reanalysis data to investigate the midsummer drought, Small et al. (2007) found that an increase in the easterly low-level flow during July and August as well as coincident positive subsidence and divergence anomalies on the Pacific side of Central America help support the suppression of precipitation in that location. Martin and Schumacher (2011) show that IPCC AR4 models that realistically simulate the occurrence of the midsummer drought also simulate the increase of the CLLJ in July. However, Amador (2008) state that more work must be done to determine whether the intensity of the drought is related to variability in the CLLJ. Therefore, recent strides have been made to recognize the CLLJ as an important contributor to the weather and climate of the Caribbean and east Pacific basins, but the CLLJ and its associated impacts still require further study.

1.4   East Pacific Easterly Waves

1.4.1   Background

Easterly waves (EWs) are westward propagating tropical disturbances that are prominent during summer and fall in the Northern Hemisphere. (e.g, Carlson 1969; Burpee 1972; Roundy and Frank 2004). EWs typically have periods of two to six days and spatial scales ranging from 2000 to 4000 km (Burpee 1972, 1974; Reed et al. 1988; Wheeler and Kiladis 1999; Kiladis et al. 2006). EWs in the east Pacific have vertical structures consisting of a cyclonic meridional wind structure maximizing near 500 hPa, a moist atmosphere peaking near 700 hPa in the region of southerly flow (with positive low-level moisture anomalies leading the wave in regions of northerly flow), and a temperature structure characterized by cold anomalies below 500 hPa and warm anomalies aloft (Serra et al. 2008). Similar to the MJO, EWs are not predicted from equatorial wave dispersion curves (Wheeler and Kiladis 1999), and their dynamics are still an ongoing topic of research in the literature (e.g., Serra et al. 2008, 2010; Diaz and Aiyyer 2013; Rydbeck and Maloney 2014, 2015; Rydbeck et al. 2017).

Thorncroft and Hodges (2001, Figure 5 of their paper and the top two panels of this figure are given as Figure 1.6 in this thesis) describe the annual EW track density based on 600 hPa vorticity for the Atlantic and east Pacific during May-October. For Atlantic EWs, high EW track density begins to the south of Lake Chad and extends westward, reaching a peak density of 14 EWs per 10^6 km^2 just off the coast of Africa, before declining over the Caribbean Sea. In the east Pacific, track density ramps up again in a more favorable environment and reaches values that are comparable, if not slightly higher than the peak in the Atlantic. Figure 1.6 also shows that EWs propagate zonally across the Atlantic, while in the east Pacific they tend to have a more northwesterly track (Thorncroft and Hodges 2001). In addition to being important sources of tropical variability, EWs have also been observed to be precursor disturbances for tropical cyclones in the Atlantic and Pacific basins (e.g., Carlson 1969; Frank 1970; Landsea 1993; Avila et al. 2003; Russell et al. 2017). In studies investigating the Atlantic basin, Russell et al. (2017) found that 61% of tropical cyclones are linked to EWs, while Landsea (1993) found that 83% of major hurricanes originated from EWs. In the east Pacific, Avila et al. (2003) notes that most tropical cyclones are related to EWs, and that in 2001 all but one named storm in the basin formed from an EW or the remnants of an Atlantic tropical cyclone. Therefore, a better understanding of the generation, development, and variability of EWs could advance our knowledge of tropical cyclogenesis as well as aid in our ability to forecast potentially devastating hurricanes.

1.4.2 Sources

EWs that exist in the Atlantic and east Pacific are typically formed from precursor convective disturbances. For EWs that travel over the Atlantic, also known as African easterly waves (AEWs), their origins lie over central Africa (e.g., Carlson 1969; Frank 1970; Burpee 1972; Thorncroft and Hodges 2001; Kiladis et al. 2006; Thorncroft et al. 2008). One leading theory for AEW generation is that convective disturbances forced by central African topography organize and develop downstream through interactions with the African easterly jet (Berry and Thorncroft 2005; Kiladis et al. 2006; Mekonnen et al. 2006; Thorncroft et al. 2008; Leroux and Hall 2009; Alaka and Maloney

2012). The African easterly jet is a region of strong mid-level easterly winds with speeds maximized at 600 hPa, and is formed through thermal wind balance caused by the low-level meridional potential temperature gradient that exists between the cool Atlantic waters to the south and warm Sahara desert to the north (Lebel et al. 2010). Thorncroft et al. (2008) used a global spectral primitive equation model to show that prescribed localized heating representing convection near the Darfur mountains and the entrance of the African easterly jet (15°N, 20°E) produced an EW response downstream that propagated toward the Atlantic. The vertical and horizontal structures of the AEWs developed by the idealized heating in the model are similar to those found in Kiladis et al. (2006) who analyzed AEW characteristics using ERA-15 reanalysis data. In addition, Alaka and Maloney (2012) found that MJO-modulated enhanced convection upstream of the African easterly jet in central and eastern Africa was followed by enhanced eddy kinetic energy and convective anomalies in western Africa in subsequent MJO phases. Thus, the authors suggest that the MJO can alter AEW activity through the modulation of convective precursor disturbances at the entrance of the jet.

In the east Pacific, sources for EWs are still being investigated but generally fall into two categories: 1) preexisting AEWs propagate across the Atlantic and into the east Pacific where they can re-intensify, and 2) EWs are generated locally in the basin from a variety of mechanisms. Annual summaries of east Pacific Hurricane seasons by the National Hurricane Center (e.g., Rappaport and Mayfield 1992; Avila and Guiney 2000; Avila et al. 2003) typically state that several east Pacific storms in a given year appear to result from AEWs. Other studies such as Shapiro (1986), Thorncroft and Hodges (2001), and Serra et al. (2008) have also found that AEWs can propagate into the Pacific. However, while Thorncroft and Hodges (2001) (Figure 1.6 in this thesis) show that some EW tracks do cross over Central America from the Caribbean, their analysis also implies that a local generation of east Pacific EWs occurs, with positive EW genesis density values occurring along the east Pacific ITCZ in the bottom panel of Figure 1.6. Serra et al. (2010) reaffirmed these results by also showing elevated EW genesis density in the east Pacific and suggested that the CLLJ may be an important mechanism for genesis, echoing previous studies on the effects of easterly flow

13

entering the basin (Zehnder 1991; Molinari et al. 1997). Ferreira and Schubert (1997) highlight ITCZ breakdown as another route to local EW genesis. In their study, the authors use a nonlinear shallow water model to show that barotropic and baroclinic instability in the ITCZ can cause it to break down into multiple EW-like tropical disturbances. Further, Toma and Webster (2010a) argue that the ITCZ is inertially unstable, which causes convection to fluctuate on synoptic timescales and potentially form EWs. Finally, Rydbeck et al. (2017) used regional modeling simulations to propose that topographically-forced diurnal convective disturbances in the Panama Bight (Mapes et al. 2003a) are able develop into east Pacific EWs. Rydbeck et al. (2017) also show that when height of the Andes and southern Sierra Madre are reduced, Panama Bight convection and EW variance in the basin are also suppressed, emphasizing the importance of Panama Bight convection to local EW generation.

1.4.3 Growth

EW development is realized through generation of eddy kinetic energy (e.g., Lau and Lau 1992; Maloney and Hartmann 2001; Maloney and Dickinson 2003; Hsieh and Cook 2007; Serra et al. 2008, 2010; Rydbeck and Maloney 2014). In the east Pacific, two main sources of EW kinetic energy are interactions with mean flow (known as barotropic conversion) and EW convective processes (the generation via diabatic heating and conversion of eddy available potential energy to eddy kinetic energy) (Maloney and Hartmann 2001; Serra et al. 2008, 2010; Rydbeck and Maloney 2014). Maloney and Hartmann (2001) found that the low-level zonal gradient in the mean zonal wind is a dominant contributor to barotropic conversion in east Pacific EWs, particularly during MJO westerly periods. Serra et al. (2008), Serra et al. (2010), and Rydbeck and Maloney (2014) show that barotropic conversion maximizes at low-levels, which emphasizes the importance of the low-level wind structure to east Pacific EWs. Rydbeck and Maloney (2014) also found that stronger EWs during westerly intraseasonal periods had enhanced mid-level barotropic conversion due to the meridional gradient in the zonal wind at these levels. On the other hand, the conversion of eddy available potential energy to eddy kinetic energy as a result of convective processes

maximizes at upper levels around 300 hPa (Serra et al. 2008, 2010). For eddy available potential energy to be generated, a positive covariance must occur between diabatic heating and temperature anomalies. Further, eddy available potential energy is converted to eddy kinetic energy where upward motion occurs in positive temperature anomalies (e.g., Rydbeck and Maloney 2014). Thus, the mean state wind structure and propensity for convective activity in the east Pacific provide an environment that is conducive to both remotely and locally generated EWs, and phenomena that alter these mean state conditions will undoubtedly also influence EWs.

1.4.4 Variability

Many studies on east Pacific EW and tropical cyclone variability have investigated the modulations induced by the MJO and related intraseasonal variability (e.g., Maloney and Hartmann 2000, 2001; Aiyyer and Molinari 2008; Rydbeck and Maloney 2014, 2015). Maloney and Hartmann (2000) found that anomalous MJO low-level westerly wind periods have double the number of named tropical cyclones than easterly periods, and that four times as many hurricanes occur in MJO westerly wind conditions. Rydbeck and Maloney (2014) calculated perturbation available potential energy and perturbation kinetic energy budgets for EWs during MJO-like intraseasonal events. This study found that westerly wind period EWs were associated with greater conversions from perturbation available potential energy to perturbation kinetic energy (associated with enhanced convective invigoration in the waves) and an enhancement of barotropic conversion compared easterly period EWs. Rydbeck and Maloney (2014) suggest that the intraseasonal modulation of the background environment, which favors convective anomalies in westerly low-level wind periods as discussed above, plays an important role in modulating the generation and subsequent conversion of perturbation available potential energy in EWs, as well as barotropic conversion due to alterations in the mean wind structure. Finally, Rydbeck and Maloney (2015) found that developing westerly period EWs are associated with stronger diluted convective available potential energy anomalies in the southwestern portion of the wave relative to easterly periods, highlighting that westerly period EWs occur in an environment that favors stronger convection. In turn, the

authors suggest that the enhanced convection in this region allows the westerly period waves to more readily develop a tilted southwest to northeast axis which aids in barotropic conversion to eddy kinetic energy (Rydbeck and Maloney 2015).

Other studies have speculated about the role of the CLLJ in tropical cyclone development and EWs in the region (e.g., Zehnder 1991; Molinari et al. 1997; Wang and Lee 2007; Serra et al. 2010). In particular, Zehnder (1991) found that low-level easterly flow related to the CLLJ produces EW-like disturbances downstream after interacting with idealized topography in a shallow water model under the assumption that the atmosphere is incompressible, homogeneous, inviscid, and hydrostatic. Serra et al. (2010) analyzed the effect of the CLLJ on EW track density and also performed an EW energetics analysis. This study found that strong CLLJ periods are associated with elevated EW track density in the east Pacific, and suggests that enhanced barotropic conversion associated with the CLLJ promotes the disparity in east Pacific track density between CLLJ periods. Finally, Serra et al. (2010) found that a strong CLLJ is correlated to enhanced (suppressed) tropical cyclone counts in the east Pacific (Atlantic) while Wang and Lee (2007) suggest that the weakening of the CLLJ in boreal fall is associated with a reduction in vertical wind shear which favors hurricane formation in the Atlantic. So, in comparing MJO and CLLJ studies, there appears to be some disagreement about which low-level wind direction provides more favorable conditions for EWs. This study investigates these discrepancies by comparing EW eddy kinetic energy and moisture budgets during MJO and CLLJ low-level wind periods.

1.5 Study Outline

Having introduced the boreal summer conditions in the east Pacific, sources of variability in the region, and easterly waves, Chapter 2 compares and contrasts the modulation of the east Pacific background state and EW energy kinetic budgets during westerly and easterly anomalous low-level wind periods associated with the MJO and CLLJ. Chapter 2 has been accepted for publication in Journal of the Atmospheric Sciences. Chapter 3 performs a vertically integrated moisture budget analysis on easterly waves during MJO and CLLJ periods to help interpret some of the results in

Chapter 2. Chapter 4 provides an overview of the study and discusses possible avenues of future work.

1.6 Chapter 1 Figures
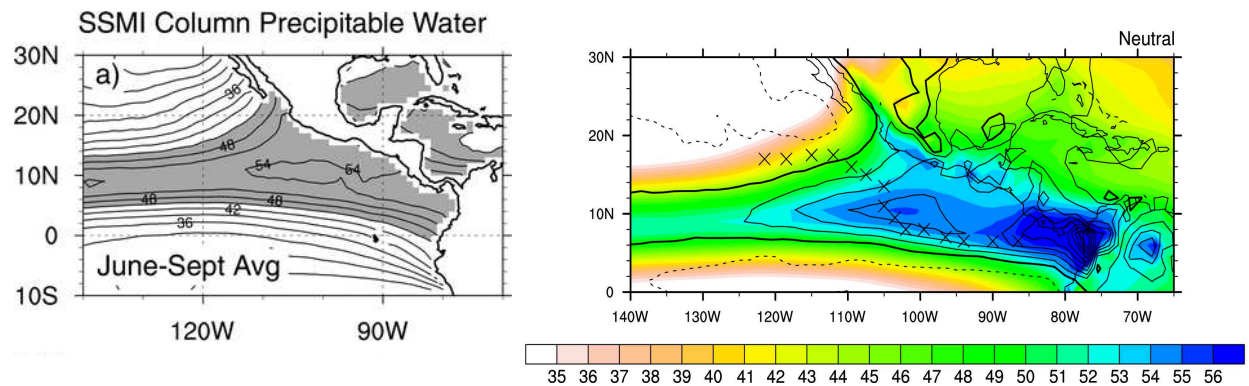
Figure 1.1: Mean boreal summer column moisture. (Left) Mean June-September SSM/I column precipitable water (mm, line contours), from Maloney and Esbensen (2007, the top panel in Figure 11 of their paper). (Right) Mean neutral intraseasonal period total precipitable water (mm, color contours) and 400 hPa vertical velocity (Pa s^{-1}, line contours), from Rydbeck and Maloney (2015, the bottom panel in Figure 7 of their paper).
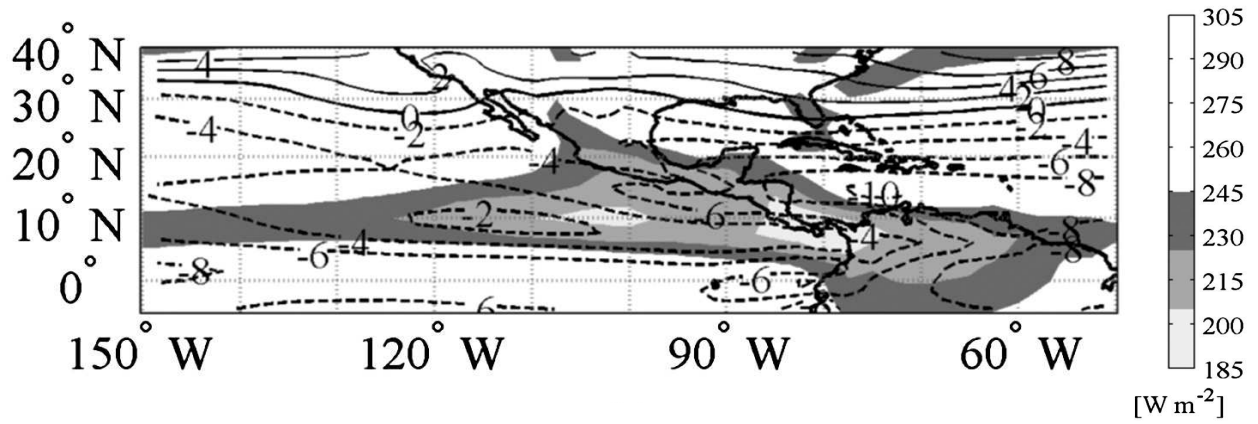
Figure 1.2: Mean June-August OLR (W m^{-2}, color contours) and 700 hPa zonal wind (m s^{-1}, line contours), from Serra et al. (2010, the top panel in Figure 1 of their paper).
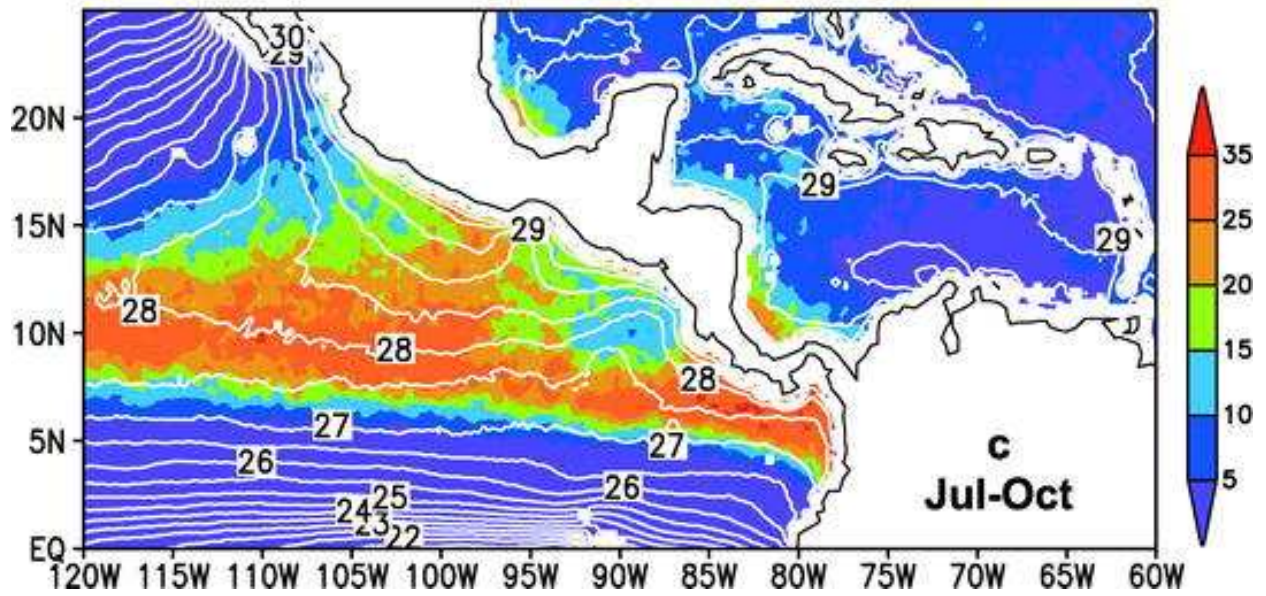
Figure 1.3: Mean July-October precipitation (mm day^{-1}, color contours) and TMI SST ($^{\circ}$C, line contours), from Xie et al. (2005, the bottom panel in Figure 8 of their paper)
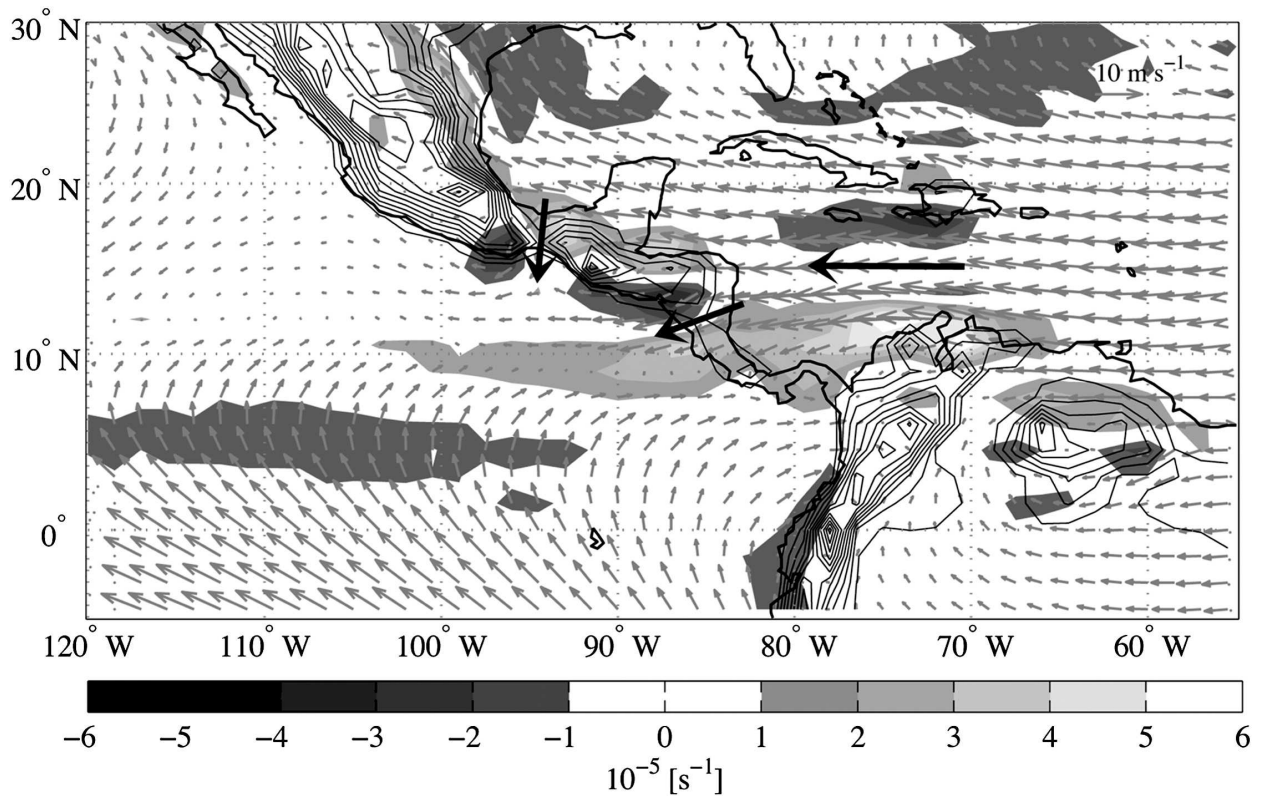
Figure 1.4: Mean June-August ERA-Interim 925 hPa wind (m s^{-1}, vectors) and relative vorticity ($\times 10^{-5}$ s^{-1}, color contours), along with orography (m, line contours every 200 m starting from 200 m), from Serra et al. (2010, Figure 2 of their paper). Solid black arrows (from east to west) represent the Caribbean low-level jet, Papagayo gap wind, and Tehuantepec gap wind.
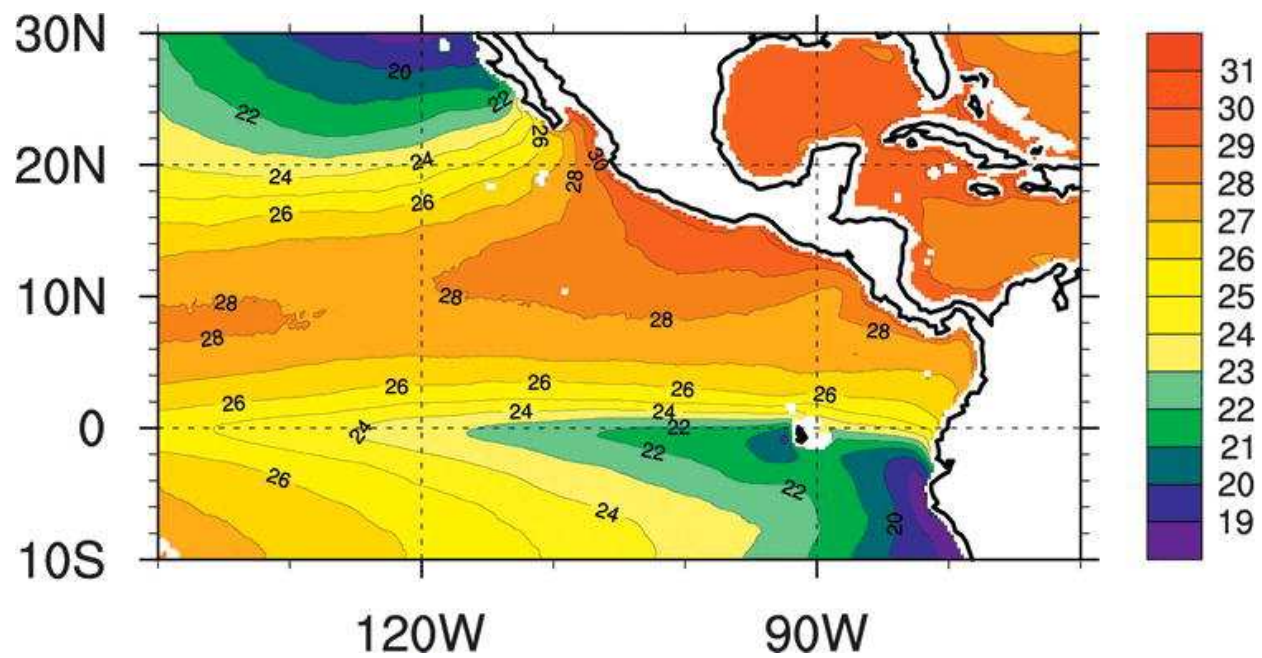
Figure 1.5: Mean June-October TMI SST (°C, color contours), from Maloney et al. (2008, Figure 1 of their paper)
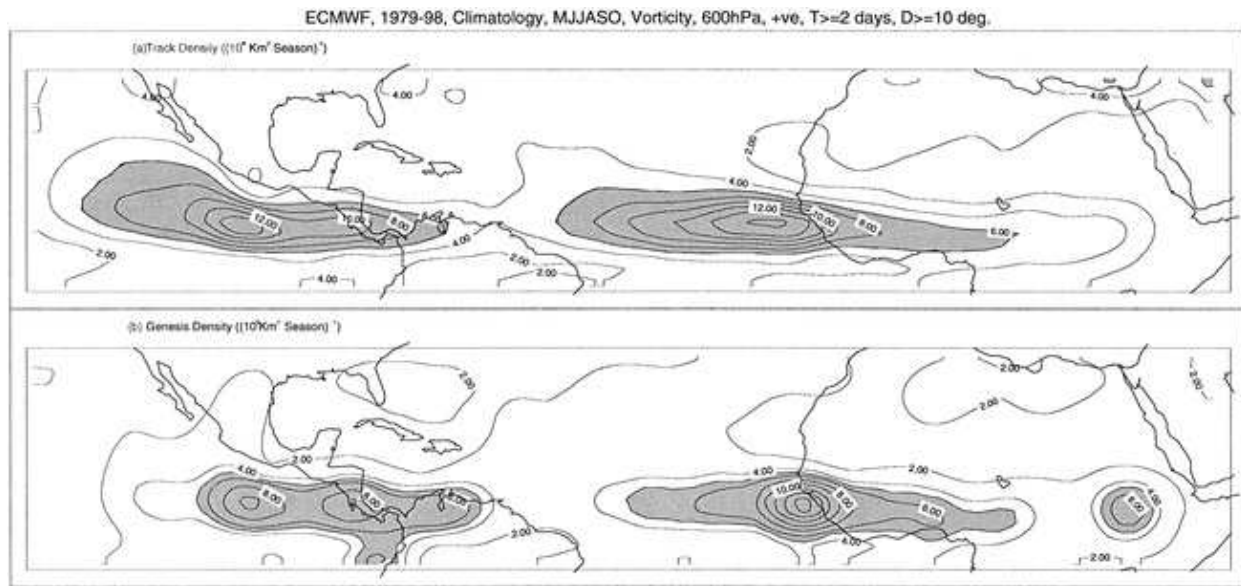
Figure 1.6: (Top) Mean 1979-1998 May-October easterly wave track density derived from 600 hPa ECMWF data, with the units of track density being the number of easterly waves per unit area (approximately 10^6 km^2) per May-October season. (Bottom) Mean easterly wave genesis density over the same time period, with the units of genesis density being the number generated easterly waves per unit area (approximately 10^6 km^2) per May-October season. Both panels of this figure are from Thorncroft and Hodges (2001, the top two panels in Figure 5 of their paper).

Chapter 2

Influence of the MJO and CLLJ on East Pacific Easterly Wave Dynamics[2]

2.1   Introduction

Easterly waves (EWs) are synoptic-scale disturbances that are important components of the weather and climate of the tropics. EWs are the primary precursor disturbances for tropical cyclones in the Atlantic and Pacific (Avila and Pasch 1992; Landsea 1993; Avila and Guiney 2000; Avila et al. 2003; Pasch et al. 2009; Russell et al. 2017), and are prominent sources of westward propagating tropical variability in wavenumber-frequency space (Wheeler and Kiladis 1999; Kiladis et al. 2006). Northern hemisphere EW activity maximizes in boreal summer and fall (Roundy and Frank 2004; Serra et al. 2008). While the origins of east Pacific EWs are still controversial, they are thought to originate either from reinvigorated African Easterly Waves (AEWs) that have propagated over the Central American isthmus (e.g., Frank 1970; Shapiro 1986; Avila and Pasch 1992; Rappaport and Mayfield 1992; Zehnder et al. 1999; Serra et al. 2008, 2010), or from local disturbances in favorable background conditions (Nitta and Takayabu 1985; Tai and Ogura 1987; Maloney and Hartmann 2001; Serra et al. 2010; Toma and Webster 2010a,b; Rydbeck and Maloney 2014; Rydbeck et al. 2017). The east Pacific warm pool, where these EWs can re-intensify or locally form, has been shown to exhibit variability on multiple timescales due to both local and remote processes. Two important phenomena that affect the east Pacific warm pool are the Madden-Julian Oscillation (MJO) and Caribbean Low-Level Jet (CLLJ). In this study, we investigate the respective influence of the MJO and CLLJ on the east Pacific background state, and their distinct impacts on EW eddy kinetic energy (EKE) budgets and tracks.

---

[2]Whitaker, J. W., and E. D. Maloney, 2018: Influence of the Madden-Julian Oscillation and Caribbean Low-Level Jet on East Pacific Easterly Wave Dynamics. *J. Atmos. Sci.*, in press. ©American Meteorological Society. Used with permission.

The MJO (Madden and Julian 1994; Zhang 2005) modulates conditions in the east Pacific warm pool on intraseasonal timescales (Maloney and Esbensen 2003; Serra et al. 2014). Previous work has found that boreal summer east Pacific precipitation, low-level convergence, low-level zonal wind, low-level relative vorticity, and vertical wind shear vary with MJO phase, although Rydbeck et al. (2013) suggest that the east Pacific can exhibit similar intraseasonal variability in these quantities independent of the MJO (e.g., Maloney and Hartmann 2000; Maloney and Esbensen 2003, 2007; Aiyyer and Molinari 2008). Maloney and Hartmann (2000) found that during anomalous MJO low-level westerly periods, a significant enhancement of east Pacific tropical cyclogenesis occurs due to strong positive anomalies in low-level relative vorticity and near-zero vertical shear of the zonal wind in the genesis region. More energetic EWs during MJO westerly periods may also contribute to this modulation of cyclogenesis (Maloney and Hartmann 2001). Anomalous MJO low-level easterly periods are associated with suppressed convection as well as anomalous low-level divergence and negative low-level relative vorticity anomalies (e.g., Maloney and Hartmann 2000, 2001). By accounting for the phase of the MJO, Slade and Maloney (2013) demonstrated increased skill at predicting east Pacific tropical cyclogenesis at 2-3 week lead times in a statistical model.

East Pacific EW activity is notably modulated by the MJO. Maloney and Hartmann (2001) found that low-level EKE is enhanced during westerly MJO phases relative to easterly phases, and that enhanced barotropic conversion helps to explain the more vigorous EWs and hence modulation of east Pacific tropical cyclones by the MJO. Using case studies from August-September 1998, Aiyyer and Molinari (2008) showed that westerly, convective phases of the MJO are associated with enhanced barotropic energy conversions along the Central American coast, while easterly, non-convective phases of the MJO have enhanced barotropic conversion along the east Pacific Intertropical Convergence Zone (ITCZ). Similarly, Crosbie and Serra (2014) found that low-level EKE and barotropic conversion increase along the Central American coast during MJO westerly periods in regional WRF model simulations, and documented shifts in moisture anomalies as a function of MJO phase. Rydbeck and Maloney (2014) highlighted that barotropic conversion and

the conversion from eddy available potential energy (EAPE) to EKE are the leading terms in the EKE budget during neutral and westerly intraseasonal events and that EAPE to EKE conversion, while still important to the energy budget, is reduced during easterly intraseasonal events. Rydbeck and Maloney (2014) also found that strong midlevel barotropic conversion occurs during westerly intraseasonal events along typical EW tracks, further indicating that westerly intraseasonal periods provide more favorable energy conditions for EW growth than easterly periods.

The CLLJ has also been shown to modify atmospheric variables that are important to EW growth and tropical cyclogenesis in the Intra-Americas Sea. Wang and Lee (2007) found that variations in the CLLJ were connected to larger scale circulations over the Atlantic, specifically the North Atlantic Subtropical High (NASH), and that pressure gradients that develop over the Caribbean Sea due to the strength and location of the NASH play an important role in enhancing or weakening the jet. Wang (2007) found that a strong easterly CLLJ in boreal summer is positively correlated with increased rainfall along the east Pacific ITCZ, but is negatively correlated with rainfall along the west coast of Central America, similar to the results of Cook and Vizy (2010). Further, the CLLJ and the mean summer easterly flow in the Caribbean have been cited as providing a favorable background state for east Pacific EWs. Using an EW tracking algorithm, Serra et al. (2010) found that strong easterly CLLJ periods are associated with a greater frequency of east Pacific EWs. Molinari et al. (1997) and Molinari and Vollaro (2000) found that the reversal of the meridional PV gradient associated with the CLLJ and its extension, the Papagayo jet, provide conditions favorable for EWs to intensify in the east Pacific. Serra et al. (2010) noted that barotropic conversion due to the CLLJ supports EW intensification in this region, while Serra et al. (2008) and Serra et al. (2010) also found that EAPE to EKE conversion is important to east Pacific EWs. Zehnder (1991) used a barotropic shallow water model to show that mean easterly flow over an idealized Sierra Madre Range led to the initiation of westward propagating Rossby waves.

The aforementioned CLLJ results, which suggest the importance of a strong easterly CLLJ to EW growth, appear to conflict with the findings presented above about the MJO; namely, that low-level westerly anomalies associated with the MJO provide more favorable background envi-

ronments and enhance EW energy conversions relative to easterly periods. The MJO also produces variations in the CLLJ (Maloney and Esbensen 2007). However, the analysis below will show that the effects of the MJO and CLLJ on EWs and the east Pacific background state are not synonymous. This study will investigate low-level zonal wind anomaly periods of the MJO and CLLJ to help distinguish which anomalous low-level wind direction is favorable for east Pacific EW development, and where and why this enhancement occurs. An EW energetics analysis will show that westerly periods of the MJO and CLLJ have similar energy budget term structures and profiles that favor EW intensification in the northeastern portion of the basin, though the influence of MJO has a more expansive reach westward into the basin. However, these phenomena produce different effects during easterly periods along the east Pacific ITCZ that are consistent with strong CLLJ period EWs relying more on convection for their energetics than in easterly MJO periods.

This paper is structured as follows. Section 2 provides an overview of the data and methods used to composite periods based on MJO and CLLJ phase, and the EW tracking algorithm that is employed. Section 3 discusses the mean state of the east Pacific and how this background state is modulated by the MJO and CLLJ. Section 4 describes the vertically averaged EKE budget during MJO and CLLJ composite events, while Section 5 looks at the vertical structure of the energy budget terms and regressed fields along the ITCZ. Section 6 discusses how EW tracks vary based on MJO and CLLJ composite phase. Section 7 provides a discussion of the results and conclusions.

2.2 Data and Methods

This study uses data from the Interim European Centre for Medium-Range Weather Forecasts Re-Analysis (ERA-Interim; Dee et al. 2011) over the years 1990-2010, and the months of May-October when EWs are most active. The ERA-Interim data employed are 6-hourly, cover 17 pressure levels from 1000 hPa to 200 hPa by 50 hPa, and have a grid spacing of $1.5°$. Further, the NOAA National Climatic Data Center outgoing longwave radiation (OLR) daily dataset (Lee 2014) from 1990-2010 is used as a proxy for deep convection. In section 3, both ERA-Interim

and OLR data are interpolated to have a 1° grid spacing and six-hour timestep for the composite analysis, similar to what is done in Rydbeck and Maloney (2014).

To investigate behavior during MJO and CLLJ events, compositing is used. MJO phases are defined using the real-time multivariate MJO (RMM; http://www.bom.gov.au/climate/mjo/) index based on Wheeler and Hendon (2004). The daily RMM index uses combined EOF analysis on equatorial-averaged 850 hPa and 200 hPa zonal wind and OLR to define eight MJO phases. Only days with RMM amplitude greater than 1 standard deviation are considered in our analysis. To distinguish different sign wind events, MJO phase 2 will represent westerly events, while MJO phase 6 will represent easterly events. For the CLLJ and its extension to the Papagayo jet, we define an index based on the ERA-Interim 925 hPa zonal wind over the domain (9-13°N, 86-89°W) for the months of May-October, similar in method to Wang (2007) and Serra et al. (2010). The CLLJ index is defined by first removing the 6-hourly climatological mean, then taking the 5-day running average of zonal wind averaged over this box. We define strong (weak) jet events as 1 standard deviation below (above) zero, where strong CLLJ events are more easterly and weak CLLJ events are more westerly compared to the mean easterly CLLJ, respectively. Only CLLJ events in which the MJO RMM index is within ±1 standard deviation are considered to limit the impact of the MJO on the CLLJ index in the analysis, since Maloney and Esbensen (2007) showed that jet events often accompany strong MJO events. In fact, roughly 33% of strong MJO westerly and easterly periods identified by the RMM index had significant jet activity that was not included in the CLLJ composite periods, and a sensitivity analysis investigating MJO periods with these jet periods removed yielded qualitatively similar results to the full MJO composite periods. By designing the CLLJ analysis this way, CLLJ periods are defined to have little to no influence by the MJO, which is a method that is unique compared to other studies involving the CLLJ in the literature. In total, 1472 MJO phase 2, 1028 MJO phase 6, 837 weak CLLJ, and 918 strong CLLJ six-hourly observations occurred over the May-October, 1990-2010 period.

Before computing the EKE budget for EWs, the effects of tropical cyclone (TC) anomalies were removed at all pressure levels using the National Hurricane Center best track data (Landsea

and Franklin 2013) for TC locations over the time domain. After the cyclone center was identified, the weighting function and process described in Aiyyer et al. (2012) and Rydbeck and Maloney (2014) was used to remove fields around the cyclone center. The weighting function is given by:

$$w(x, y) = 1 - exp(-\frac{r^2 ln(4)}{2R^2}), \quad (2.1)$$

where $r = r(x, y)$ is the distance of a grid point from the TC center and R = 500 km is the length scale of the weighting function. The weighting function is applied to a $6° \times 6°$ box centered on the location of a TC at all time steps and over all pressure levels of data. By removing TCs, the EKE budget will more accurately display the energy conversions for EWs.

In Section 6, we investigate how May-October EW and TC tracks vary during phases of the MJO and CLLJ. To do this, we utilize the newly created NOAA National Centers for Environmental Information African Easterly Wave Climatology dataset at 600 hPa (Belanger et al. 2014), which provides track information about individual easterly wave events and TCs. The EW track data is used to illustrate the general spatial characteristics of EW activity and whether EW activity is favored in certain regions of the east Pacific during particular MJO and CLLJ periods, as opposed to investigating individual EWs that may be modulated by these phenomena. The 6-hourly track data used is derived from ERA-Interim data and an EW tracking algorithm described in Belanger et al. (2016) that uses curvature vorticity anomalies, among other variables, to identify and track EWs and TCs. To ensure that only typical, more robust EWs are included, we mandate that EWs must persist for more than 2 days and travel at least $15°$ in Pythagorean distance, at least $12°$ to the west in longitude, and no more than $4°$ to the south in latitude relative to their genesis location. EW track information is presented using track density, which is calculated by binning EW track observations every $2°$ and scaled to produce units of the number waves per May-October season, similar to work done by Serra et al. (2010) and others. Finally, a centered $8° \times 8°$ two-dimensional Gaussian weighting box with $\sigma = 1.4°$ is applied over the track density plots for smoothing.

2.3 MJO and CLLJ influence on the East Pacific background state

To indicate where east Pacific EWs and TCs tend to occur, Figure 2.1 shows average EW track density over May-October of 1990-2010, along with line contours of mean boreal summer OLR. Track density is in units of $\frac{EW}{4^{\circ 2} year}$, and represents the number of EW and TC observations that occur in a given grid box per May-October season. The mean track density shown has similar features to results shown by Thorncroft and Hodges (2001), Serra et al. (2010), and Belanger et al. (2016). In the eastern Atlantic, track density values are mostly around 7 to 8 $\frac{EW}{4^{\circ 2} year}$ near the exit of the African easterly jet, and slightly lower values continue westward across the north Atlantic hurricane main development region. Further, a relative minimum in track density occurs in the western Caribbean Sea as waves weaken after traversing the Atlantic. In the east Pacific, EWs and eventually TCs travel in a more southeast to northwest oriented path that is parallel to the Central American coast, with values over 8.5 $\frac{EW}{4^{\circ 2} year}$. This area of high track density will henceforth be referred to as the main EW path. The transition from low track density in the western Atlantic to high track density in the east Pacific is consistent with previous studies on EW tracks (Thorncroft and Hodges 2001; Serra et al. 2010; Belanger et al. 2016), and supports the notion that while some waves may propagate from the Atlantic into the Pacific, the local conditions and energetics in the east Pacific warm pool may be sufficient enough for EW generation (e.g., Maloney and Hartmann 2001; Serra et al. 2010; Rydbeck and Maloney 2014). Track density is also fairly high along the east Pacific ITCZ, with the location of the ITCZ being associated with the lower mean OLR values in the basin that extend from 80°W to 140°W and from 7°N and 10°N. This ITCZ EW activity is potentially related to preexisting AEWs and Panama Bight convective disturbances having more of a zonal track in the basin, or from EWs which form locally in the ITCZ due to processes like ITCZ breakdown (Ferreira and Schubert 1997) or inertial instability in the ITCZ that results from cross-equatorial pressure gradients (Toma and Webster 2010a).

Having discussed locations of east Pacific EW activity, it is important to investigate how the MJO and CLLJ affect the environmental conditions of this basin. Figure 2.2 shows the monthly frequency of occurrence for MJO and independent CLLJ low-level westerly and easterly events. MJO phase 2 events in our sample have a modest preference for the months of June-September, with August having a frequency of around 0.2. MJO phase 6 events in our sample have a modest preference for the months of May and October, with May having a frequency of about 0.25. Significant jet events independent from the MJO appear to favor the later months of boreal summer and into fall. Interestingly, although Chelton et al. (2000a) notes that jet activity is particularly strong in boreal winter, the bottom panels of Figure 2.2 indicate that substantial jet activity also occurs in summer months. For weak jet periods, the months of August-October all have frequencies over 0.2, while May and July values are below 0.1. For strong jet periods, October has the highest frequency of around 0.25, while June is the second highest month of occurrence. Although Wang (2007) notes that the CLLJ has a boreal summer maximum in July, our index finds that July is not the most prominent month with strong CLLJ activity. This difference may be due to the emphasis on synoptic timescale activity and the removal of high amplitude MJO events in our CLLJ index.

To analyze the influence of the MJO and CLLJ on the east Pacific warm pool large-scale environment, composite anomalies are computed relative to the 6-hourly climatological mean for all fields. Figures 2.3 and 2.4 show anomalous total column water vapor and 850 hPa relative vorticity during westerly and easterly periods of the MJO and CLLJ. For the MJO and CLLJ, westerly low-level wind anomaly periods are associated with enhanced moisture and positive relative vorticity anomalies along the main EW path shown in Figure 2.1, while negative moisture and vorticity anomalies occur along the ITCZ. Easterly low-level wind anomaly periods for both phenomena are associated with negative moisture and relative vorticity anomalies along the main EW path, and have positive moisture and relative vorticity anomalies along the ITCZ. Although general similarities exist between these MJO and CLLJ composites, there are also some notable differences in how they modulate the east Pacific background state. For example, a greater modulation of moisture occurs along the ITCZ for the CLLJ relative to the MJO, particularly during easterly pe-

31

riods. Strong CLLJ periods have moisture anomalies that are around 1 kg m^{-2} above those found in MJO phase 6. In particular, CLLJ moisture anomalies are much higher along the ITCZ east of 105W relative to MJO easterly periods. The increase in ITCZ moisture anomalies during strong CLLJ periods may provide a more favorable environment for ITCZ EWs relative to MJO phase 6. Further, it appears that the MJO has a more spatially extensive influence along the coast from Nicaragua to the Baja California Peninsula relative to the CLLJ, while the absolute value of the anomalies during both CLLJ periods are higher than in MJO periods. MJO moisture and vorticity anomalies have more of a northward and westward extent over the main EW path than those for the CLLJ, with CLLJ moisture anomalies being more concentrated in the immediate vicinity of the Central American coast. The strong influence along the entirety of the main EW path by the MJO provides additional evidence of its role as a major modulator of east Pacific EWs and TCs.

Figures 2.5 and 2.6 show mean May-October OLR and anomalous composite OLR to highlight the MJO's more expansive influence along the main EW path and the stronger modulation of ITCZ convection by the CLLJ. The time mean contours indicate that during boreal summer, deep convection is prominent in the Panama Bight region, with values below 200 W m^{-2}. This OLR minimum then extends westward between 7°N and 10°N, again highlighting the mean position of the east Pacific ITCZ. The composite OLR anomalies indicate that strong (weak) CLLJ periods are associated with a suppression (enhancement) of convection near the Central American coast, but these anomalies are more localized relative to the MJO periods, similar to what was seen for the moisture anomalies in Figures 2.3 and 2.4. Negative (positive) OLR anomalies occur more extensively along the main EW path during MJO phase 2 (6) periods. CLLJ periods are associated with a greater modulation of convection along and to the south of the ITCZ with a sign opposite to that near the Central American coast. During strong CLLJ periods, negative OLR anomalies at ITCZ latitudes begin around 90°W, while MJO phase 6 anomalies only start to become negative around 110°W, underscoring that the influence of these easterly periods on the east Pacific is not synonymous. This result is consistent with Figures 2.3 and 2.4, which show higher moisture anomalies occurring along the ITCZ in strong CLLJ periods relative to MJO phase

32

6. Westerly period composite OLR anomalies also emphasize the greater influence the CLLJ has on ITCZ convection. Weak CLLJ period positive OLR anomalies also start around 90°W while positive MJO anomalies only begin west of 105°W. Though differences in westerly MJO and CLLJ period anomalies are notable, differences in the modulation of moisture and convection are most strongly apparent for easterly periods along the ITCZ, and the differences between easterly MJO and CLLJ periods will be explored further in subsequent sections. Overall, these findings indicate that while the MJO has a more extensive spatial influence along the main EW path, the modulation of moisture and deep convection along and to the south of the ITCZ is stronger and more extensive from the CLLJ. The enhancement of ITCZ moisture and convection during strong CLLJ periods may be associated with stronger moisture convergence due to the CLLJ, as mentioned by Wang (2007). However, understanding the differing responses of the east Pacific to the MJO and CLLJ is a topic for future research.

2.4   Eddy Kinetic Energy Budgets

To support the notion that both MJO and CLLJ westerly low-level wind anomaly periods are more favorable for EW growth in the northeastern portion of the east Pacific basin, and to show that EWs during easterly periods of the MJO and CLLJ are influenced differently along the ITCZ, an EKE budget (vertically averaged from 1000 to 200 hPa) is computed. As in Rydbeck and Maloney (2014), EKE is defined as:

$$KE = \frac{1}{2}(\overline{u'^2} + \overline{v'^2}), \tag{2.2}$$

where a bar represents the 11-day running mean, and a prime represents a deviation from the 11-day running mean. The EKE budget describes the components of the EKE tendency equation, which is given by:

$$\frac{\partial \overline{KE}}{\partial t} = -\overline{v}_h \cdot \nabla_h \overline{KE} - \overline{v'_h \cdot \nabla_h KE} + \left[-\overline{u'u'}\frac{\partial \bar{u}}{\partial x} - \overline{u'v'}\frac{\partial \bar{u}}{\partial y} - \overline{u'v'}\frac{\partial \bar{v}}{\partial x} - \overline{v'v'}\frac{\partial \bar{v}}{\partial y} \right]$$
$$- \nabla \cdot \left(\overline{\vec{v}'\Phi'} \right) - \frac{R}{p}\left(\overline{\omega'T'} \right) + D, \tag{2.3}$$

where $\vec{v}$ is the three dimensional wind vector, $\vec{v}_h = \vec{v}(u,v)$ is the two dimensional wind vector, Φ is the geopotential, R is the gas constant for dry air, p is the pressure, ω is the vertical pressure velocity, T is the temperature, and D is the budget residual. The first and second terms on the right-hand side of the EKE tendency equation, $-\overline{\vec{v}_h} \cdot \nabla_h \overline{KE}$ and $-\overline{\vec{v}_h' \cdot \nabla_h KE}$, account for the advection of EKE by the time-mean and perturbation flow, respectively. The third term, $-\overline{u'u'}\frac{\partial \bar{u}}{\partial x} - \overline{u'v'}\frac{\partial \bar{u}}{\partial y} - \overline{u'v'}\frac{\partial \bar{v}}{\partial x} - \overline{v'v'}\frac{\partial \bar{v}}{\partial y}$, accounts for barotropic conversion, or the conversion of mean-state kinetic energy to EKE. The fourth term, $-\nabla \cdot \left(\overline{\vec{v}'\Phi'} \right)$, accounts for the generation of EKE by geopotential flux convergence. The fifth term, $-\frac{R}{p}\left(\overline{\omega'T'} \right)$, accounts for the conversion of EAPE to EKE. Serra et al. (2008) documented that a maximum in EAPE to EKE conversion occurs between 400hPa and 200hPa in the east Pacific, suggesting that EAPE is generated by convection in this region. EAPE is converted to EKE where ascent occurs in areas of warm temperature anomalies and descent occurs in areas of cold anomalies. The final term, D, is the budget residual and accounts for any uncalculated sources or sinks of EKE, such as friction due to turbulent mixing or smaller-scale processes, and also contains any budget residuals due to analysis increments or errors that arise from imprecise calculations.

Figures 2.7 and 2.8 show the contrast between the westerly and easterly low-level wind anomaly period EKE for the MJO and CLLJ, respectively, vertically averaged from 1000 to 200 hPa. A strong meridional gradient in EKE exists due to increasing synoptic scale wind perturbations with latitude, likely associated with midlatitude systems. MJO phase 2 is characterized by a local maximum of EKE in the east Pacific around 12°N, 105°W, with values reaching 11.5 m^2 s^{-2}, and a local minimum in the Panama Bight with values as low as 6.5 m^2 s^{-2}. For MJO phase 2, the area where the local maximum occurs is enhanced by around 2 m^2 s^{-2} relative to phase 6, and is a statistically significant difference in EKE at the 90% confidence level using a bootstrapping re-sampling method by generating over 2000 random samples with replacement. Further, MJO phase 6 EKE values are also low in the Panama Bight, and lower values extend westward to the south of the ITCZ. Given the relatively weak modulation of precursor disturbances in the Bight of Panama region, the expansive modulation of the east Pacific background state shown in Figures 2.3 and 2.5

by the MJO is most likely responsible for why stronger EWs occur along the main EW path during MJO phase 2 relative to phase 6.

Figure 2.8 shows that weak CLLJ periods resemble MJO phase 2 in that an extension of higher EKE values occurs southward, however the local maximum is observed further east than for MJO westerly periods, near the Central American coast and the Gulf of Tehuantepec. Values in this area are on the order of 11 m^2 s^{-2}, which are enhanced relative to the mean-state EKE (not shown). However, during strong CLLJ periods, the total EKE in the east Pacific is reduced both relative to weak CLLJ periods and the easterly MJO phase 6. This result highlights that MJO and CLLJ westerly periods are associated with stronger EWs relative to their respective easterly periods, and seemingly goes against the notion that a strong CLLJ is associated with strong EW development. In particular, near the Central American coast weak CLLJ period EKE enhancements up to 2 m^2 s^{-2} occur relative to strong CLLJ periods, which are statistically significant at the 90% level after bootstrapping. However, this enhancement of EKE for weak CLLJ periods is not as extensive along the main EW path, or as large in magnitude relative to the MJO periods shown in Figure 2.7. It is also noted that at the latitude of the ITCZ, the reduction in EKE for strong CLLJ periods relative to weak CLLJ periods is relatively modest and not significant, consistent with a possible role for convection in maintaining EW activity in these regions as argued in the context of Figures 2.4 and 2.6 above. This feature is not seen for the MJO in Figure 2.7. In addition, the EKE during weak CLLJ periods is significantly enhanced to the west of 120°W in the equatorial region south of the ITCZ. This signal is also not present in the MJO composites. The mean-state equatorial 200 hPa zonal wind west of 120°W during weak CLLJ periods is characterized by total westerly winds that are also westerly in an anomalous sense relative to strong CLLJ periods (not shown). Thus, a potential explanation for this increase in equatorial EKE could be cross equatorial wave propagation through westerly ducts, as described in Webster and Holton (1982). However, further testing of this hypothesis is left for future work.

Interestingly, EKE values in the Panama Bight show only modest differences between strong and weak CLLJ periods, similar to the MJO composite results shown in Figure 2.7. During MJO

phase 2, EKE in the Panama Bight is actually lowest when EKE in the east Pacific warm pool is highest. One implication of these results is that variability in the strength of east Pacific EW activity may be more dependent on variations in the large-scale downstream environment than the initial strength of diurnal convective disturbances that can grow upscale into EWs (e.g., Rydbeck et al. 2017).

The leading terms of the EKE budget (barotropic conversion and EAPE to EKE conversion) for the anomalous westerly and easterly composites of the MJO and CLLJ are provided in Figures 2.9 and 2.10, respectively. Barotropic conversion in MJO phase 2 has a tendency to orient parallel to the Central American coast, and has a local maximum of 3×10^{-5} m^2 s^{-3} that is roughly in the same location as the EKE maximum seen in Figure 2.7. In comparison to the weak CLLJ periods in Figure 2.10, the barotropic conversion signature during MJO phase 2 extends more along the main EW path, although the values are roughly on the same order of magnitude around 2×10^{-5} m^2 s^{-3}. Consistent with results in Figures 2.4, 2.6, and 2.8, the area of higher EW barotropic conversion is shifted closer to the Central American coast for weak CLLJ periods relative to MJO phase 2. MJO phase 6 barotropic conversion has more of a zonal orientation that is shifted southward toward the ITCZ, and has lower values along the main EW path compared to MJO phase 2, except for the exit region of the Papagayo jet. A southward shift in barotropic conversion toward the ITCZ also occurs during strong CLLJ periods and an enhancement of this term also extends westward from the Papagayo jet, which lines up well with the enhanced relative vorticity anomalies in this region for easterly periods in Figures 2.3 and 2.4. These results indicate that topographic effects due to an enhancement of the basic state easterly flow through the Central American mountain gaps may play a role in providing a more favorable environment to initiate or reinvigorate EWs downstream during easterly periods, similar to what was found in Zehnder (1991), Molinari et al. (1997), and Molinari and Vollaro (2000).

For the EAPE to EKE conversion term, MJO and CLLJ westerly periods are more comparable to each other than for the easterly period composites. For example, an enhancement of this term, which is consistent with convective invigoration, extends from the Central American coast into

36

the main EW path during both low-level westerly periods. EAPE to EKE conversion values over 4×10^{-5} m^2 s^{-3} occur in this region during westerly periods. In addition, both periods have a relative minimum in EAPE to EKE conversion over the Costa Rica Dome region where relatively cool sea surface temperatures help disfavor convection climatologically (Xie et al. 2005). Both westerly period EAPE to EKE conversion composites are consistent with the anomalies shown in Figures 2.3-2.6, namely that enhanced convection and moisture along the main EW path and near the Central American coast can help produce EAPE which then is converted to EKE. Both easterly period composites have higher EAPE to EKE conversion along 10°N and the ITCZ. The magnitude of the EAPE to EKE conversion term values for strong CLLJ periods are stronger than for the MJO. Strong CLLJ periods also have a broader area of enhanced EAPE to EKE conversion along the ITCZ, which lines up with the negative OLR anomalies seen in Figure 2.6. The more widespread and stronger EAPE to EKE values along the ITCZ during strong CLLJ periods than for easterly MJO periods suggests that this term plays more of a role in EW development relative to MJO phase 6, given their similar structures and magnitudes in barotropic conversion. Interestingly, all composite phases of the MJO and CLLJ have high EAPE to EKE conversion in the Panama Bight region, suggesting convective invigoration there. This finding indicates that regardless of the modulation to the east Pacific background state by the MJO or CLLJ, deep convective disturbances in the Panama Bight will continue to initiate and provide seed disturbances that are favorable for downstream EW development.

To provide a sense of the relative importance of the leading EKE budget terms in the composite periods, Figures 2.11 and 2.12 provide the ratio of vertically averaged barotropic conversion to EAPE to EKE conversion in areas were the sum of the absolute values of both of the terms in Figures 2.9 and 2.10 is at least 1.5×10^{-5} m^2 s^{-3}. Ratio values greater (less) than 1 indicate higher (lower) barotropic conversion values relative to EAPE to EKE conversion. Overall, westerly MJO and weak CLLJ periods appear to have many similarities, while their respective easterly periods have different responses. For MJO phase 2 and weak CLLJ periods, most of the main EW path is associated with a greater proportion of EKE generation stemming from EAPE to EKE conversion.

Given the increased moisture and negative OLR anomalies east of 105°W in Figures 2.3-2.6, we would expect convective processes to play an important role in EWs along the main track during both westerly periods. The ratios observed for weak CLLJ periods are lower than those during MJO phase 2 and are the lowest overall, indicating that weak CLLJ period EW growth is most dependent on convective generation of all the composite periods. However, when comparing both easterly periods, the ratios for EW energetics show greater differences along the ITCZ. In phase 6, the ITCZ is associated with higher barotropic conversion to EAPE to EKE conversion ratios than during MJO phase 2. Hence, it appears that convection is relatively less important for EW growth during easterly MJO periods, which agrees with the positive OLR anomalies found around the ITCZ in Figure 2.5. This result is also consistent with Rydbeck and Maloney (2015), who found that weak convective coupling occurs in EWs during easterly intraseasonal events, and may suggest that EWs during easterly MJO periods act more like dry dynamical waves, growing due to interactions with the mean flow. Conversely, the strong CLLJ period ratios seem to indicate more of a contribution from convective invigoration to EW growth along the ITCZ relative to MJO phase 6. Along the ITCZ, statistically significant differences in the ratios occur between strong CLLJ periods and MJO phase 6 at the 90% confidence level using bootstrapping (not shown). When calculating the average of the ratio fields meeting the magnitude threshold for plotting in Figures 2.11 and 2.12 over a box encompassing the mean ITCZ (6-13°N, 88.5-120°W), the average ratio is 1.27 for strong jet periods to 1.52 for MJO phase 6. If the strength threshold used for plotting is relaxed, strong CLLJ periods have an average ratio in the ITCZ box of 1.68, while for MJO phase 6 the ratio is 5.11. Thus, strong CLLJ periods have more of a reliance on convection for EKE growth, reflected in the conversion from EAPE to EKE, than during MJO phase 6 periods. This greater dependence on convection is consistent with the stronger modulation in moisture along the ITCZ during strong CLLJ periods shown in Figure 2.4, and from the more extensive and stronger negative OLR anomalies along and south of the ITCZ for strong CLLJ periods versus the positive OLR anomalies east of 110°W in the ITCZ associated with MJO phase 6 (Figures 2.5 and 2.6).

2.5   ITCZ Vertical Structure

Given the differences in the east Pacific basic state modulation and vertically averaged EKE budget terms near the ITCZ for the MJO and CLLJ, this section discusses the vertical structure of EKE budget terms along the ITCZ to diagnose their contributions to the growth of EWs during the MJO and CLLJ events. To do this, vertical cross sections along the ITCZ at 10.5°N from 85.5°W to 135°W are computed.

Figure 2.13 shows the composite vertical cross sections of EKE from east (right) to west (left) along the ITCZ. Overall, a distinct vertical gradient in EKE exists associated with the stronger wind perturbations at upper levels. MJO phase 2 has a secondary maximum (with values over 11.5 $m^2 s^{-2}$) of EKE between 600 and 400 hPa near 10.5°N, 102°W, and higher values that extend down through the column to the surface. Additionally, weak CLLJ periods also have an extension of higher EKE at midlevels, though the values are not as strong. The midlevel extensions are consistent with regions of increased EKE during westerly periods in the main EW track shown in Figures 2.7 and 2.8. Although westerly periods for both the MJO and CLLJ exhibit similar behavior, easterly periods have more notable differences in their EKE structure relative to one another. For MJO phase 6 very little structure exists at midlevels. However, strong CLLJ periods have an enhancement of midlevel EKE relative to MJO phase 6 along the ITCZ on the order of 1 $m^2 s^{-2}$. The enhancement of midlevel EKE during strong CLLJ periods may be consistent with the notion that convective invigoration helps support EWs more during strong CLLJ periods relative to MJO phase 6, as suggested in Figures 2.9-2.12.

Having shown the changes to the EKE vertical structure, we will now discuss composite changes in barotropic conversion and EAPE to EKE conversion in a vertical cross-section along the ITCZ (Figures 2.14 and 2.15). The structure of the energy generation fields along the ITCZ expands upon previous work done by Rydbeck and Maloney (2014) for a cross section along the main EW path, and shows the importance of lower level barotropic conversion and upper level EAPE to EKE conversion for ITCZ EWs east of 120°W. This analysis also expands upon the findings of Serra et al. (2010), who showed in meridional cross sections along 95°W that strong EAPE to EKE

conversion occurs at upper levels and enhanced barotropic conversion occurs at lower levels near 10°N.

Consistent with previous results in this study, MJO and CLLJ westerly periods have similar vertical cross sections of their leading budget terms along the ITCZ, while easterly periods have notable differences. For example, Figure 2.14 shows that MJO phase 2 is associated with strong midlevel barotropic conversion near 102°W, with values on the order of 4×10^{-5} m^2 s^{-3}, and high values at low levels exist throughout the cross section. Similarly, weak CLLJ period barotropic conversion shown in Figure 2.15 is enhanced near 400 hPa and has its highest values below 900 hPa. Both westerly MJO and weak CLLJ periods have strong EAPE to EKE conversion at upper levels to the east of 115°W, with values over 1.4×10^{-4} m^2 s^{-3}. Thus, even though lower and midlevel barotropic conversion is important to developing EWs, the values of EAPE to EKE conversion at upper levels are large enough to keep the ratios shown in Figures 2.11 and 2.12 along the ITCZ during both westerly composites below one to the east of 115°W. So, it appears that these areas may favor the generation of EKE by convective invigoration relative to barotropic conversion.

However, easterly MJO and strong CLLJ composite cross sections of the leading budget terms show differences important to the energetics of ITCZ EWs. While strong CLLJ periods have a similar, though weaker, midlevel extension of barotropic conversion up to 400 hPa, which is consistent with the results of Serra et al. (2010), MJO phase 6 periods have only weak midlevel barotropic conversion. Strong CLLJ periods have stronger and somewhat deeper EAPE to EKE conversion at upper levels relative to MJO phase 6 periods, and this feature is located above the enhanced midlevel barotropic conversion feature, similar to what occurs during the westerly composites.

A one-tailed difference of means Student's t-test at the 90% confidence level was conducted to examine the statistical significance of this strong CLLJ period EAPE to EKE conversion enhancement relative to MJO phase 6 in Figure 2.14. The sample sizes of the composite periods used in the significance test are the number of individual events spanning at least 2 consecutive days over the composites—45 strong CLLJ and 52 MJO phase 6 events were used, respectively. Indeed, the enhanced EAPE to EKE conversion feature for strong CLLJ periods is significantly different at

the 90% confidence level then during MJO phase 6 (Figure 2.14), shown by the hatching in the bottom right panel of Figure 2.15. This more prominent area of EAPE to EKE conversion during strong CLLJ periods supports the results of Figures 2.11 and 2.12, namely that strong CLLJ period EWs along the ITCZ rely more on convective processes relative to MJO phase 6. This result is also consistent with the greater modulation of ITCZ moisture and convection during strong CLLJ periods relative to MJO phase 6 seen in Figures 2.4 and 2.6. Thus, while the westerly MJO and CLLJ composite budget term cross sections are comparable in structure and magnitude, the easterly MJO and CLLJ composites are not synonymous and support the idea that strong CLLJ period waves depend more on convective invigoration than MJO phase 6 waves along the ITCZ.

To further explain why strong CLLJ period EWs are invigorated more by convection relative to MJO phase 6 EWs, linear regressions of bandpass filtered apparent heat source (Q_1), ω and temperature onto bandpass filtered 700 hPa vorticity were calculated for easterly MJO and CLLJ periods. A positive covariance between anomalies of Q_1 and temperature leads to EAPE generation, which subsequently can be converted to EKE through a negative covariance of ω and temperature as shown in Figures 2.14 and 2.15. The method behind this analysis is described here. The expression for Q_1 is calculated as in Yanai and Johnson (1993), and is given by:

$$Q_1 = \frac{\partial \overline{s}}{\partial t} + \overline{\boldsymbol{v}} \cdot \nabla \overline{s} + \overline{\omega} \frac{\partial \overline{s}}{\partial p}, \tag{2.4}$$

where $s = c_p T + gz$ is the dry static energy, $\boldsymbol{v}$ is the horizontal wind velocity, p is the pressure, and ω is the vertical pressure velocity. In this expression, the bars represent an average over a grid cell. For the linear regression, 700 hPa relative vorticity filtered from 2.5 to 12 days in frequency space and to westward wavenumbers of 6-30 is used as the reference time series at a base point of 10.5°N, 111°W for investigating ITCZ EWs during the respective composite periods. Anomalous Q_1, ω, and temperature on EW time scales are computed at all pressure levels by the same bandpass filtering approach as for the 700 hPa relative vorticity. These anomalous fields are linearly regressed on to the filtered vorticity reference time series during easterly and westerly periods of the CLLJ and MJO to yield regression coefficients. These regression coefficients are

41

then scaled by a 1 standard deviation value of the respective composite period filtered vorticity time series (to represent the passage of a typical EW) for plotting.

Figure 2.16 shows ITCZ vertical cross sections (averaged between 10.5°N and 12°N) of regressed anomalous temperature and Q_1 (top row), and temperature and ω (bottom row) for MJO phase 6 and strong CLLJ composite periods. The temperature profiles for EWs in both periods, and particularly in strong CLLJ periods, agree with Serra et al. (2008), who found that east Pacific EWs have an eastward tilt of warm temperature anomalies with height. Further, EWs in both periods have anomalous apparent heating that maximizes in the middle to upper troposphere, suggesting that both deep convection and stratiform structures are present in these waves, which is consistent with the observational results of Petersen et al. (2003). Strong CLLJ period EWs appear to have stronger apparent heating and temperature anomalies and smaller wavelengths compared to MJO phase 6 waves, and appear to more efficiently produce EAPE due to a stronger covariability of temperature and Q_1. For example, out in front of the wave there is anomalous cooling co-located with negative temperature anomalies that are more vertically coherent relative to MJO phase 6. Similarly, anomalous heating and positive temperature anomalies are more co-located behind the wave axis in strong CLLJ period waves. The analysis of regressed ω and temperature reveals a consistent story, that a better co-location of opposite signed and stronger ω and temperature anomalies occurs for strong CLLJ period waves relative to MJO phase 6 waves, particularly in front of the wave axis. The enhanced negative covariance between ω and temperature indicates that strong CLLJ period waves seem to more efficiently convert the generated EAPE to EKE, supporting the results of Figures 2.14 and 2.15. Therefore, strong CLLJ period EWs rely more on convective invigoration for their energetics relative to MJO phase 6. A potential explanation for the more coherent dynamical structures along the ITCZ that lead to more efficient EAPE to EKE conversion associated with convection during strong CLLJ periods could be the stronger moisture gradients along and to the north of the ITCZ relative to MJO phase 6, inferred from Figures 2.3 and 2.4. The enhanced moisture gradients during strong CLLJ periods may cause stronger moisture advection anomalies in ITCZ EWs relative to MJO phase 6, leading to a stronger locking of convection to

the waves. An examination of the moisture budget during these composite periods will be a topic for future work.

2.6 Easterly Wave Tracking

To provide a measure of the number and location of EWs to supplement the strength metric of EKE applied in Sections 4 and 5, this section uses the recently released NOAA National Centers for Environmental Information African Easterly Wave Climatology dataset at 600 hPa to look at the influence of the MJO and CLLJ on EW and TC tracks. As a reminder, the May-October 1990-2010 track density is given by Figure 2.1. As previously stated, the units for track density in Figure 2.1 are $\frac{EW}{4°^2 year}$ and are created from binning all track observations at a resolution of 2°x2°.

To discern the impact of the MJO and CLLJ on EW tracks, the difference in composite EW track density is shown in Figure 2.17, where the difference is calculated as the westerly minus the easterly period. Track density in these plots represents the difference in the total number of track observations per grid box per year over each respective composite period ($\frac{EW}{4°^2 year}$). To do this, the number of waves per grid box over each composite period is calculated, similar to Figure 2.1. Next, this value is divided by the number of days that goes into the composite period, and then is scaled by the length of the active season, May-October (184 days) to represent a year. Along the main EW path in MJO phase 2, there are areas with up to 10 additional track observations per grid box per year compared to phase 6. More tracks occur along 6 to 8°N during MJO phase 6 relative to phase 2. This result is likely related to the southward shift of the vertically averaged barotropic and EAPE to EKE conversion terms toward the ITCZ shown in Figure 2.9.

For the CLLJ composites, a strong modulation of tracks between wind periods occurs along the ITCZ. Strong CLLJ periods have higher EW observations along and north of the ITCZ relative to weak CLLJ periods, consistent with the OLR anomalies shown in Figure 2.6, but along the main EW path not as clear of a distinction exists between wind phases as was observed with the MJO. An analysis of MJO and CLLJ composite periods against the climatology (not shown) reveals that, indeed, MJO phase 2 (phase 6) is associated with higher (lower) track density relative to

the climatology along the main EW path while weak (strong) CLLJ period track density is close to (slightly above) climatology in this region. For the easterly composites, strong CLLJ periods and MJO phase 6 are associated with higher ITCZ track density relative to climatology, though strong CLLJ periods have broader and generally stronger areas of higher track counts along the ITCZ relative to MJO phase 6. Thus, the MJO modulates the number of tracks along the main EW path to a much greater degree than the CLLJ, while both the CLLJ and MJO favor more EWs occurring along the ITCZ during easterly events, although the modulation by the CLLJ appears to be stronger. The stronger invigoration by convection that occurs during strong CLLJ periods relative to easterly MJO periods may support the higher ITCZ EW track density.

2.7 Discussion and Conclusions

The background state of the east Pacific is modulated on a variety of time scales by events such as the MJO and CLLJ. These phenomena are associated with changes in the low-level wind structure, low-level vorticity, moisture, and convection in the basin, which are important to EW development and TC genesis. Previous studies have found that low-level westerly events associated with the MJO or intraseasonal events were linked to enhanced EW activity (Maloney and Hartmann 2001), tropical cyclogenesis (Maloney and Hartmann 2000; Aiyyer and Molinari 2008), favorable EW energetics (Crosbie and Serra 2014; Rydbeck and Maloney 2014), and stronger convective coupling in EWs (Rydbeck and Maloney 2015). Contrastingly, other studies indicate that strong easterly flow related to the CLLJ is associated with a greater frequency of EWs (Serra et al. 2010), east Pacific EW intensification (Molinari et al. 1997; Molinari and Vollaro 2000), and a possible source of EWs due to interactions of the flow with Central American topography (e.g., Zehnder 1991). This study presents a composite analysis and an EKE budget for MJO and CLLJ low-level wind phases to discern whether westerly or easterly low-level wind anomalies associated with these events provide more favorable conditions for east Pacific EW development. Our results show that MJO and CLLJ low-level wind periods provide differing anomalous responses in the east Pacific background state. The CLLJ is a stronger modulator of moisture and convection along the ITCZ,

44

with strong CLLJ periods having enhanced moisture and reduced OLR anomalies relative to MJO phase 6. Strong CLLJ periods are also associated with enhanced ITCZ EW track density relative to MJO phase 6. MJO and CLLJ westerly periods are associated with enhanced convection, moisture, and low-level vorticity in the northeastern portion of the basin, with MJO anomalies extending further westward across the main EW path.

EKE budgets for the composite periods reveal that westerly MJO and weak CLLJ periods are associated with significantly higher vertically averaged EKE along the main EW track as compared to their respective easterly phases. Along the ITCZ, however, the difference in total EKE between weak and strong CLLJ periods is not statistically significant, which differs from the corresponding MJO result, potentially indicating the importance of convection in supporting strong CLLJ period EW activity. Easterly periods for both phenomena are associated with enhanced barotropic and EAPE to EKE conversion along the ITCZ. However, easterly MJO and strong CLLJ period ITCZ EWs have different dependencies on their sources of EKE, with strong CLLJ period EWs relying more on EAPE to EKE conversion due to convective generation for their energetics. This result is consistent with the non-significant decrease in strong CLLJ period ITCZ EKE relative to weak CLLJ periods and the enhancement in ITCZ EW track density relative to MJO phase 6. Further, the greater reliance on EAPE to EKE conversion by strong CLLJ period waves is likely related to the relatively enhanced moisture and convection anomalies in this period seen in Figures 2.4 and 2.6. Westerly MJO and weak CLLJ periods are associated with enhanced barotropic and EAPE to EKE conversion along the main EW path relative to easterly MJO and strong CLLJ periods (with the MJO having a more expansive westward reach along the main EW path). This result seems to contrast with previous CLLJ studies by suggesting that weak CLLJ periods, as opposed to strong CLLJ periods, may be associated with more favorable conditions for strong EW development in the northeastern portion of the basin. Regardless of composite low-level wind period, a maximum in EAPE to EKE conversion occurs in the Panama Bight, which suggests that favorable energy conversions in this region are consistently occurring to support local disturbances that can develop and propagate into the east Pacific warm pool and seed downstream EW growth.

Vertical cross sections along the ITCZ reveal that easterly MJO and CLLJ periods have differing vertical structures of EKE budget terms, which also suggest the greater relative importance of convective processes to strong CLLJ period EWs. Strong CLLJ periods have enhanced midlevel barotropic conversion and stronger upper-level EAPE to EKE conversion from 114°W to 99°W relative to MJO phase 6. Linear regressions of Q_1, ω, and temperature anomalies on to filtered low-level vorticity also suggest that strong CLLJ period EWs appear to be able to more efficiently generate EAPE and then convert it to EKE relative to MJO phase 6 period waves. This result is consistent with the enhanced convective activity and column moisture anomalies found along the ITCZ in Figures 2.4 and 2.6 for strong CLLJ periods.

EW track data is employed to show how the MJO and CLLJ alter the count and spatial characteristics of EWs. Easterly MJO and strong CLLJ periods are characterized by increased track density along the ITCZ. However, the CLLJ appears to be a stronger modulator of EW tracks in this area, likely associated with the greater modulation of moisture and convection anomalies along the ITCZ relative to the MJO. Along the main EW path, the CLLJ does not modulate EW track density to the same degree as the MJO.

The CLLJ index developed for our analysis is uniquely defined such that significant strong and weak CLLJ periods have limited influence by the MJO, since Maloney and Esbensen (2007) found that the MJO can also cause variations in the CLLJ. This study highlights the importance of convective invigoration to strong CLLJ period ITCZ EWs relative to MJO phase 6 waves, but more work must be done to understand why this occurs. We hypothesize that the greater modulation of moisture and convection along the ITCZ during strong CLLJ periods leads to enhanced ITCZ moisture gradients, which causes stronger moisture advection and convective coupling to the waves. We plan to conduct a detailed moisture budget analysis for MJO and CLLJ periods to address this hypothesis. In addition, we plan to use regional modeling in subsequent analyses to support mechanistic understanding of how and why MJO and CLLJ events have distinct influences on the east Pacific warm pool, EKE budget, and EW tracks, and to further explore the role convection has in the development and maintenance of EWs in this region. These experiments may

include alternately constraining the basic state and Bight of Panama convective disturbances to test their respective influences on east Pacific EW formation. Future work may also explore how the MJO and CLLJ affect east Pacific EWs in a future climate, and whether the relationships observed in this study still hold. Overall, these findings suggest that subsequent studies involving the east Pacific background state and EWs must consider the distinct influences the MJO and CLLJ have on the region.

2.8   Chapter 2 Figures
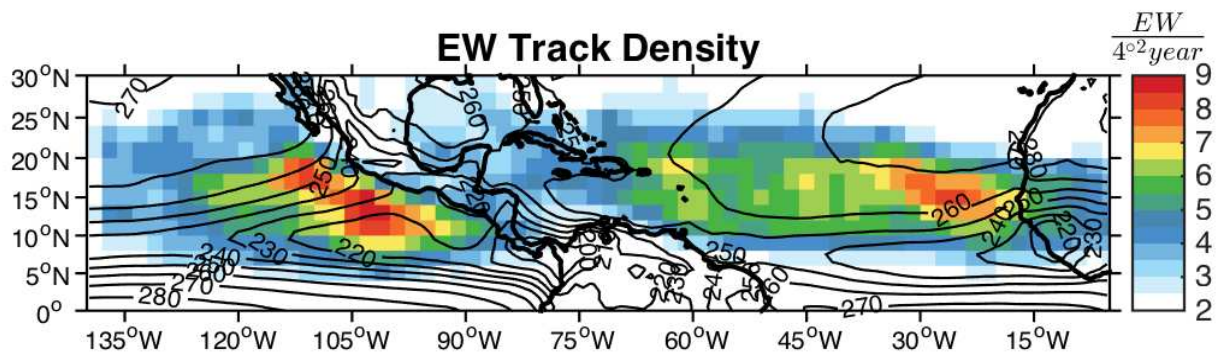
Figure 2.1: 1990-2010 May-October easterly wave track density ($\frac{EW}{4^{\circ 2} year}$, color contours) and mean OLR (W m^{-2}, line contours). The OLR interval is 10 W m^{-2}.
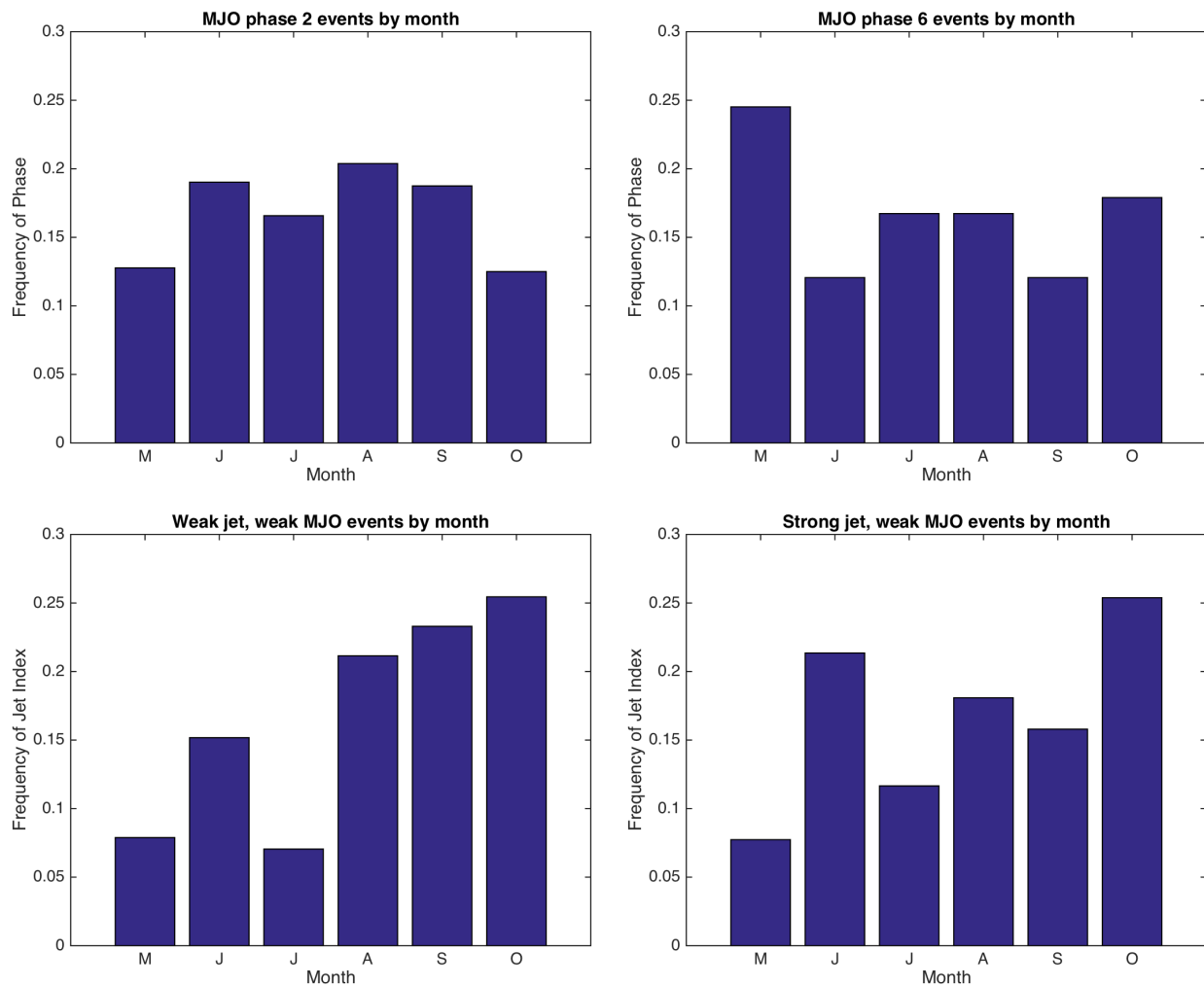
Figure 2.2: Frequency of 1990-2010 MJO (top row) and CLLJ observations (bottom row) as a function of month for May-October. Westerly events (left column) are MJO phase 2 and weak CLLJ periods, while easterly events (right column) are MJO phase 6 and strong CLLJ periods.

MJO phase 2

Westerly (MJO Phase 2):
Convectively Enhanced

MJO phase 6

Easterly (MJO Phase 6):
Convectively Suppressed
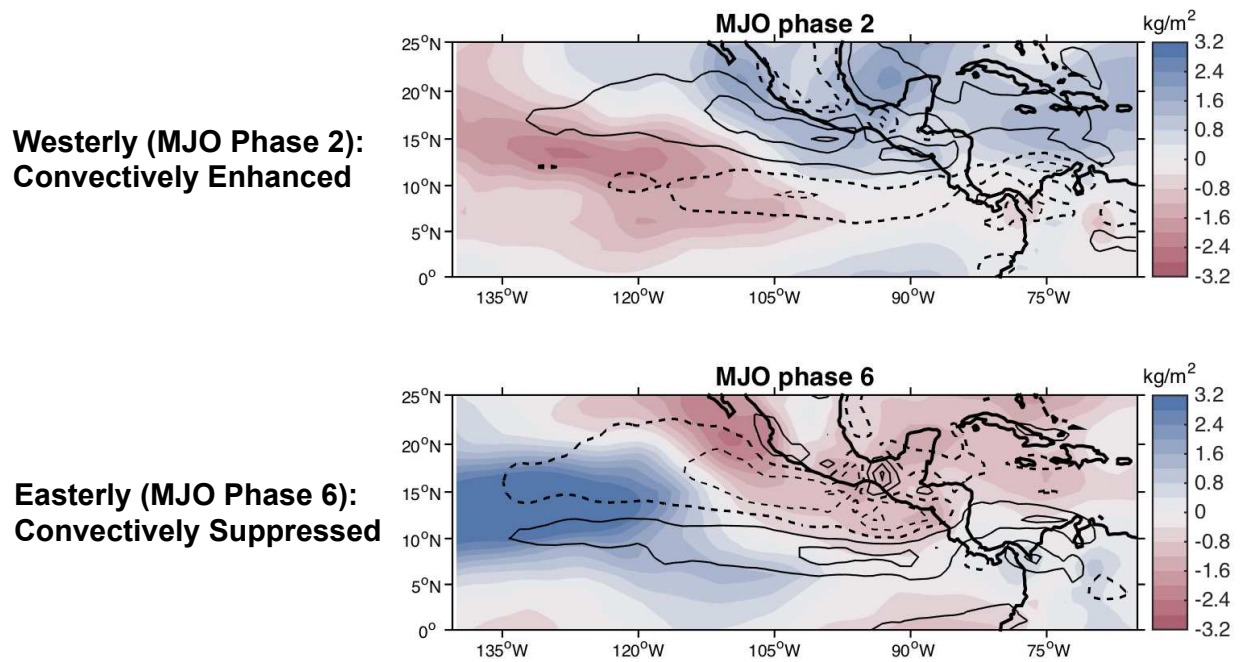
Figure 2.3: Composite total column water vapor (kg m^{-2}, color contours) and 850 hPa vorticity anomalies ($\times 10^{-6}$ s^{-1}, line contours) associated with phase 2 (top) and phase 6 (bottom) of the MJO. Total column water vapor anomaly interval is 0.4 kg m^{-2} and the vorticity anomaly interval is 4×10^{-6} s^{-1} starting at 2×10^{-6} s^{-1} (solid, ascending) and -2$\times 10^{-6}$ s^{-1} (dashed, descending).
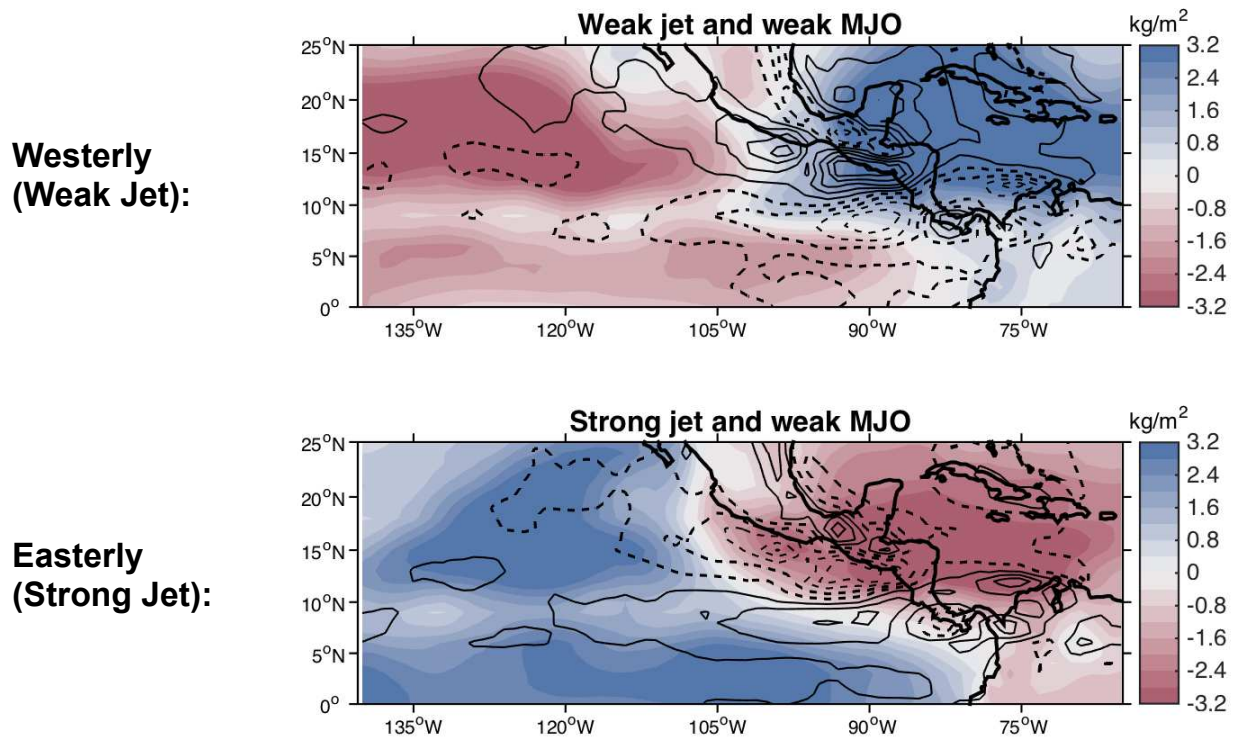
Figure 2.4: Composite total column water vapor (kg m^{-2}, color contours) and 850 hPa vorticity anomalies ($\times 10^{-6}$ s^{-1}, line contours) associated with weak jet (top) and strong jet (bottom) phases of the CLLJ. Total column water vapor anomaly interval is 0.4 kg m^{-2} and the vorticity anomaly interval is 4×10^{-6} s^{-1} starting at 2×10^{-6} s^{-1} (solid, ascending) and -2×10^{-6} s^{-1} (dashed, descending).

MJO phase 2

Westerly (MJO Phase 2): Convectively Enhanced
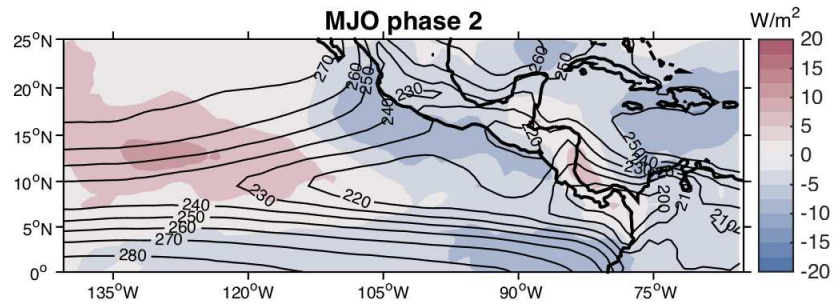
MJO phase 6

Easterly (MJO Phase 6): Convectively Suppressed
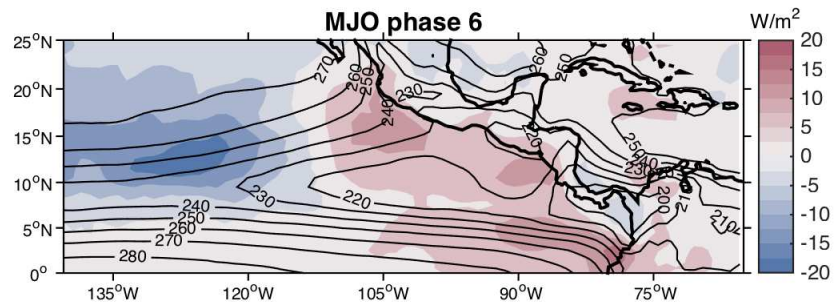
Figure 2.5: Composite OLR (W m^{-2}, color contours) anomalies associated with phase 2 (top) and phase 6 (bottom) of the MJO and mean May-October OLR (W m^{-2}, line contours). OLR anomaly interval is 2.5 W m^{-2} and the mean OLR interval is 10 W m^{-2}.

Westerly (Weak Jet):
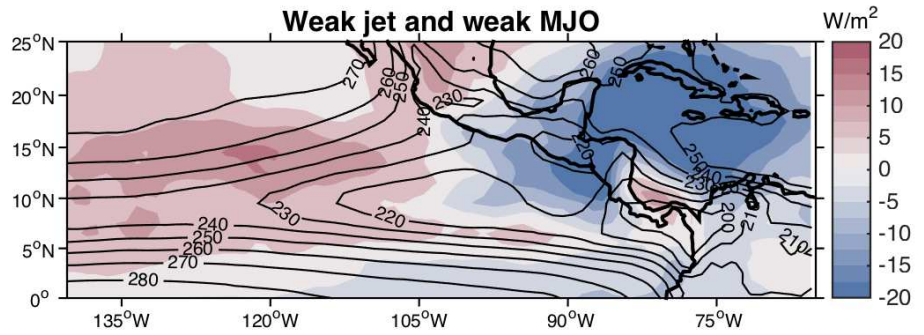
Easterly (Strong Jet):
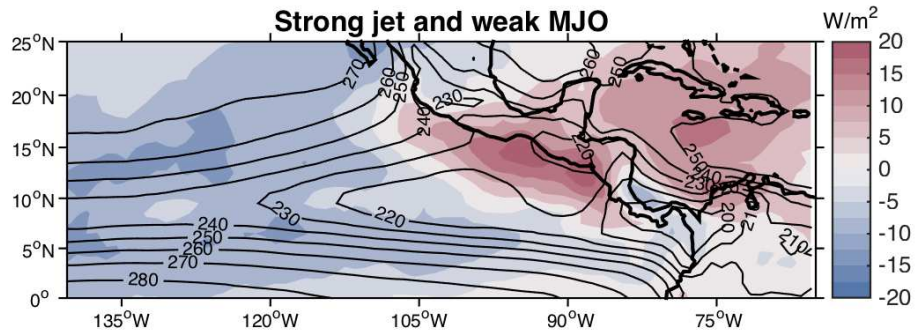
Figure 2.6: Composite OLR (W m^{-2}, color contours) anomalies associated with weak jet (top) and strong jet (bottom) phases of the CLLJ and mean May-October OLR (W m^{-2}, line contours). OLR anomaly interval is 2.5 W m^{-2} and the mean OLR interval is 10 W m^{-2}.
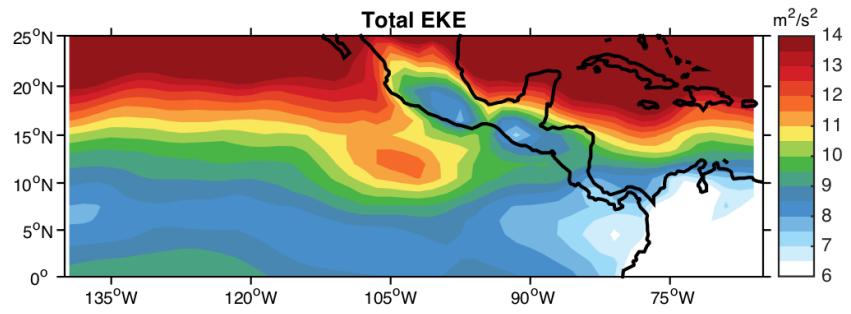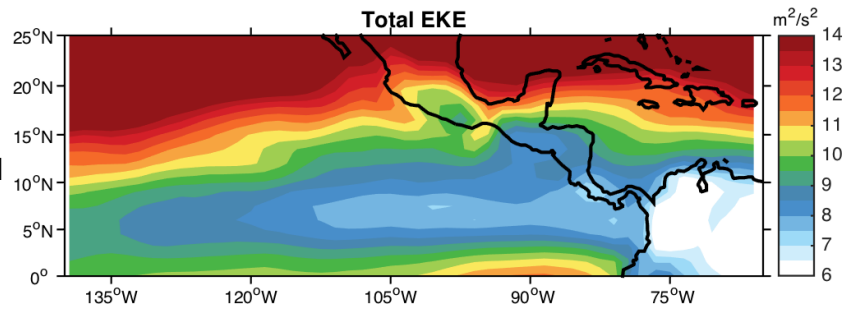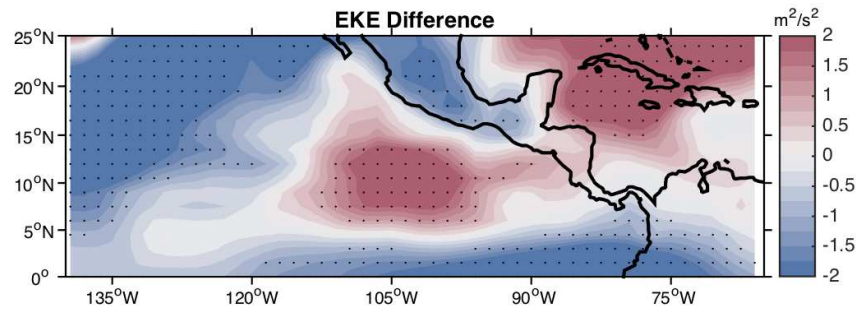
Figure 2.7: Vertically averaged total EKE (m^2 s^{-2}) for phase 2 (top) and phase 6 (middle) of the MJO. The difference between these phases (bottom) is defined as the westerly phase minus the easterly phase and stippling indicates areas of 90% statistical significance after bootstrapping over 2000 random samples with replacement.
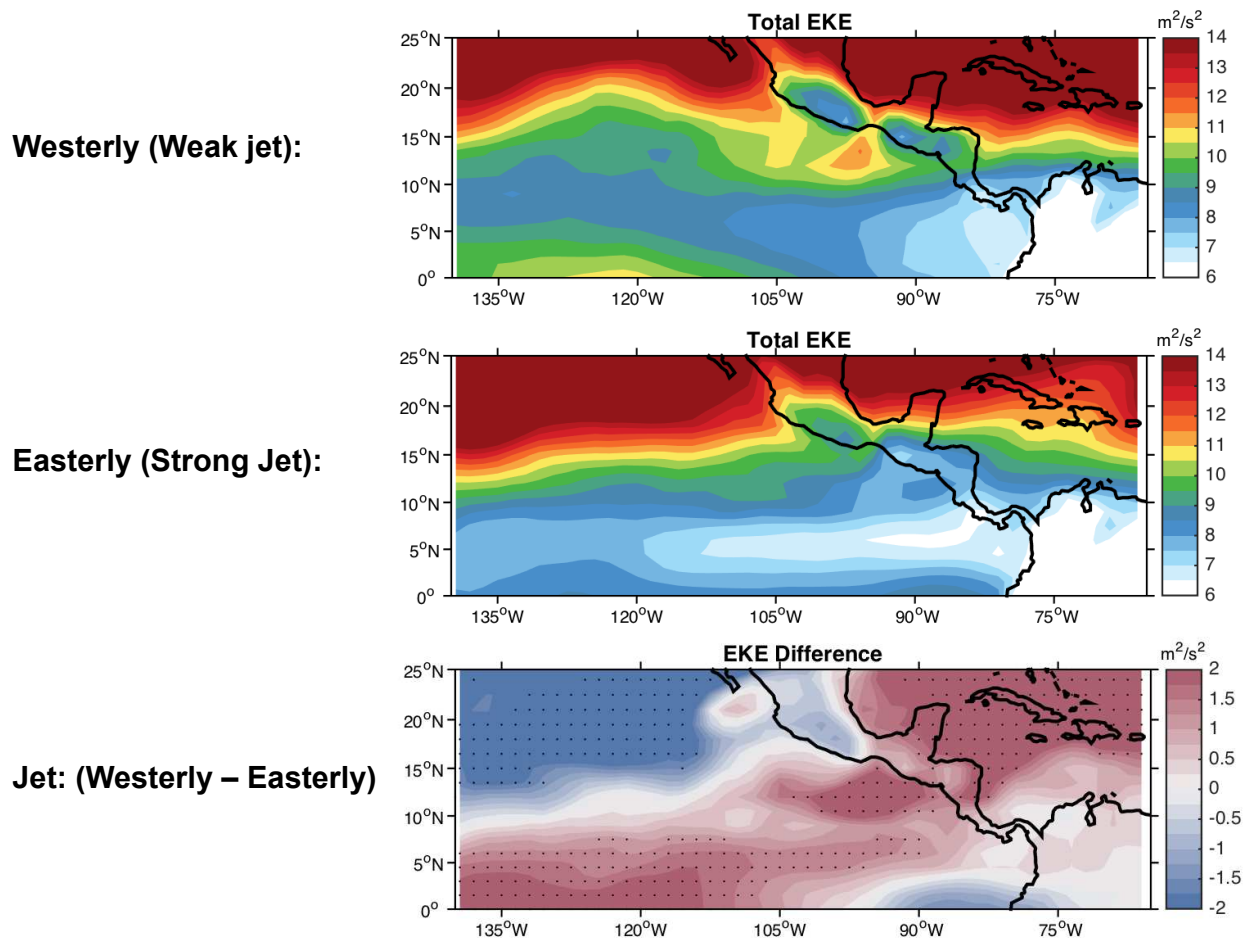
Figure 2.8: Vertically averaged total EKE (m^2 s^{-2}) for weak jet (top) and strong jet (middle) phases of the CLLJ. The difference between these phases (bottom) is defined as the westerly phase minus the easterly phase and stippling indicates areas of 90% statistical significance after bootstrapping over 2000 random samples with replacement.

Westerly (MJO Phase 2):
Convectively Enhanced

Easterly (MJO Phase 6):
Convectively Suppressed
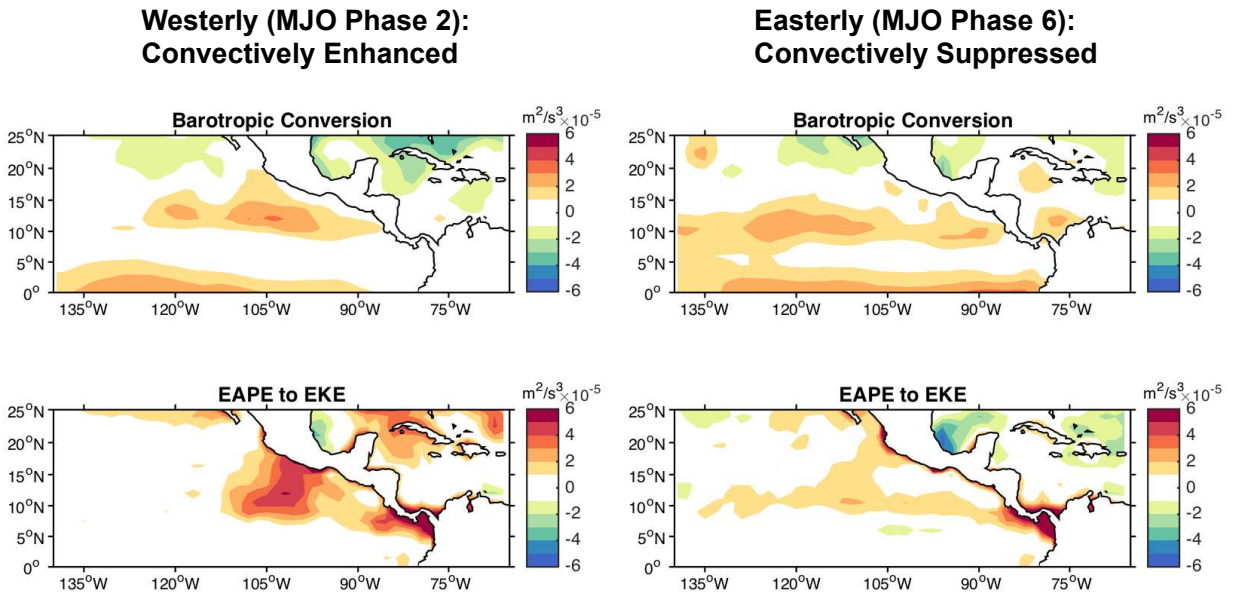
Figure 2.9: Vertically averaged barotropic conversion (first row) and EAPE to EKE conversion (second row) from the EKE budget for MJO phase 2 (left column) and phase 6 (right column). Values are $\times 10^{-5}$ m^2 s^{-3}.
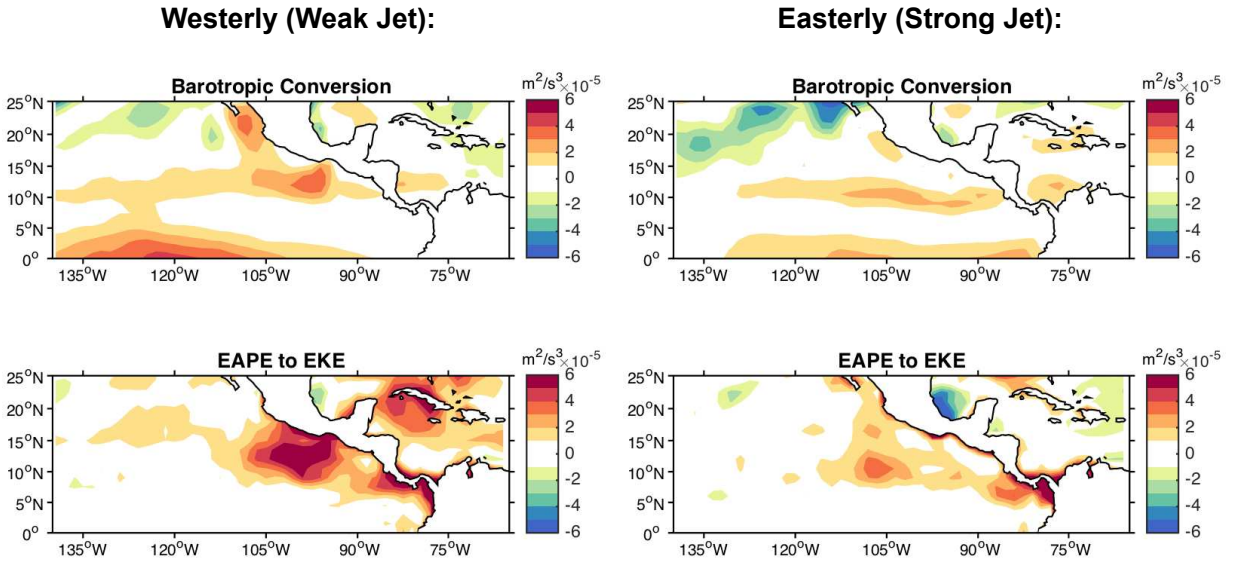
Figure 2.10: Vertically averaged barotropic conversion (first row) and EAPE to EKE conversion (second row) from the EKE budget for the weak jet phase (left column) and strong jet phase (right column) of the CLLJ. Values are $\times 10^{-5}$ m^2 s^{-3}.

Westerly (MJO Phase 2):
Convectively Enhanced
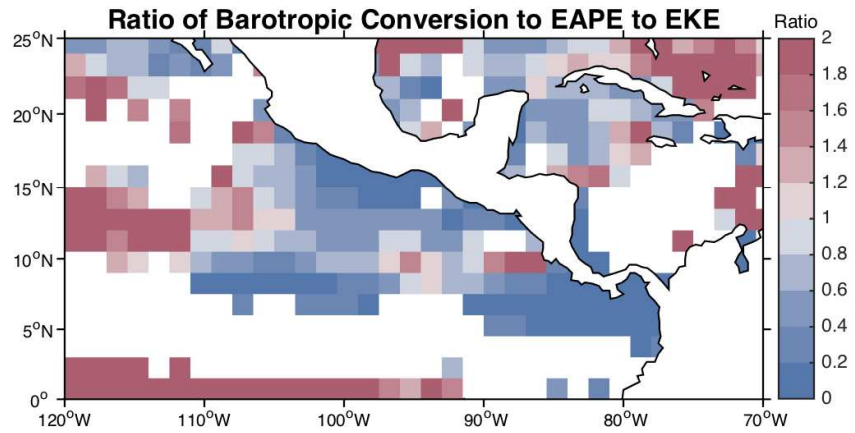
Easterly (MJO Phase 6):
Convectively Suppressed
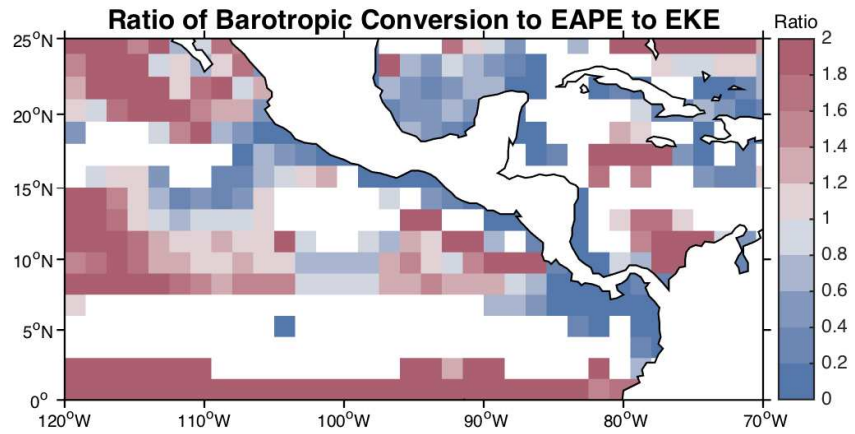
Figure 2.11: Ratio of vertically averaged barotropic conversion to EAPE to EKE conversion for MJO phase 2 (top) and phase 6 (bottom). Only areas where the sum of the absolute values of barotropic conversion and EAPE to EKE conversion are above 1.5×10^{-5} m^2 s^{-3} are shown.
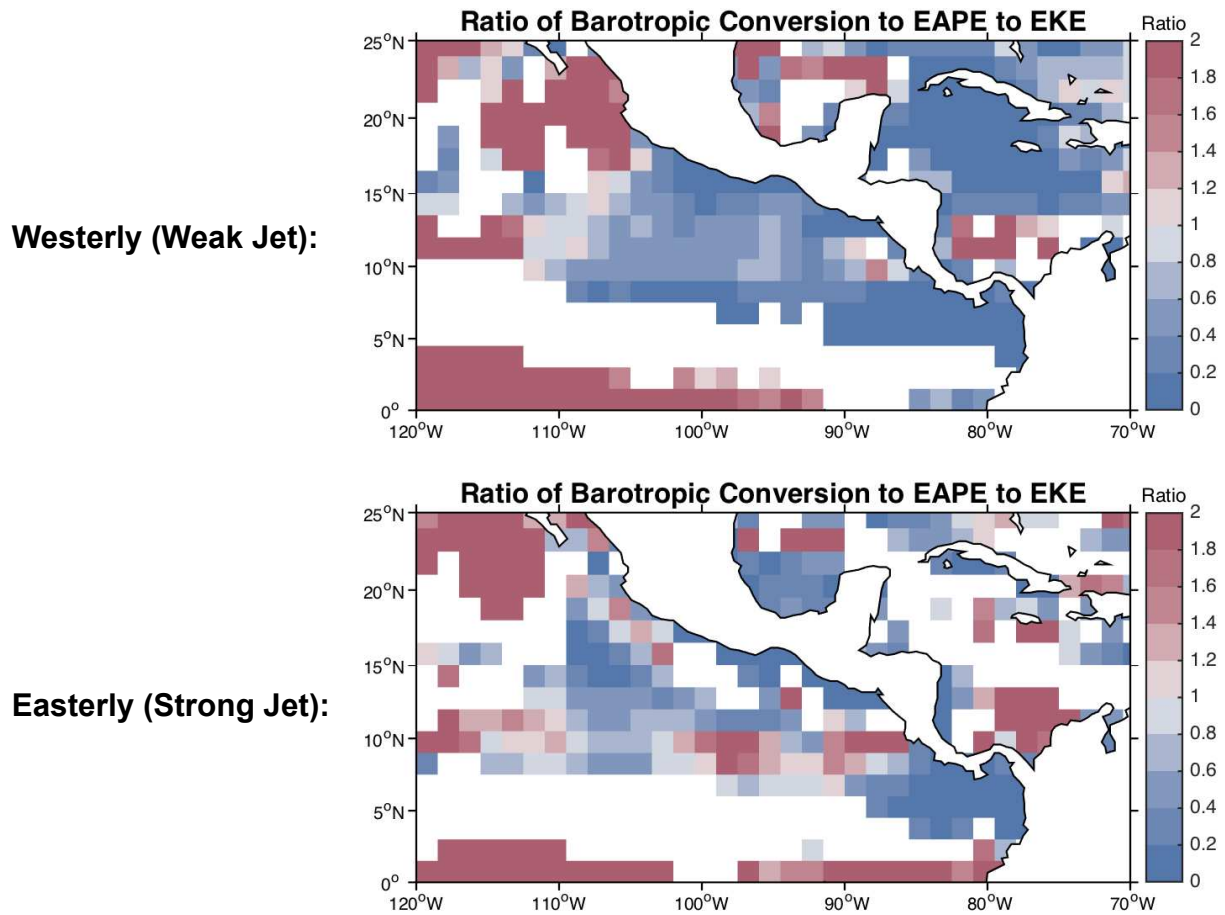
Figure 2.12: Ratio of vertically averaged barotropic conversion to EAPE to EKE conversion for the weak jet phase (top) and strong jet phase (bottom) of the CLLJ. Only areas where the sum of the absolute values of barotropic conversion and EAPE to EKE conversion are above 1.5×10^{-5} m^2 s^{-3} are shown.

MJO Phase 2:

MJO Phase 6:

Westerly (Weak) Jet:

Easterly (Strong) Jet:
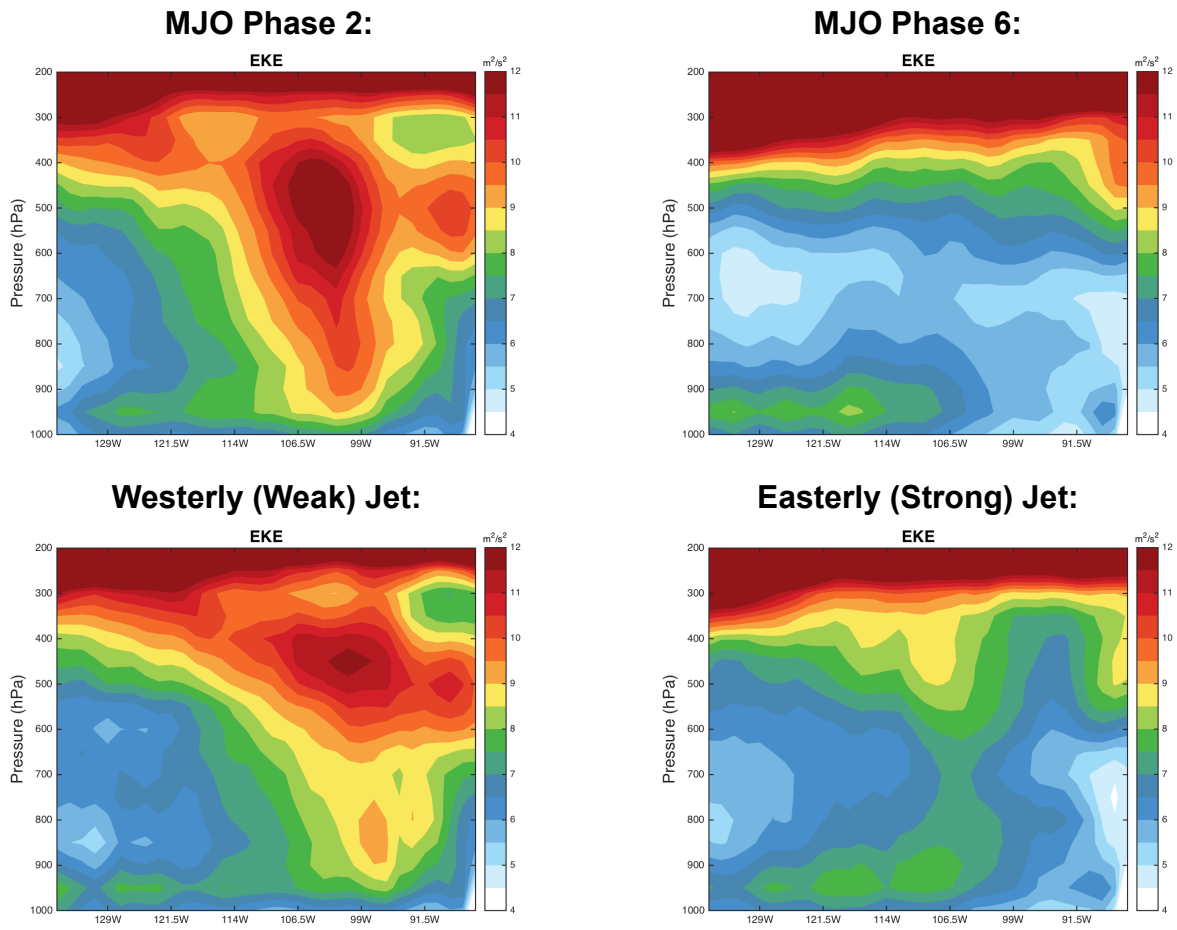
Figure 2.13: West to east vertical cross sections along 10.5°N of EKE for composite periods (MJO phase 2, top left; MJO phase 6, top right; weak CLLJ , bottom left; strong CLLJ, bottom right). Values are $m^2 \, s^{-2}$.
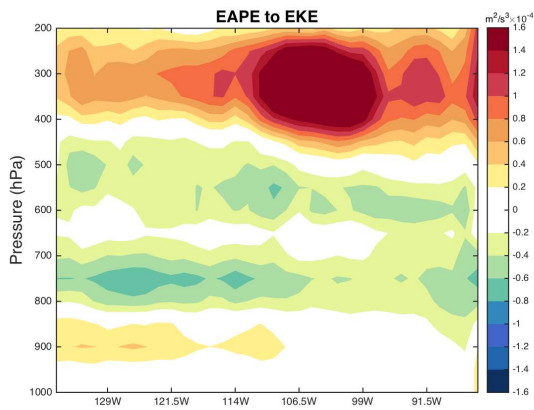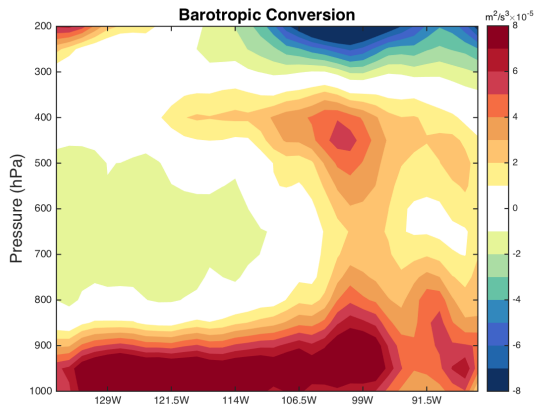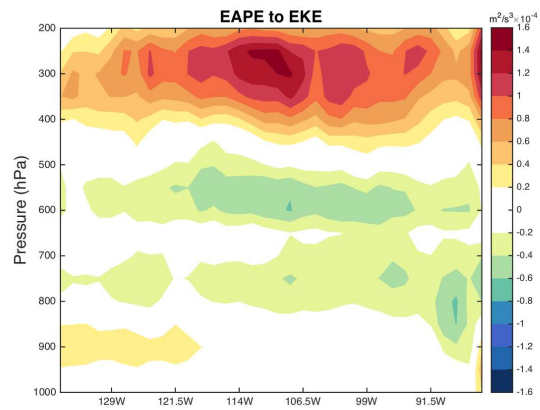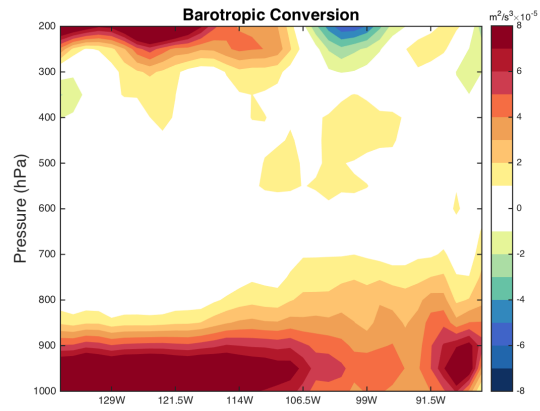
Figure 2.14: West to east vertical cross sections along $10.5°$ N of barotropic conversion (top row) and EAPE to EKE conversion (bottom row) for MJO phase 2 (left column) and phase 6 (right column). Values are $\times 10^{-5}$ m^2 s^{-3} for barotropic conversion and $\times 10^{-4}$ m^2 s^{-3} for EAPE to EKE conversion.
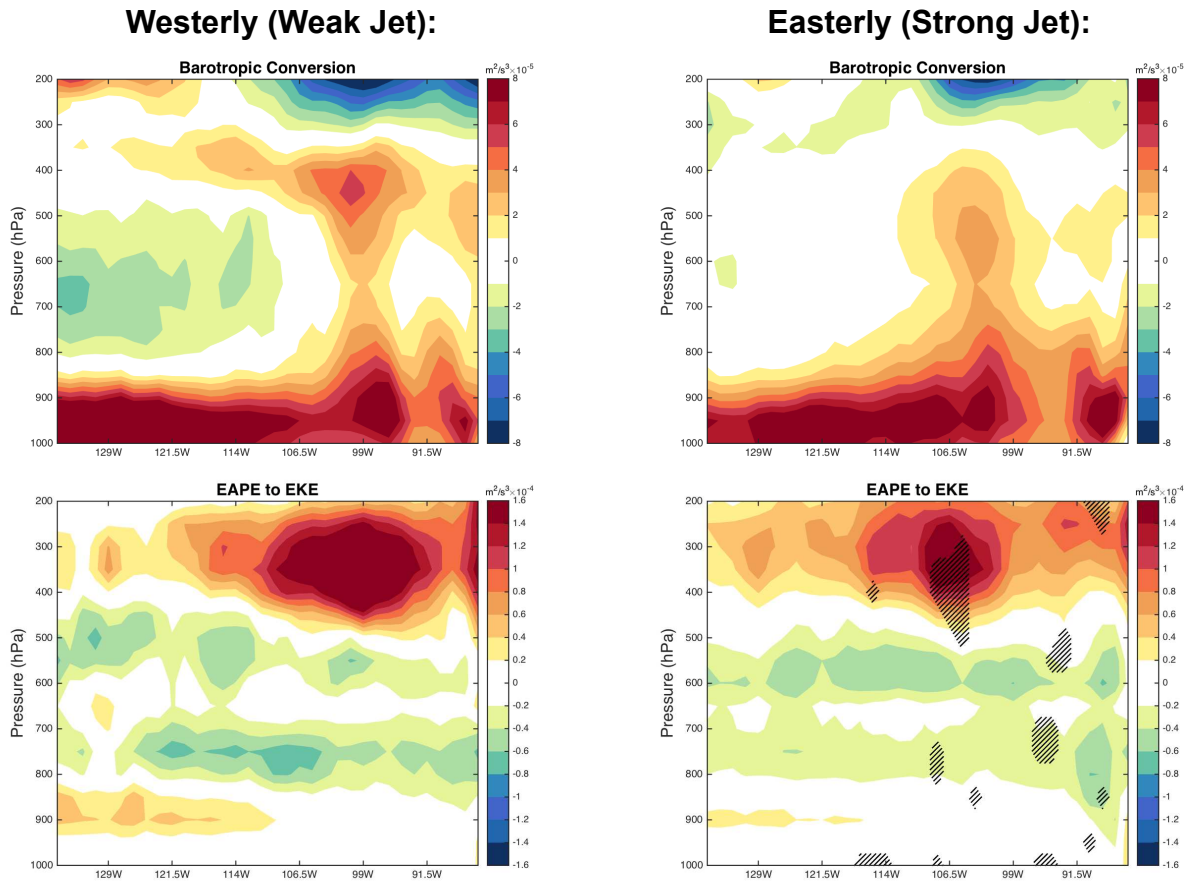
Figure 2.15: West to east vertical cross sections along $10.5°$N of barotropic conversion (top row) and EAPE to EKE conversion (bottom row) for the weak jet phase (left column) and strong jet phase (right column) of the CLLJ. Values are $\times 10^{-5}$ m^2 s^{-3} for barotropic conversion and $\times 10^{-4}$ m^2 s^{-3} for EAPE to EKE conversion. Areas of hatching in the bottom right panel indicate areas of 90% statistical significance from a one-tailed difference of means Student's t-test between strong CLLJ period and MJO phase 6 EAPE to EKE conversion, shown in Figures 2.15 and 2.14, respectively.
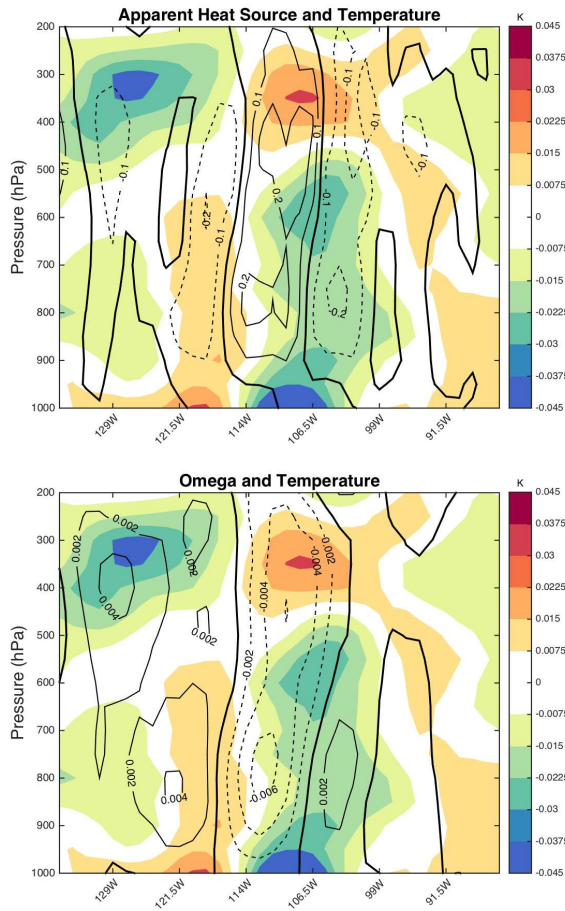
MJO Phase 6:　　　　　　　　　　　**Strong CLLJ:**
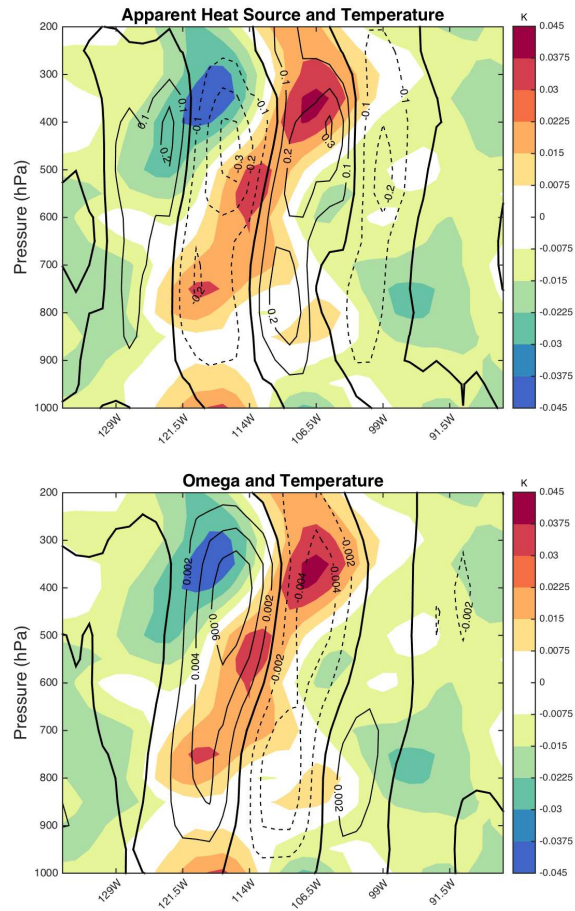
Figure 2.16: Linear regressions of bandpass filtered apparent heat source (line contours) and temperature (color contours) (top row) and ω (line contours) and temperature (color contours) (bottom row) on 700 hPa bandpass filtered vorticity at a base point of 10.5°N, 111°W for MJO phase 6 (left) and strong CLLJ (right) periods. Units are K day^{-1} for apparent heat source, Pa s^{-1} for ω, and K for temperature.

MJO:
Phase 2 - Phase 6
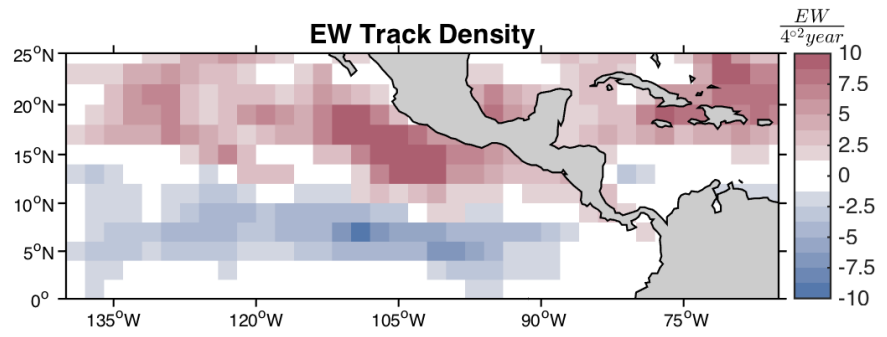
CLLJ:
Westerly - Easterly
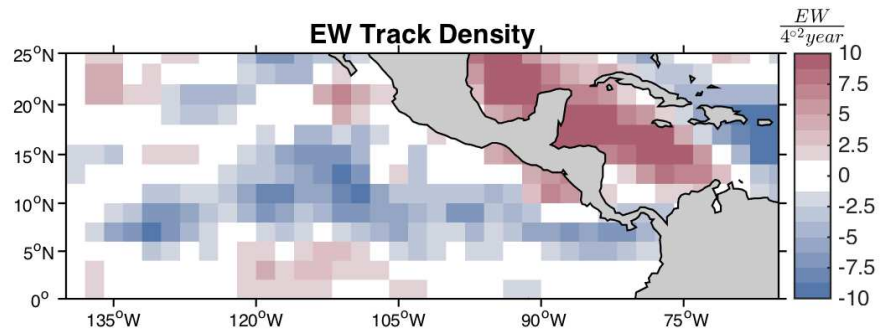
Figure 2.17: Easterly wave track density difference for the MJO (top, phase 2- phase 6) and CLLJ (bottom, weak - strong jet). Units are $\frac{EW}{4°^2year}$.

Chapter 3

Vertically Integrated Moisture Budget analysis of East Pacific Easterly Waves influenced by the MJO and CLLJ

3.1 Introduction

Easterly waves (EWs) are cyclonic disturbances that exist on synoptic time scales and are prevalent throughout the tropical atmosphere. During boreal summer, EWs can serve as important components to tropical cyclogenesis in the Atlantic and Pacific oceans (Avila and Pasch 1992; Avila et al. 2003; Dunkerton et al. 2009; Pasch et al. 2009; Russell et al. 2017). The east Pacific, which accounts for approximately 19% of all global tropical cyclones and has the highest tropical cyclone density of any basin (Ramsay 2017), is also characterized by elevated track and genesis densities of precursor EW disturbances (Thorncroft and Hodges 2001; Serra et al. 2010). East Pacific EWs intensify and sustain themselves through barotropic and baroclinic conversions to eddy kinetic energy (Maloney and Hartmann 2001; Serra et al. 2008; Rydbeck and Maloney 2014), and the relative role of these conversions in EWs can be modulated by phenomenon such as the Madden-Julian Oscillation (MJO) and Caribbean low-level jet (CLLJ) (Rydbeck and Maloney 2014; Whitaker and Maloney 2018, manuscript in press in *J. Atmos. Sci.* and Chapter 2 of this thesis). Ultimately, an important contributor to these energy conversions as well as the overall structure of east Pacific EWs is tropical convection. Convective latent heating generates eddy available potential energy, which can then be converted to eddy kinetic energy (Maloney and Esbensen 2003; Serra et al. 2008; Rydbeck and Maloney 2014), while local vorticity convergence due to convection in the southwest part of developing disturbances can tilt an EW axis from southwest to northeast to enhance the extraction of mean kinetic energy from the basic state flow (Rydbeck and Maloney 2015).

Free-tropospheric moisture has been shown to influence tropical convection and precipitation (e.g., Bretherton et al. 2004; Peters and Neelin 2006; Holloway and Neelin 2009). In particular, the entrainment of environmental air plays an important role in modulating convection; the entrainment of moister air into an air parcel leads to increased buoyancy relative to the entrainment of drier air, with the overall effect of entrainment being the reduction of parcel buoyancy (Holloway and Neelin 2009; Zhang 2009). As convection helps to initiate EWs near the entrance of the African easterly jet (e.g., Thorncroft et al. 2008) and is an important source of east Pacific EW eddy kinetic energy (e.g., Serra et al. 2008, 2010; Rydbeck and Maloney 2014), it follows that the distribution of mean and anomalous moisture would impact their respective generation and development in these regions. Indeed, Alaka and Maloney (2012) found that anomalous moistening near the entrance of the African easterly jet by the MJO preceded enhanced convective anomalies in this region, and they hypothesize that the enhanced convection can serve as precursor disturbances to EWs that develop downstream. Rydbeck and Maloney (2015) used an EW-timescale vertically integrated moisture budget to show that horizontal advection of east Pacific Intertropical Convergence Zone (ITCZ) moisture by EWs results in anomalous moistening ahead of the southwest portion of the EW that is then followed by enhanced convection in that region. Further, Rydbeck and Maloney (2015) suggest that differences in the east Pacific basic state moisture (in this case through intraseasonal modulations) can lead to varying levels of convective activity in the waves, with enhanced convective coupling being associated with stronger EW development.

Chapter 2 of this thesis highlights that EWs during anomalously easterly CLLJ periods are more reliant on convective invigoration than waves that occur during easterly MJO periods. This is due in part to the enhanced generation of eddy available potential energy and its subsequent stronger conversion to eddy kinetic energy observed along the ITCZ during easterly CLLJ periods shown in Chapter 2. It is hypothesized that a greater basic state modulation of moisture helps produce a more favorable convective environment along the east Pacific ITCZ, which in turn supports CLLJ period waves being more convectively active. The enhanced ITCZ moisture is thought to be advected by EW cyclonic circulations as the waves travel westward, and leads to a stronger coupling of

convection to the waves during the anomalous easterly CLLJ periods. To this end, a vertically integrated moisture budget analysis will be used to provide additional insight as to why EWs during low-level easterly wind periods of the MJO and CLLJ have differing dependencies on convection. Further, to investigate the impacts of environmental moisture on entraining convection in both the background state and in EWs, diluted convective available potential energy (CAPE) is calculated. Diluted CAPE will be used to elucidate which background state most favors convection and to highlight differences in EW convection between CLLJ and MJO periods.

The remaining sections of this chapter are organized as follows: Section 2 highlights the data and methods used, along with providing details about the diluted CAPE calculation that is performed. Section 3 discusses the results of the vertically integrated moisture budget and diluted CAPE calculation during easterly MJO and CLLJ periods, both from a plan view and ITCZ vertical cross section perspective. Section 4 discusses the results and conclusions of this study.

3.2   Data and Methods

Specific humidity, vertical pressure velocity, winds, surface evaporation, precipitation, and temperature data from the European Centre for Medium-Range Weather Forecast Interim Reanalysis (ERA-Interim; Dee et al. 2011) are used from May-October, over the years 1990-2010 to match the time frame used in Chapter 2. The 6-hourly data have grid spacing of $1.5°$, and cover 17 pressure levels from 1000 hPa to 200 hPa in 50 hPa increments. Further, 6-hourly interpolated, $1°$ grid-spaced outgoing longwave radiation (OLR) from the NOAA National Climatic Data Center daily dataset (Lee 2014) over the same time period as the ERA-Interim data is used.

As in Chapter 2, we composite MJO and CLLJ periods based on the real-time multivariate MJO index (RMM; http://www.bom.gov.au/climate/mjo/) from Wheeler and Hendon (2004), and the CLLJ index developed in Chapter 2. The daily RMM index creates eight MJO phases by performing a combined EOF analysis on zonal wind at 850 hPa and 200 hPa and OLR averaged over the equator. Westerly (easterly) intraseasonal events are represented by MJO phase 2 (6), as done in Chapter 2. The CLLJ index uses 925 hPa zonal wind to determine when strong (anomalously

easterly) and weak (anomalously westerly) jet periods occur. Further details about the methods used to select anomalous low-level wind periods for the MJO and CLLJ can be found in Chapter 2.

For the EW vertically integrated moisture budget and linearized horizontal advection calculation, anomalies associated with tropical cyclones are removed using the weighting function and procedure explained in Aiyyer et al. (2012). Additional details into the specifics of how tropical cyclone anomalies are identified and removed from the data can be found in Chapter 2. Diluted CAPE is calculated in a similar manner to Neale et al. (2010), where an entraining plume model is used to incorporate the effects of mixing environmental air into convection. Environmental humidity and entropy (defined and calculated from the average of fields between the current level and the level below) are mixed into the entraining plume separately to determine a new temperature profile for the mixture which can then be used to determine diluted CAPE. For the purpose of this analysis, we adapted and simplified the "buoyan_dilute" subroutine from the source code of the NCAR Community Earth System model, version 1.2 (http://www.cesm.ucar.edu/models/cesm1.2/ cesm/cesmBbrowser/html_code/cam/zm_conv.F90.html#BUOYAN_DILUTE) to provide us with an estimation of diluted CAPE using ERA-Interim data with the following assumptions: a constant entrainment rate of 0.004 hPa^{-1} is used from 950 hPa upward similar to Rydbeck and Maloney (2015), the entraining parcel does not have to be saturated at 1000 hPa, and the effects of freezing and condensation are not included in the mixture. The expression for diluted CAPE used in our calculation and adapted from the model code is given by:

$$CAPE_{diluted} = \int_{950hPa}^{LNB} R_d(T_{v,p} - T_v)d\ln\left(\frac{p_{n-1}}{p_n}\right), \tag{3.1}$$

where R_d is the gas constant for dry air, p_n is the pressure of the current evaluated level, p_{n-1} is the pressure of the level below the evaluated level, $T_{v,p}$ is the virtual temperature of the entraining parcel at p_n, T_v is the virtual temperature of the environment at p_n, and LNB is the level of neutral buoyancy, which is defined in-between the instance of two consecutive negative buoyancy levels (when $T_{v,p} < T_v$). Overall, the entrainment of environmental air works to reduce undilute CAPE

values, and emphasizes the importance of environmental free tropospheric humidity for calculating the effective convective instability (Zhang 2009).

3.3 Moisture Budget Results

To highlight the importance of the ITCZ in the development of EWs, Figure 3.1 shows the variance of May-October filtered OLR for the 2.5-12 day period band and for wavenumbers 6-30. Along with the high EW OLR variance in the northeastern portion of the basin, there is also notable EW variability along the east Pacific ITCZ near 9°N, indicating that while some EWs have a more southeast to northwest track paralleling the Central American coast, others travel in a more westward direction along the ITCZ. The ITCZ signal begins near the Panama Bight region with values near $140\frac{W^2}{m^4}$, where locally generated mesoscale convective systems have been shown to impact EW variability (Rydbeck et al. 2017), and extends westward reaching variance values over $200\frac{W^2}{m^4}$ near 105°W. ITCZ moisture has been shown to support convection in developing EWs (Rydbeck and Maloney 2015) and in Chapter 2 it was shown that the CLLJ is a stronger modulator of ITCZ moisture than the MJO. The stronger moisture anomalies along the ITCZ during strong CLLJ periods were hypothesized in Chapter 2 as an important factor in providing differences in EW energy budgets between easterly MJO and CLLJ periods, with easterly CLLJ periods having stronger convective contributions to eddy kinetic energy.

To test the hypothesis from Chapter 2 that differences in ITCZ moisture anomalies between easterly low-level wind periods of the MJO and CLLJ lead to strong CLLJ period waves being more reliant on convection, a mass-weighted vertically integrated moisture budget is computed. As in Rydbeck and Maloney (2015), the moisture budget equation is given by:

$$\left[\frac{\partial q}{\partial t}\right]' = -[\vec{v}_h \cdot \nabla_h q]' - \left[\omega\frac{\partial q}{\partial p}\right]' + E' - P',\tag{3.2}$$

where $\vec{v}_h = \vec{v}(u,v)$ is the two dimensional wind vector, q is the specific humidity, ω is the vertical pressure velocity, p is the pressure, E is evaporation, and P is precipitation. Brackets represent the

mass-weighted vertical integral from 1000 hPa to 200 hPa, and primes represent filtering for the 2.5-12 day band and for wavenumbers 6-30. The term on the left hand side of the moisture budget equation is the time tendency of vertically integrated specific humidity. The first and second terms on the right hand side of the moisture budget equation represent horizontal and vertical advection of moisture, respectively. The third term is the change in column moisture due to evaporation from the surface, while the fourth term accounts for moisture changes due to precipitation.

Figure 3.2 shows linear regressions of moisture budget terms and filtered total column water vapor (TCWV) onto EW filtered 700 hPa vorticity during easterly MJO and CLLJ periods. As was explained in Chapter 2, the 700 hPa relative vorticity time series is filtered from 2.5 to 12 days in frequency space and to westward wavenumbers of 6-30 and is used as the reference time series at a base point of 10.5°N, 111°W. The regressed fields are also scaled by a 1 standard deviation value of the respective composite period filtered vorticity time series (to represent the passage of a typical EW) for plotting. As in Rydbeck and Maloney (2015), we chose to combine the effects of vertical advection and precipitation by calculating a vertical advection minus precipitation term as the residual of the other budget terms. This is done due to inaccuracies in representing the sum of these two terms in reanalysis data. Strong CLLJ period EWs have enhanced specific humidity time tendency and horizontal advection terms relative to MJO phase 6, with regressed values over 0.75 $\frac{mm}{day}$, while evaporation and vertical advection minus precipitation terms contribute very weakly to the moisture tendency. The stronger horizontal moisture advection in strong CLLJ period EWs leads the maximum in regressed TCWV, which is also enhanced relative to MJO phase 6 waves, suggesting that strong CLLJ waves are able to more effectively moisten the environment that they are approaching to help sustain themselves. As a result of the enhanced horizontal moisture advection combined with a moister background environment, strong CLLJ period waves may produce stronger convective variability relative to MJO phase 6 waves, which in turn favors a stronger generation and conversion of eddy available potential energy to eddy kinetic energy by EW convection, as discussed in the context of an eddy kinetic energy budget in Chapter 2. Vertical cross sections linking horizontal advection and EW precipitation will be discussed later on in Figure 3.7.

Because horizontal advection is the dominant term in producing changes in moisture, it is useful to linearize the term to look at how the zonal and meridional mean state winds and EW circulation act on mean and anomalous moisture during both composite periods to help explain the differences in moistening. Linearized horizontal advection is computed as in Rydbeck and Maloney (2015), and is given by:

$$-[\vec{v}_h \cdot \nabla_h q]' = -\left[u''\frac{\partial \bar{q}}{\partial x}\right]' - \left[v''\frac{\partial \bar{q}}{\partial y}\right]' - \left[\bar{u}\frac{\partial q''}{\partial x}\right]' - \left[\bar{v}\frac{\partial q''}{\partial y}\right]' - \left[u''\frac{\partial q''}{\partial x}\right]' - \left[v''\frac{\partial q''}{\partial y}\right]', \quad (3.3)$$

where a bar represents the 11-day running mean, a double prime represents a deviation from the 11-day running mean, and the brackets again represent the mass-weighted vertical integral from 1000 hPa to 200 hPa. The first two component terms of horizontal advection represent EW-timescale anomalous winds acting on mean moisture. The third and fourth terms represent the mean winds advecting EW-timescale anomalous moisture. The fifth and sixth terms represent anomalous EW winds advecting anomalous EW moisture.

Figure 3.3 shows the contributions of these linearized terms to horizontal advection, and they are regressed along with 700 hPa filtered vorticity during MJO phase 6 and strong CLLJ periods. Horizontal advection for EWs during both periods has strong contributions from terms 2 and 3, $-\left[v''\frac{\partial \bar{q}}{\partial y}\right]'$ and $-\left[\bar{u}\frac{\partial q''}{\partial x}\right]'$, respectively, while strong CLLJ period waves also have a modest contribution from term 6, $-\left[v''\frac{\partial q''}{\partial y}\right]'$, to horizontal advection not seen in MJO phase 6. Interestingly, strong CLLJ period waves appear to have stronger meridional contributions to horizontal advection (enhancement of terms 2 and 6), while MJO phase 6 waves favor zonal contributions (enhancement of term 3). A sensitivity test (not shown) revealed that the enhancement of term 2 in strong CLLJ period waves relative to MJO phase 6 is due to enhanced values of the magnitude of v'' as opposed to the mean meridional moisture gradient. This result implies that the stronger horizontal advection observed in strong CLLJ waves is due to the fact that the waves themselves, as evidenced by their enhanced circulations, are stronger than in MJO phase 6, and that differences in mean moisture and its gradients seem to not play as large of a role in the stronger moisture advection. However,

71

even though composite changes in background moisture are not as important to the enhancement in EW horizontal advection as the stronger EW circulations, background moisture changes may still be responsible for helping produce the stronger EW circulations in strong CLLJ periods by providing an environment that is more conducive for convection.

Figures 3.4 and 3.5 show vertical cross sections along 7.5°N of the leading linearized horizontal advection terms for MJO phase 6 and strong CLLJ EWs to highlight the disparity in linearized terms involving the EW meridional circulation, v'', between these periods. Figure 3.4 contrasts the strongest vertically integrated linearized terms in MJO and CLLJ periods. In Figure 3.4, strong CLLJ EWs have relatively stronger advection of mean moisture by the anomalous meridional winds at mid-levels and at lower levels (term 2, color contours), with values that are on the order of 50% higher than during MJO phase 6 near 500 and 900 hPa. On the other hand, for the advection of perturbation moisture by the mean zonal flow (term 3, line contours) there is not as stark of contrast between the easterly periods, with MJO phase 6 waves having slightly elevated values near 650 hPa. Thus, while the leading horizontal advection term in MJO phase 6 periods is largely matched in strong CLLJ periods, the leading contribution to horizontal advection in strong CLLJ periods (associated with the EW meridional circulation) is much stronger than in MJO phase 6, highlighting the enhanced intensity of strong CLLJ waves. Figure 3.5 emphasizes the importance meridional circulation terms have on the total horizontal advection in strong CLLJ periods. Along with the strong term 2 (now line contours) contributions listed above, strong CLLJ period waves also have enhanced advection of anomalous moisture by the EW circulation (term 6, color contours) around 700 hPa. In MJO phase 6 waves, however, term 6 is significantly reduced. A potential explanation for why strong CLLJ EWs have enhanced horizontal advection relative to MJO phase 6 waves appears to be the relative enhancement of terms 2 and 6 throughout mid and lower levels, which are associated with an increased EW circulation. The enhanced EW circulations present in strong CLLJ waves may be the result of the EWs developing in a more convectively active background environment earlier in their lifetimes.

Figure 3.6 shows the mean moisture as well as regressed filtered vorticity and wind averaged over low-levels (700 to 1000 hPa) for both composite periods to provide context for the environment the waves propagate in. Strong CLLJ period waves have enhanced regressed vorticity and wind contours relative to MJO phase 6, emphasizing the strong circulation contribution to horizontal advection in the waves seen in Figures 3.3, 3.4, and 3.5. Strong CLLJ periods are also characterized by higher mean moisture extending along the ITCZ (that also has a wider meridional extent) relative to MJO phase 6. This enhanced low-level ITCZ moisture during strong CLLJ periods may help provide a more convectively active environment for growing EWs, and allow them to develop the stronger and more expansive circulations seen in the regressed vorticity and wind fields. Understanding the differences in the development of EW circulations during MJO and CLLJ periods will be a topic of future study.

To further highlight the relationship between advection, moisture, and convection in strong CLLJ waves, Figure 3.7 shows a vertical cross section along $7.5°N$ of regressed total horizontal advection and specific humidity, along with a line graph of regressed total precipitation averaged over $7.5°N$ to $9°N$. In comparing the easterly periods, horizontal advection is indeed stronger in strong CLLJ waves consistent with that shown above, both in magnitude and vertical extent throughout the mid and lower levels. Further, the regressed specific humidity in strong CLLJ waves is enhanced throughout the column with a maximum in moisture near 800 hPa and higher values extending up to 500 hPa. Strong CLLJ period waves also have a more defined convective signal in terms of regressed precipitation, with a relatively stronger peak precipitation rate occurring at the same latitude as the maximum in EW moisture. The increased moisture in the column due to horizontal advection, along with the moister basic state conditions and enhanced EW precipitation rates during strong CLLJ periods reinforce the results of Figure 3.2, and indicate that stronger convective invigoration occurs in the waves relative to during MJO phase 6, supporting the findings in Chapter 2.

To investigate the differences in EW convective activity between easterly MJO and CLLJ periods, and to further underscore that strong CLLJ periods have more favorable convective envi-

ronments which lead to the waves having enhanced circulations, diluted CAPE is calculated. The diluted CAPE calculation employs a simplified entraining plume model with a constant entrainment rate of 0.004 hpa^{-1}. Figure 3.8 shows the mean diluted CAPE for May-October 1990-2010. Diluted CAPE is maximized in the Panama Bight region, with values on the order of 250 J kg^{-1} and higher values extend westward along the ITCZ, indicating strong convective instability in these regions. Overall, diluted CAPE values are reduced compared to undiluted CAPE values calculated for zero entrainment, while the calculated zero entrainment undiluted CAPE compares reasonably to ERA-Interim undiluted CAPE values in the region (not shown).

Comparing the modulation of diluted CAPE by ITCZ EWs in easterly MJO and CLLJ periods, Figure 3.9 shows regressed filtered diluted CAPE (displayed as the percentage of the May-October mean), TCWV, and wind. Strong CLLJ period EWs in the regression have diluted CAPE anomalies that not only consist of a higher percentage of the mean diluted CAPE, but also are much more expansive along the wave axis relative to MJO phase 6 EWs. In fact, near the area of the highest TCWV anomalies, which is enhanced in strong CLLJ waves, positive diluted CAPE anomalies are nearly double that of MJO phase 6 in terms of the percentage of the mean, reaching up to 8%. Finally, while strong CLLJ waves are associated with a strong modulation of diluted CAPE (oriented in a southwest to northeast manner extending from 0°N to the Central American coast), MJO phase 6 waves only appear to have weak anomalies confined to the core of the regressed TCWV, limiting potential convective invigoration in the waves.

Further, while strong CLLJ EWs are associated with larger diluted CAPE anomalies, it is also important to consider the convective activity of the background state in which they occur. Figure 3.10 shows the mean diluted CAPE during strong CLLJ and MJO phase 6 periods calculated from the three-dimensional composite mean of specific humidity and temperature, along with composite regressed 700 hPa vorticity. In these calculations, a 1% increase in 1000 hPa mean moisture was included to provide reasonable diluted CAPE values based on the basic state conditions. In general, the contributions from the composite background states resemble the structure of the mean diluted CAPE shown in Figure 3.8, with enhanced values extending from the Panama Bight across the

74

ITCZ. Notably, strong CLLJ periods are associated with enhanced diluted CAPE along the ITCZ relative to MJO phase 6, highlighting that the mean state during strong CLLJ periods appears to be more supportive of convection. Further, the enhanced convective instability along the ITCZ is likely associated with the relatively stronger positive moisture anomalies that occur in the region during strong CLLJ periods, as tropospheric humidity is an important contributor to diluted CAPE. As a result, a positive feedback that links the background environment, EW intensification, and EW convection appears to be occurring that favors more convectively active EWs during strong CLLJ periods. This feedback begins with a moister, more favorable basic state that fosters more convective activity, which then supports stronger EW development and cyclonic circulations in EWs relative to MJO phase 6 (as seen in Figures 3.3 and 3.6). Next, these enhanced EW circulations may then further aid EW convection through stronger horizontal moisture advection, highlighting the results of Figure 3.7.

These results for the diluted CAPE calculation indicate that ITCZ EWs during strong CLLJ periods are associated with enhanced convective invigoration relative to MJO phase 6, and that the convective instability of the background environment may explain why strong CLLJ EWs intensify into stronger waves. Due to the positive feedback linking a more favorable background state to enhanced convective activity in EWs, strong CLLJ period waves should have stronger contributions by convection in their eddy kinetic energy budgets along the ITCZ relative to MJO phase 6 waves, as was indeed shown in the findings in Chapter 2. Although it seems clear that the importance of convection to EWs and the mean state during MJO phase 6 and strong CLLJ periods (which have similar easterly low-level wind anomalies in the basin) differs, we are still unsure as to why relatively higher mean moisture, and subsequently diluted CAPE, exists in the basin during strong CLLJ events as opposed to during MJO phase 6. Future work into why the observed differences in moisture and convection between these phenomena exist for the same-signed anomalous low-level wind period would be useful.

3.4 Discussion and Conclusions

Tropical deep convection is an important component of energy conversions in east Pacific EWs. Convection works to generate eddy available potential energy through a positive covariance between apparent heat source and temperature anomalies, and then converts this potential energy into eddy kinetic energy through the anomalous rising of warm air anomalies (Maloney and Esbensen 2003; Serra et al. 2008, 2010; Rydbeck and Maloney 2014). The presence of environmental moisture plays a role in modulating convection, and subsequently EW energy conversions; a convecting air parcel will have higher buoyancy when the surrounding environment is moist, as opposed to dry, due to the effects convective entrainment (Zhang 2009; Holloway and Neelin 2009). In Chapter 2 of this thesis, it was discovered that EWs during low-level easterly wind anomaly periods of the MJO and CLLJ have differing dependencies on convection, with strong CLLJ period EWs having relatively stronger convective anomalies and contributions to their eddy kinetic energy budget. This chapter addresses the hypothesis that differences in basic state moisture along the ITCZ played a role in this observed difference in convective activity between these composite periods.

Vertically integrated moisture budget regressions reveal that horizontal advection of moisture is the dominant contributor to moisture tendency changes in ITCZ EWs. Strong CLLJ EWs have stronger horizontal advection of moisture ahead of the wave, which contributes to the enhanced moisture anomalies along the wave axis relative to MJO phase 6. Linearized components of horizontal advection are computed and show that while the overall horizontal advection term is dominant in both periods, strong CLLJ EW overall horizontal advection is enhanced due to contributions involving the meridional EW circulation, rather than mean moisture, highlighting the importance of the relative strength of the waves compared to MJO phase 6 for the moisture budget. Hence, differences in EW circulation strength are largely responsible for the differences in moisture tendency between strong CLLJ and MJO phase 6 EWs. However, the moister background environment during strong CLLJ periods likely helps produce the stronger EW circulations in the first place, by supporting enhanced convective activity as the waves develop.

Vertical cross sections along the ITCZ highlight that strong CLLJ waves are characterized by stronger horizontal advection at lower levels. Stronger EW circulations, likely established from enhanced convection along a moister mean state ITCZ, help produce this stronger moisture advection. The subsequent positive moisture tendency leading the waves aids the already enhanced lower-level moisture anomalies in the waves, which have been shown to be important to invigorating convection (e.g., Bretherton et al. 2004; Holloway and Neelin 2009). Likely through this combination of a moister, more convective background state and enhanced EW moisture advection, strong CLLJ EWs are associated with higher precipitation anomalies relative to MJO phase 6. Calculations of diluted CAPE for these periods reemphasize the importance of convection in strong CLLJ waves, which more notably modulate diluted CAPE along their wave axis. The moister background state during strong CLLJ periods is associated with enhanced diluted CAPE along the ITCZ relative to MJO phase 6, and appears to more favorably support convective development in the region. Thus, we hypothesize that a positive feedback for EWs is occurring that may help explain the differences in convective activity for EWs between these periods. The enhanced background moisture and convective instability along the ITCZ during strong CLLJ periods helps to generate stronger EW circulations, which further support stronger EW convective invigoration as the waves mature through horizontal advection. This hypothesis also supports the results of Chapter 2, which indicated that convection was helping to drive stronger conversions from eddy available potential energy to eddy kinetic energy in strong CLLJ period EWs.

The mean state of the east Pacific, and its variability due to local and remote processes, plays an important role in modulating EWs. In this chapter, we investigate easterly periods of the MJO and CLLJ, which are associated with a general enhancement in ITCZ EW activity as shown in Chapter 2, and find that ITCZ EWs during strong CLLJ periods appear to be more convectively active than MJO phase 6 due to a relative enhancement in basic state moisture. Topics of future work may include investigating why easterly periods associated with the CLLJ produce a relatively moister ITCZ region and where EW circulations in these composite periods form and intensify. Overall, we note that the MJO and CLLJ have distinct influences on east Pacific EWs and the east Pacific

background state, and that additional investigations into the details of their modulating influences would further elucidate our understanding of the region and potentially aid in tropical cyclone forecasting.

3.5 Chapter 3 Figures
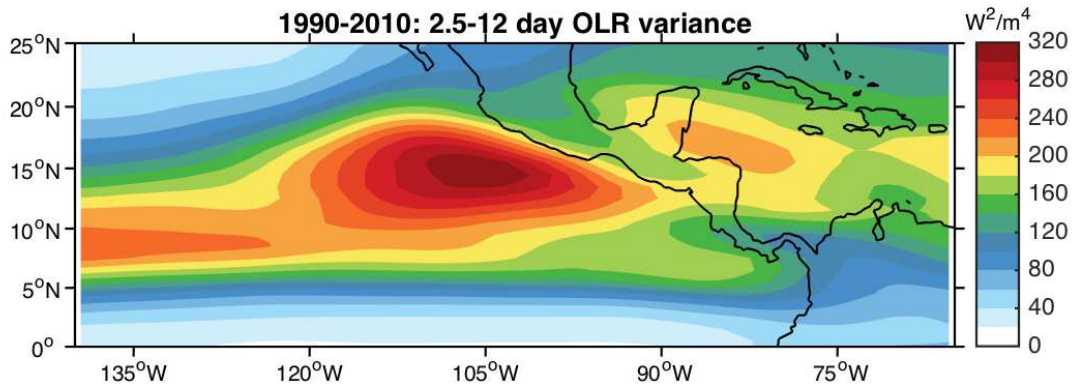
Figure 3.1: 1990-2010 May-October EW wavenumber-frequency filtered OLR variance. Units are $\frac{W^2}{m^4}$.
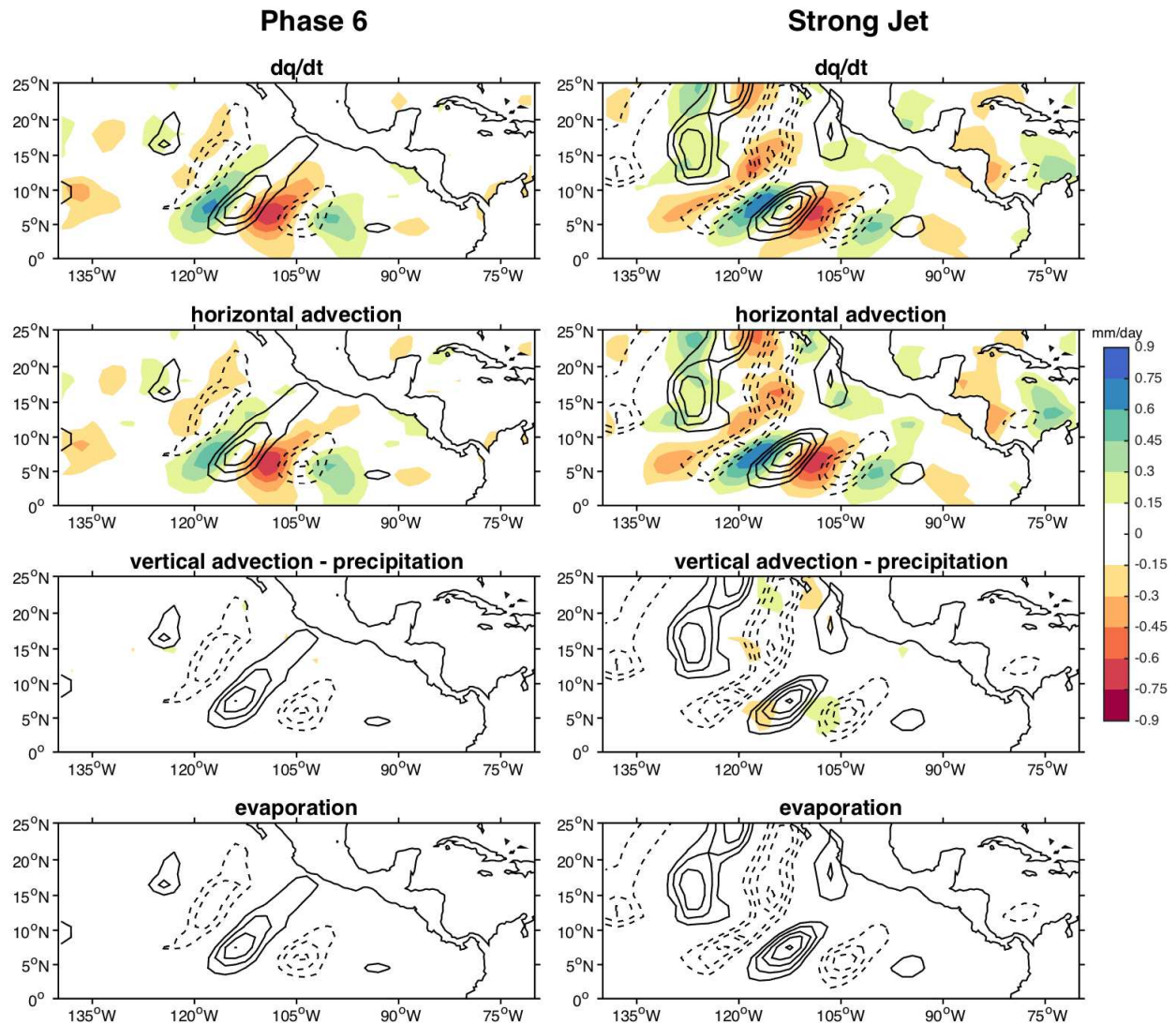
Figure 3.2: Regressions of vertically integrated moisture budget terms ($\frac{mm}{day}$, color contours) and EW wavenumber-frequency filtered total column water vapor (kg m^{-2}, line contours with a contour interval of 0.1 kg m^{-2}, ascending from 0.2 kg m^{-2} for solid lines and descending from -0.2 kg m^{-2} for dashed lines) for MJO phase 6 (left) and strong CLLJ (right) periods. Moisture budget terms are: (first row) time tendency of moisture, (second row) horizontal advection, (third row) vertical advection minus precipitation, (fourth row) evaporation.
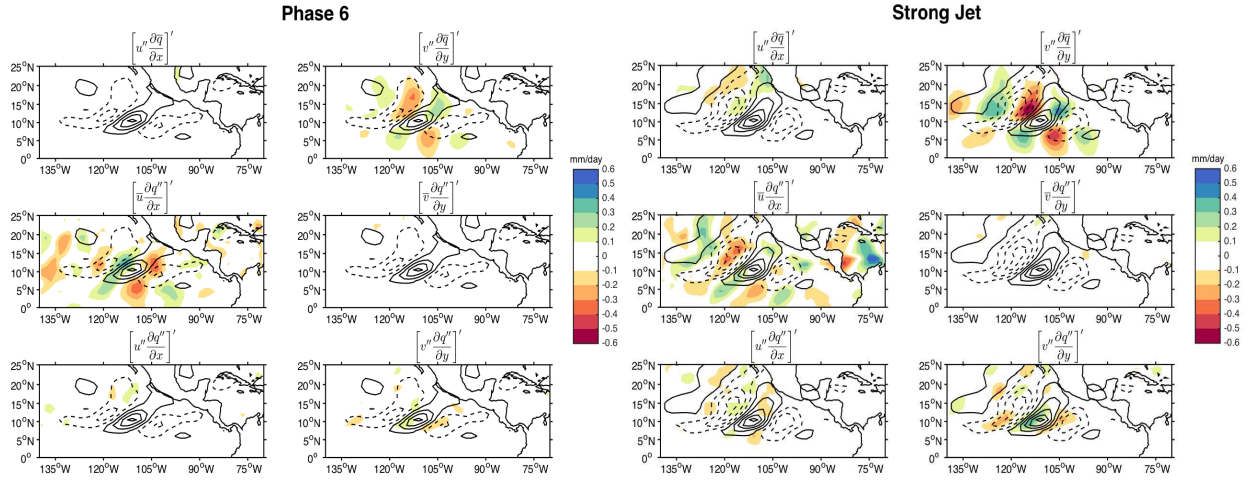
Figure 3.3: Regressions of linearized horizontal advection terms ($\frac{mm}{day}$, color contours) and EW wavenumber-frequency filtered 700 hPa vorticity (s^{-1}, line contours with a contour interval of 2×10^{-6} s^{-1}, ascending from 1×10^{-6} s^{-1} for solid lines and descending from -1×10^{-6} s^{-1} for dashed lines) for MJO phase 6 (left) and strong CLLJ (right) periods.

81
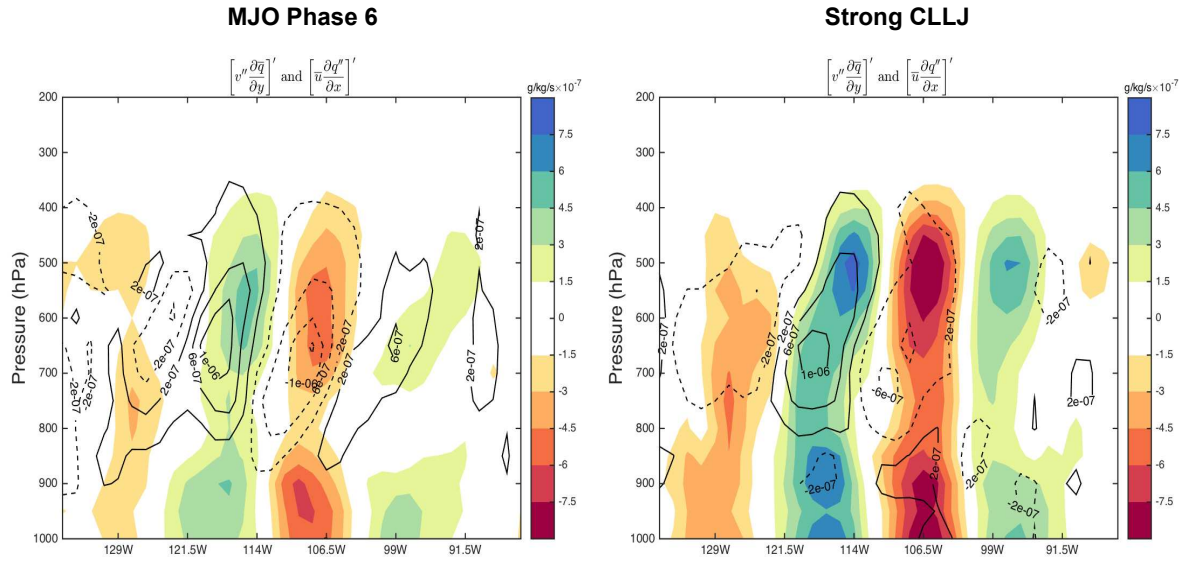
Figure 3.4: West to east vertical cross sections along 7.5°N of regressed linearized horizontal advection terms $\left[v''\frac{\partial\overline{q}}{\partial y}\right]'$ (g kg^{-1} s^{-1}, color contours) and $\left[\overline{u}\frac{\partial q''}{\partial x}\right]'$ (g kg^{-1} s^{-1}, line contours with a contour interval of 4×10^{-7} g kg^{-1} s^{-1}, ascending from 2×10^{-7} g kg^{-1} s^{-1} for solid lines and descending from -2×10^{-7} g kg^{-1} s^{-1} for dashed lines) for MJO phase 6 (left) and strong CLLJ (right) periods.
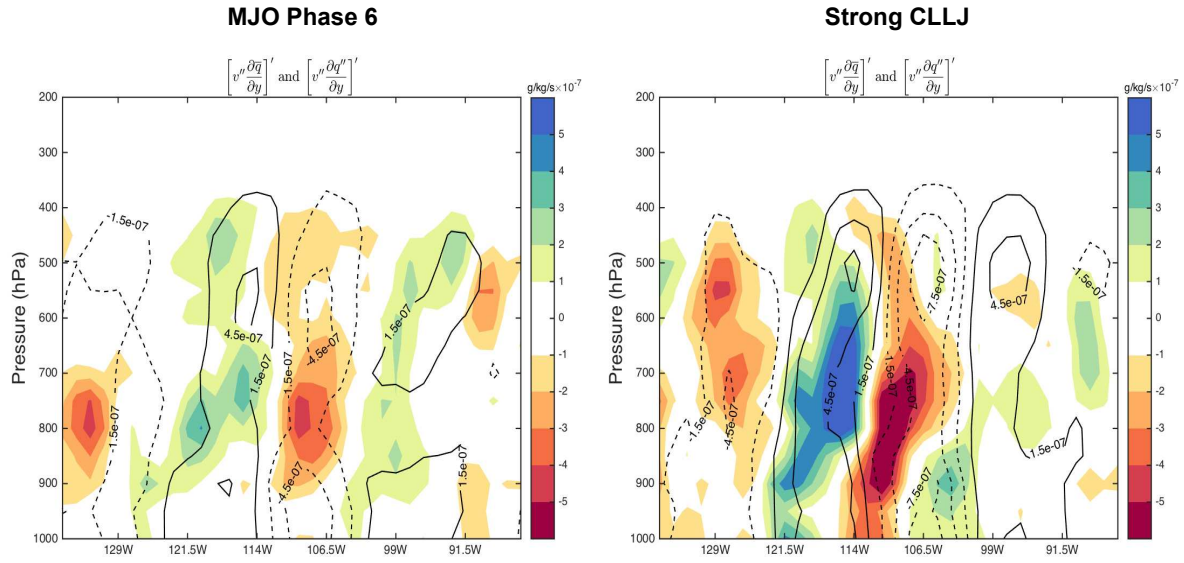
Figure 3.5: West to east vertical cross sections along 7.5°N of regressed linearized horizontal advection terms $\left[v''\frac{\partial q''}{\partial y}\right]'$ (g kg^{-1} s^{-1}, color contours) and $\left[v''\frac{\partial \bar{q}}{\partial y}\right]'$ (g kg^{-1} s^{-1}, line contours with a contour interval of 3×10^{-7} g kg^{-1} s^{-1}, ascending from 1.5×10^{-7} g kg^{-1} s^{-1} for solid lines and descending from -1.5×10^{-7} g kg^{-1} s^{-1} for dashed lines) for MJO phase 6 (left) and strong CLLJ (right) periods.
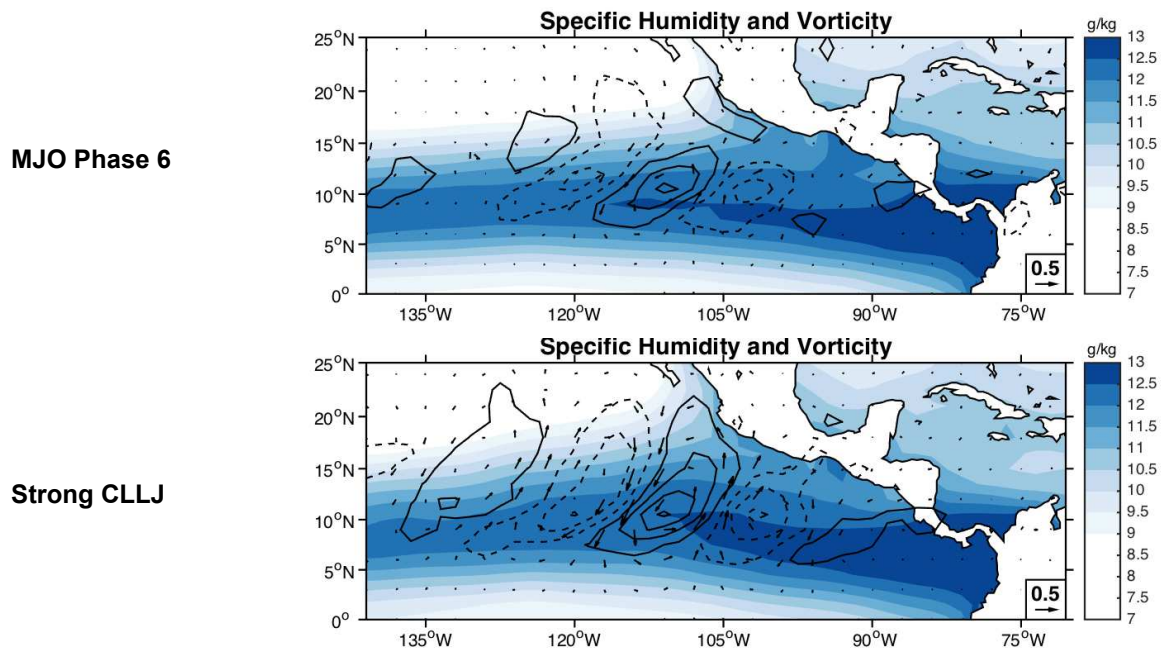
Figure 3.6: Composite mean specific humidity (g kg^{-1}, color contours) and regressed EW wavenumber-frequency filtered wind (m s^{-1}) and vorticity (s^{-1}, line contours with a contour interval of 1×10^{-6} s^{-1}, ascending from 0.5×10^{-6} s^{-1} for solid lines and descending from -0.5×10^{-6} s^{-1} for dashed lines) for MJO phase 6 (top) and strong CLLJ (bottom) periods. All fields are averaged over 700-1000 hPa.
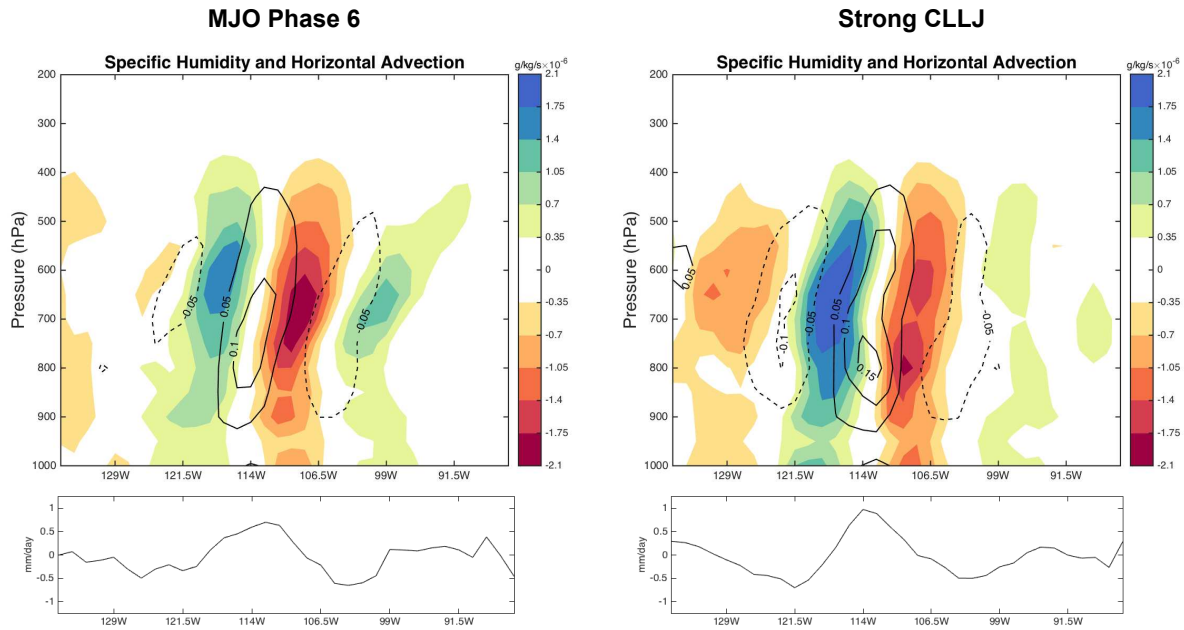
Figure 3.7: West to east vertical cross sections along 7.5°N (top) of regressed total horizontal advection (g kg^{-1} s^{-1}, color contours) and EW wavenumber-frequency filtered specific humidity (g kg^{-1}, line contours with a contour interval of 0.05 g kg^{-1}, ascending from 0.05 g kg^{-1} for solid lines and descending from -0.05 g kg^{-1} for dashed lines), along with (bottom) regressed precipitation ($\frac{mm}{day}$) averaged over 7.5°N and 9°N for MJO phase 6 (left) and strong CLLJ (right) periods.
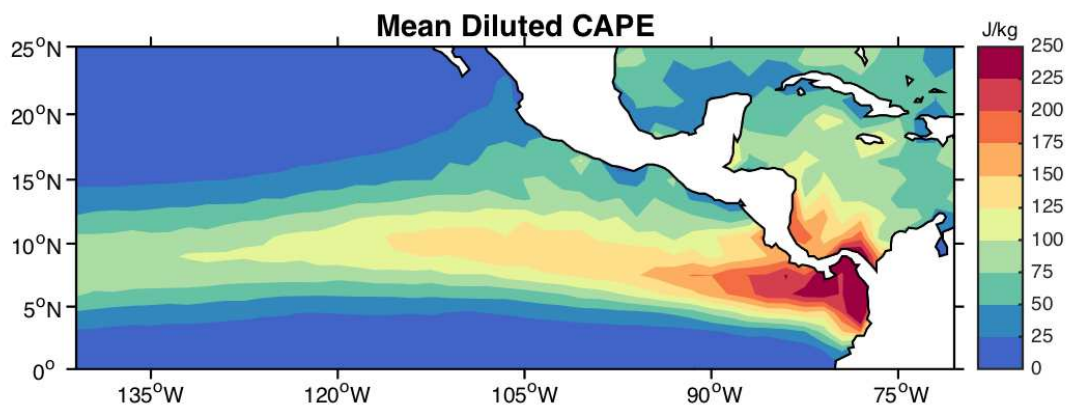
Figure 3.8: 1990-2010 May-October mean diluted CAPE. Units are J kg^{-1}.
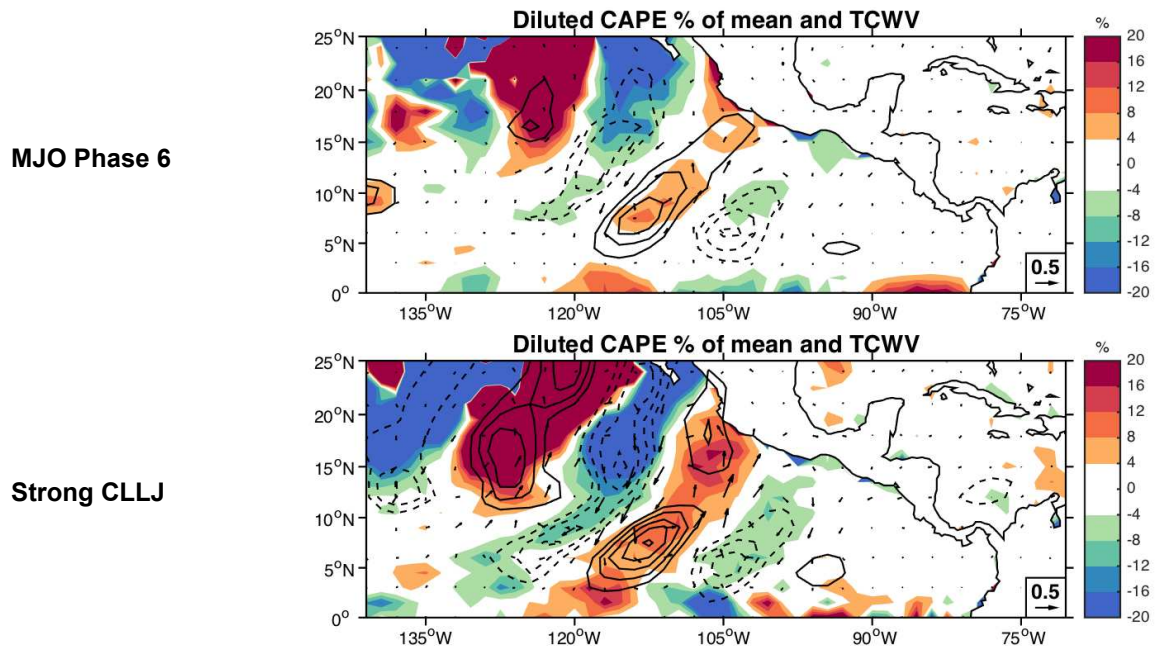
Figure 3.9: Regressions of EW wavenumber-frequency filtered diluted CAPE (expressed as the percentage of the mean diluted CAPE, color contours), total column water vapor (kg m^{-2}, line contours with a contour interval of 0.1 kg m^{-2}, ascending from 0.2 kg m^{-2} for solid lines and descending from -0.2 kg m^{-2} for dashed lines), and 700-1000 hPa averaged wind (m s^{-1}) for MJO phase 6 (top) and strong CLLJ (bottom) periods.
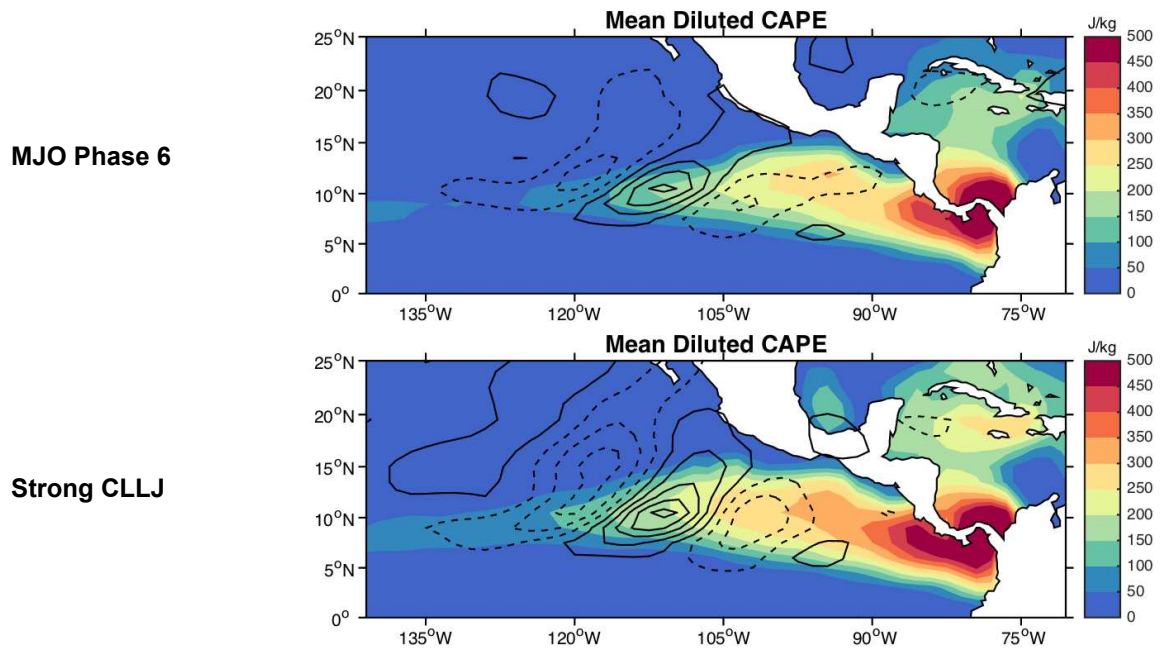
Figure 3.10: Composite mean diluted CAPE (J kg^{-1}, color contours) based on basic state temperature and specific humidity, and regressed EW wavenumber-frequency filtered 700 hPa vorticity (s^{-1}, line contours with a contour interval of 2×10^{-6} s^{-1}, ascending from 1×10^{-6} s^{-1} for solid lines and descending from -1×10^{-6} s^{-1} for dashed lines) for MJO phase 6 (top) and strong CLLJ (bottom). A centered $6^\circ \times 6^\circ$ two-dimensional Gaussian weighting box is applied to the calculated diluted CAPE for smoothing.

Chapter 4

Study Overview and Future Work

This study compares and contrasts the effects that the MJO and CLLJ have on the east Pacific background state and EWs. The east Pacific is a unique tropical ocean basin due the influence of the surrounding topography on local processes, its physical separation from the Caribbean Sea by a land isthmus, and the wide variety of atmospheric and oceanic phenomena that it harbors. Easterly waves that propagate in the basin have either been generated locally or remotely and are substantially affected by variations in the mean state conditions.

In Chapter 2, a local CLLJ index is developed and used along with a widely employed MJO index to investigate anomalous low-level wind periods associated with the MJO and CLLJ to try and resolve somewhat differing ideas in the literature about the importance of low-level wind direction to EW development. One key finding is that the MJO and CLLJ are distinct in their effects on the basic state. In particular, the CLLJ appears to be a stronger modulator of the ITCZ. Strong CLLJ periods are also associated with enhanced moisture anomalies along the ITCZ relative to easterly MJO periods, which may support enhanced convection during this time. An eddy kinetic energy budget is performed to analyze the relative roles of energy budget terms to EW development during these periods. It is found that EWs during strong CLLJ periods have stronger convective contributions to eddy kinetic energy and elevated track density along the ITCZ relative to easterly MJO period EWs. Westerly MJO and CLLJ periods are characterized by elevated barotropic and EAPE to EKE conversion along the Central American coast, which indicates the potential for strong EW development in this region. Another notable result from Chapter 2 is that contributions to eddy kinetic energy from Panama Bight convection seemed to remain elevated regardless of the composite period.

In Chapter 3, we test a hypothesis developed in Chapter 2 that changes in ITCZ moisture helped contribute to the convective differences seen in easterly period MJO and CLLJ ITCZ EWs. A vertically integrated moisture budget is computed and highlights that the horizontal advection

of moisture is the dominant contributor to overall changes in moisture in ITCZ EWs in these composite periods. It is found that easterly period CLLJ EWs are associated with stronger horizontal advection and positive moisture changes in front of the wave axis relative to easterly MJO period EWs in the ITCZ. However, it appears that these enhancements are mostly due to stronger EW circulations rather than differences in background moisture. Calculations of diluted CAPE using a simple entraining plume model are performed, and highlight that the overall basic state diluted CAPE is higher during easterly CLLJ periods versus easterly MJO periods. In addition, ITCZ EWs in easterly CLLJ periods are also associated with stronger and more expansive regressed diluted CAPE anomalies. Therefore, we hypothesize that the easterly CLLJ basic state is more conducive to convective invigoration, and therefore may allow EWs to develop stronger circulations than in easterly MJO periods, producing the stronger moisture advection noted above.

Although this study highlights important differences between the MJO and CLLJ modulation of the east Pacific and EWs, there are some caveats to be noted. First, although the CLLJ index developed in Chapter 2 limits the influence of strong MJO events on CLLJ composites, MJO events and easterly waves in these periods may still be influenced by the CLLJ and mountain jets entering the basin (Chelton et al. 2000a). Additionally, as both of these phenomena are related to the large-scale global circulation, indirect connections between the remote MJO and more local CLLJ may occur in the indices used. For example, because the MJO has been shown to alter the mid-latitude circulation (e.g., Henderson et al. 2016), it may also influence the location of the North American subtropical high, which has been shown to influence the strength of the CLLJ (Wang and Lee 2007). Thus, while the direct impact of the MJO on the CLLJ is mitigated in this study, a possible indirect relationship between the MJO and CLLJ via the global circulation has not been taken into account in our indices and may lead to some minor biasing in our composites. Further, the diluted CAPE calculation performed in Chapter 3 is based on a simplified entraining plume model (Neale et al. 2010) to provide a general sense for the impact of environmental moisture on convection in MJO and CLLJ periods, and could be improved on in future work. For example, the constant entrainment rate used in our study may preferentially favor moisture anomalies at certain

heights, and ignoring the effects of condensation and freezing may lead to further differences in the estimation of convective instability between MJO and CLLJ periods. So, while our CAPE calculation is useful for highlighting a difference in convective instability between composite periods, the specific magnitude of these differences could be improved on in additional studies. Finally, as most of the data used in this study was from ERA-Interim reanalysis (Dee et al. 2011), the results presented may be subject to potential biases in the reanalysis model that may differ from the actual observed conditions in the region. Therefore, differences between the reanalysis data and observations may need to be taken into account when thinking of this work from an operational or forecasting context.

Overall, this study seems to be consistent with works involving the MJO, while some differences arise with conclusions found in previous studies investigating the CLLJ and EWs. This thesis finds that MJO westerly periods are associated with more favorable conditions for EWs along the main EW path in terms of the mean state, EKE budget, and EW tracks, relative to easterly periods, which is consistent with previous studies such as Maloney and Hartmann (2001), Crosbie and Serra (2014), and Rydbeck and Maloney (2014). Further, EW track density and EKE budget terms are more focused along the ITCZ for MJO easterly periods, which agrees with the findings of Crosbie and Serra (2014) and Rydbeck and Maloney (2014). In terms of the CLLJ results, we also find that westerly periods are conducive to EW development along the Central American coast, which contrasts with the findings of Serra et al. (2010). On the other hand, we do show that EW track density along the ITCZ and in the east Pacific is enhanced during easterly CLLJ periods, when compared to CLLJ westerly periods, which is consistent with Serra et al. (2010). Thus, more work must be done to elucidate aspects of EW variability during composite periods of these phenomena.

From this study, there are many avenues of future work. As this study found differences between easterly MJO and CLLJ periods along the ITCZ, it would be interesting to investigate the mechanisms for why the CLLJ appears to be a stronger modulator of the ITCZ and why the ITCZ appears to be more convectively active during CLLJ easterly periods. Within this framework, observations and modeling of ITCZ breakdown during composite MJO and CLLJ periods may be a

useful exercise. Next, because we found that large background state changes in the east Pacific occurred during MJO and CLLJ periods but the Panama Bight region contained high EAPE to EKE conversion in all composite periods, future work may focus on the relative roles of the east Pacific background environment versus the strength of the precursor disturbance (e.g., Panama Bight convective systems or AEWs) to EW formation and development, and potentially tropical cyclogenesis. Sensitivity tests could be performed with reduced topography to suppress Panama Bight convection (Rydbeck et al. 2017) and removed African easterly waves during MJO and CLLJ periods to see how these composite periods influence EW activity without the aid of a precursor disturbance. Additionally, it may be interesting to investigate local EW genesis or AEW reinvigoration in the east Pacific using a high resolution model. Notable cases found in observational data could be simulated for both categories to see what mechanisms are important to EW genesis, and if they differ for the local and remote disturbances. Finally, observational studies of convective process in EWs as well as local EW generation could be made from the findings of the Organization of Tropical East Pacific Convection (OTREC) field campaign scheduled for summer 2019. OTREC will be based in Costa Rica and proposes using aircraft to deploy dropsondes over the western Caribbean and east Pacific, along with airborne and land-based radar to observe convective processes in the region. The data from this field campaign could also be used to better understand the east Pacific mean state, as well as to construct observational EW EKE and moisture budgets that could be compared against the results of this study to help validate the important developmental processes in EWs. Overall, the generation, development, and variability of east Pacific EWs still provide valuable research questions that should be addressed in subsequent investigations.

References

Adames, A. F., and D. Kim, 2016: The MJO as a Dispersive, Convectively Coupled Moisture Wave: Theory and Observations. *J. Atmos. Sci.*, **73**, 913–941.

Aiyyer, A., and J. Molinari, 2008: MJO and Tropical Cyclogenesis in the Gulf of Mexico and Eastern Pacific: Case Study and Idelaized Numerical Modeling. *J. Atmos. Sci.*, **65**, 2691–2704.

Aiyyer, A., A. Mekonnen, and C. J. Schreck, 2012: Projection of Tropical Cyclones on Wavenumber-Frequency-Filtered Equatorial Waves. *J. Climate*, **25**, 3653–3658.

Alaka, G. J., and E. D. Maloney, 2012: The Influence of the MJO on Upstream Precursors to African Easterly Waves. *J. Climate*, **25**, 3219–3236.

Amador, J. A., 1998: A Climatic Feature of Tropical Americas: The Trade Wind Easterly Jet. *Top. Meteor. Oceanogr.*, **5**, 91–102.

Amador, J. A., 2008: The Intra-Americas Sea Low-level Jet. *Ann. N.Y. Acad. Sci.*, **1146**, 153–188.

Avila, L. A., and R. J. Pasch, 1992: Atlantic tropical systems of 1991. *Mon. Wea. Rev.*, **120**, 2688–2696.s

Avila, L. A., and J. L. Guiney, 2000: Eastern North Pacific hurricane season of 1998. *Mon. Wea. Rev.*, **128**, 2990–3000.

Avila, L. A., R. J. Pasch, J. L. Beven, J. L. Franklin, M. B. Lawrence, S. R. Stewart, and J. G. Jiing, 2003: Eastern North Pacific hurricane season of 2001. *Mon. Wea. Rev.*, **131**, 249–262.

Back, L. E., and C. S. Bretherton, 2009: On the Relationship between SST Gradients, Boundary Layer Winds, and Convergence over the Tropical Oceans. *J. Climate*, **22**, 4182–4196.

Belanger, J. I., M. T. Jelinek, and J. A. Curry, 2014: African Easterly Wave Climatology, Version 1. NOAA National Centers for Environmental Information. ERA-Interim, 600hPa. Access Date: 10/25/2016, doi:10.7289/V5ZC80SX.

Belanger, J. I., M. T. Jelinek, and J. A. Curry, 2016: A climatology of easterly waves in the tropical Western Hemisphere. *Geosci. Data J.*, **3**, 40–49.

Berry, G. J., and C. D. Thorncroft, 2005: Case Study of an Intense African Easterly Wave. *Mon. Wea. Rev.*, **133**, 752–766.

Bjerknes, J., 1969: Atmospheric Teleconnections From the Equatorial Pacific. *Mon. Wea. Rev.*, **97 (3)**, 163–172.

Bretherton, C. S., M. E. Peters, and L. E. Back, 2004: Relationships between Water Vapor Path and Precipitation over the Tropical Oceans. *J. Climate*, **17**, 1517–1528.

Burpee, R. W., 1972: The Origin and Structure of Easterly Waves in the Lower Troposphere of North Africa. *J. Atmos. Sci.*, **29**, 77–90.

Burpee, R. W., 1974: Characteristics of North African Easterly Waves During the Summers of 1968 and 1969. *J. Atmos. Sci.*, **31**, 1556–1570.

Carlson, T. N., 1969: Synoptic histories of three African disturbances that developed into Atlantic hurricanes. *Mon. Wea. Rev.*, **97**, 256–276.

Chelton, D. B., M. H. Freilich, and S. K. Esbensen, 2000a: Satellite Observations of the Wind Jets off the Pacific Coast of Central America. Part I: Case Studies and Statistical Characteristics. *Mon. Wea. Rev.*, **128**, 1993–2018.

Chelton, D. B., M. H. Freilich, and S. K. Esbensen, 2000b: Satellite Observations of the Wind Jets off the Pacific Coast of Central America. Part II: Regional Relationships and Dynamical Considerations. *Mon. Wea. Rev.*, **128**, 2019–2043.

Cook, K. H., and E. K. Vizy, 2010: Hydrodynamics of the Caribbean Low-Level Jet and Its Relationship to Precipitation. *J. Climate*, **23**, 1477–1494.

Crosbie, E., and Y. Serra, 2014: Intraseasonal Modulation of Synoptic-Scale Disturbances and Tropical Cyclone Genesis in the Eastern North Pacific. *J. Climate*, **27**, 5724–5745.

Dee, D. P., and Coauthors, 2011: The ERA-Interim reanalysis: configuration and performance of the data assimilation system. *Quart. J. Roy. Meteor. Soc.*, **137**, 553–597.

Diaz, M., and A. Aiyyer, 2013: Energy Dispersion in African Easterly Waves. *J. Atmos. Sci.*, **70**, 130–145.

Dima, I. M., and J. M. Wallace, 2003: On the Seasonality of the Hadley Cell. *J. Atmos. Sci.*, **60**, 1522–1527.

Dunkerton, T. J., M. T. Montgomery, and Z. Wang, 2009: Tropical cyclogenesis in a tropical wave critical layer: easterly waves. *Atmos. Chem. Phys.*, **9**, 5587–5646.

Ferreira, R. N., and W. H. Schubert, 1997: Barotropic Aspects of ITCZ Breakdown. *J. Atmos. Sci.*, **54**, 261–285.

Frank, N. L., 1970: Atlantic tropical systems of 1969. *Mon. Wea. Rev.*, **98**, 307–314.

Henderson, S. A., E. D. Maloney, and E. A. Barnes, 2016: The Influence of the Madden-Julian Oscillation on Northern Hemisphere Winter Blocking. *J. Climate*, **29**, 4597–4616.

Holloway, C. E., and J. D. Neelin, 2009: Moisture Vertical Structure, Column Water Vapor, and Tropical Deep Convection. *J. Atmos. Sci.*, **66**, 1665–1683.

Hsieh, J.-S., and K. H. Cook, 2007: A Study of the Energetics of African Easterly Waves Using a Regional Climate Model. *J. Atmos. Sci.*, **64**, 421–440.

Jiang, X., and D. E. Waliser, 2008: Northward propagation of the subseasonal variability over the eastern pacific warm pool. *Geophys. Res. Lett.*, **35**, L09814.

Kiladis, G. N., C. D. Thorncroft, and N. M. J. Hall, 2006: Three-Dimensional Structure and Dynamics of African Easterly Waves. Part I: Observations. *J. Atmos. Sci.*, **63**, 2212–2230.

Krishnamurthy, L., G. A. Vecchi, R. Msadek, A. Wittenberg, T. L. Delworth, and F. Zeng, 2015: The Seasonality of the Great Plains Low-Level Jet and ENSO Relationship. *J. Climate*, **28**, 4525–4544.

Landsea, C. W., 1993: A Climatology of Intense (or Major) Atlantic Hurricanes. *Mon. Wea. Rev.*, **121**, 1703–1713.

Landsea, C. W., and J. L. Franklin, 2013: Atlantic Hurricane Database Uncertainty and Presentation of a New Database Format. *Mon. Wea. Rev.*, **141**, 3576–3592.

Lau, K.-H., and N.-C. Lau, 1992: The Energetics and Propagation Dynamics of Tropical Summertime Synoptic-Scale Disturbances. *Mon. Wea. Rev.*, **120**, 2523–2539.

Lebel, T., and Coauthors, 2010: The AMMA field campaigns: Multiscale and multidisciplinary observations in the West African region. *Quart. J. Roy. Meteor. Soc.*, **136**, 8 – 33.

Lee, H.-T., 2014: Climate Algorithm Theoretical Basis Document (C-ATBD): Outgoing Longwave Radiation (OLR) - Daily. NOAA's Climate Data Record (CDR) Program, CDRP-ATBD-0526, 46 pp.

Leroux, S., and N. M. J. Hall, 2009: On the Relationship between African Easterly Waves and the African Easterly Jet. *J. Atmos. Sci.*, **66**, 2303–2316.

Lu, J., G. A. Vecchi, and T. Reichler, 2007: Expansion of the Hadley cell under global warming. *Geophys. Res. Lett.*, **34**, L06805.

Madden, R. A., and P. R. Julian, 1994: Observations of the 40-50-Day Tropical Oscillation – A Review. *Mon. Wea. Rev.*, **122**, 814–837.

Magana, V., J. A. Amador, and S. Medina, 1999: The Midsummer Drought over Mexico and Central America. *J. Climate*, **12**, 1577–1588.

Maloney, E. D., and D. L. Hartmann, 1998: Frictional Moisture Convergence in a Composite Life Cycle of the Madden-Julian Oscillation. *J. Climate*, **11**, 2387–2403.

Maloney, E. D., and D. L. Hartmann, 2000: Modulation of Eastern North Pacific Hurricanes by the Madden-Julian Oscillation. *J. Climate*, **13**, 1451–1460.

Maloney, E. D., and D. L. Hartmann, 2001: The Madden-Julian Oscillation, Barotropic Dynamics, and North Pacific Tropical Cyclone Formation. Part I: Observations. *J. Atmos. Sci.*, **58**, 2545–2558.

Maloney, E. D., and J. T. Kiehl, 2002: MJO-Related SST Variations over the Tropical Eastern Pacific during Northern Hemisphere Summer. *J. Climate*, **15**, 675–689.

Maloney, E. D., and M. J. Dickinson, 2003: The Intraseasonal Oscillation and the Energetics of Summertime Tropical Western North Pacific Synoptic-Scale Disturbances. *J. Atmos. Sci.*, **60**, 2153–2168.

Maloney, E. D., and S. K. Esbensen, 2003: The Amplification of East Pacific Madden-Julian Oscillation Convection and Wind Anomalies during June-November. *J. Climate*, **16**, 3482–3497.

Maloney, E. D., and S. K. Esbensen, 2007: Satellite and Buoy Observations of Boreal Summer Intraseasonal Variability in the Tropical Northeast Pacific. *Mon. Wea. Rev.*, **135**, 3–19.

Maloney, E. D., D. B. Chelton, and S. K. Esbensen, 2008: Subseasonal SST Variability in the Tropical Eastern North Pacific during Boreal Summer. *J. Climate*, **21**, 4149–4167.

Mapes, B. E., T. T. Warner, M. Xu, and A. J. Negri, 2003a: Diurnal Patterns of Rainfall in Northwestern South America. Part I: Observations and Context. *Mon. Wea. Rev.*, **131**, 799–812.

Mapes, B. E., T. T. Warner, and M. Xu, 2003b: Diurnal Patterns of Rainfall in Northwestern South America. Part III: Diurnal Gravity Waves and Nocturnal Convection Offshore. *Mon. Wea. Rev.*, **131**, 830–844.

Martin, E. R., and C. Schumacher, 2011: The Caribbean Low-Level Jet and Its Relationship with Precipitation in IPCC AR4 Models. *J. Climate*, **24**, 5935–5950.

McPhaden, M. J., and Coauthors, 1998: The Tropical Ocean-Global Atmosphere observing system: A decade of progress. *J. Geophys. Res.*, **103**, 14 169–14 240.

Mekonnen, A., C. D. Thorncroft, and A. R. Aiyyer, 2006: Analysis of Convection and Its Association with African Easterly Waves. *J. Climate*, **19**, 5405–5421.

Molinari, J., D. Knight, M. Dickinson, D. Vollaro, and S. Skubis, 1997: Potential Vorticity, Easterly Waves, and Eastern Pacific Tropical Cyclogenesis. *Mon. Wea. Rev.*, **125**, 2699–2708.

Molinari, J., and D. Vollaro, 2000: Planetary- and Synoptic-Scale Influences on Eastern Pacific Tropical Cyclogenesis. *Mon. Wea. Rev.*, **128**, 3296–3307.

Mundhenk, B. D., E. A. Barnes, and E. D. Maloney, 2016: All-Season Climatology and Variability of Atmospheric River Frequencies over the North Pacific. *J. Climate*, **29**, 4885–4903.

Munoz, E., A. J. Busalacchi, S. Nigam, and A. Ruiz-Barradas, 2008: Winter and Summer Structure of the Caribbean Low-Level Jet. *J. Climate*, **21**, 1260–1276.

Neale, R. B., and Coauthors, 2010: Description of the NCAR Community Atmosphere Model (CAM 4.0). NCAR Tech. Note NCAR/TN-485+STR, National Center for Atmospheric Research, Boulder, CO, 212 pp.

Nitta, T., and Y. Takayabu, 1985: Global Analysis of the Lower Tropospheric Disturbances in the Tropics During the Northern Summer of the FGGE Year. Part II: Regional Characteristics of the Disturbances. *Pure Appl. Geophys.*, **123**, 272–292.

Pasch, R. J., and Coauthors, 2009: Eastern North Pacific hurricane season of 2006. *Mon. Wea. Rev.*, **137**, 3–20.

Peters, O., and J. D. Neelin, 2006: Critical phenomena in atmospheric precipitation. *Nature Phys.*, **2**, 393–396.

Petersen, W. A., R. Cifelli, D. J. Boccippio, S. A. Rutledge, and C. Fairall, 2003: Convection and Easterly Wave Structures Observed in the Eastern Pacific Warm Pool during EPIC-2001. *J. Atmos. Sci*, **60**, 1754–1773.

Ramsay, H. A., 2017: The Global Climatology of Tropical Cyclones. *Oxford Research Encyclopedia of Natural Hazard Science*, doi:10.1093/acrefore/9780199389407.013.79.

Rappaport, E. N., and M. Mayfield, 1992: Eastern North Pacific hurricane season of 1991. *Mon. Wea. Rev.*, **120**, 2697–2708.

Raymond, D. J., C. S. Bretherton, and J. Molinari, 2006: Dynamics of the Intertropical Convergence Zone of the East Pacific. *J. Atmos. Sci.*, **63**, 582–597.

Reed, R. J., E. Klinker, and A. Hollingsworth, 1988: The Structure and Characteristics of African Easterly Wave Disturbances as Determined from the ECMWF Operational Analysis/Forecast System. *Meteorl. Atmos. Phys.*, **38**, 22–33.

Roundy, P. E., and W. M. Frank, 2004: A Climatology of Waves in the Equatorial Region. *J. Atmos. Sci.*, **61**, 2105–2132.

Russell, J. O., A. Aiyyer, J. D. White, and W. Hannah, 2017: Revisiting the connection between African Easterly Waves and Atlantic tropical cyclogenesis. *Geophys. Res. Lett.*, **4**, 587–595.

Rydbeck, A. V., E. D. Maloney, S.-P. Xie, J. Hafner, and J. Shaman, 2013: Remote Forcing versus Local Feedback of East Pacific Intraseasonal Variability during Boreal Summer. *J. Climate*, **26**, 3573–3596.

Rydbeck, A. V., and E. D. Maloney, 2014: Energetics of East Pacific Easterly Waves during Intraseasonal Events. *J. Climate*, **27**, 7603–7621.

Rydbeck, A. V., and E. D. Maloney, 2015: On the Convective Coupling and Moisture Organization of East Pacific Easterly Waves. *J. Atmos. Sci*, **72**, 3850–3870.

Rydbeck, A. V., E. D. Maloney, and G. J. Alaka, 2017: In Situ Initiation of East Pacific Easterly Waves in a Regional Model. *J. Atmos. Sci.*, **74**, 333–351.

Serra, Y. L., G. N. Kiladis, and M. F. Cronin, 2008: Horizontal and Vertical Structure of Easterly Waves in the Pacific ITCZ. *J. Atmos. Sci.*, **65**, 1266–1284.

Serra, Y. L., G. N. Kiladis, and K. I. Hodges, 2010: Tracking and Mean Structure of Easterly Waves over the Intra-Americas Sea. *J. Climate*, **23**, 4823–4840.

Serra, Y. L., X. Jiang, B. Tian, J. Amador-Astua, E. D. Maloney, and G. N. Kiladis, 2014: Tropical Intraseasonal Modes of the Atmosphere. *Ann. Rev. Environ. Resour.*, **39**, 189–215.

Shapiro, L. J., 1986: The Three Dimensional Structure of Synoptic-Scale Disturbances over the Tropical Atlantic. *Mon. Wea. Rev.*, **114**, 1876–1891.

Slade, S. A., and E. D. Maloney, 2013: An Intraseasonal Prediction Model of Atlantic and East Pacific Tropical Cyclone Genesis. *Mon. Wea. Rev.*, **141**, 1925–1942.

Small, R. J. O., S. P. de Szoeke, and S.-P. Xie, 2007: The Central American Midsummer Drought: Regional Aspects and Large-Scale Forcing. *J. Climate*, **20**, 4853–4873.

Small, R. J., S.-P. Xie, E. D. Maloney, S. P. de Szoeke, and T. Miyama, 2011: Intraseasonal variability in the far-east pacific: investigation of the role of air–sea coupling in a regional coupled model. *Climate Dyn.*, **36**, 867–890.

Sobel, A., and E. D. Maloney, 2012: An Idealized Semi-Empirical Framework for Modeling the Madden-Julian Oscillation. *J. Atmos. Sci.*, **69**, 1691–1705.

Sobel, A., and E. D. Maloney, 2013: Moisture Modes and the Eastward Propagation of the MJO. *J. Atmos. Sci.*, **70**, 187–192.

Tai, K.-S., and Y. Ogura, 1987: An Observational Study of Easterly Waves over the Eastern Pacific in the Northern Summer Using FGGE Data. *J. Atmos. Sci.*, **44**, 339–361.

Thorncroft, C., and K. Hodges, 2001: African Easterly Wave Variability and Its Relationship to Atlantic Tropical Cyclone Activity. *J. Climate*, **14**, 1166–1179.

Thorncroft, C. D., N. M. J. Hall, and G. N. Kiladis, 2008: Three-Dimensional Structure and Dynamics of African Easterly Waves. Part III: Genesis. *J. Atmos. Sci.*, **65**, 3596–3607.

Toma, V. E., and P. J. Webster, 2010a: Oscillations of the Intertropical Convergence Zone and the genesis of easterly waves. Part I: diagnostics and theory. *Clim. Dyn.*, **34**, 587–604.

Toma, V. E., and P. J. Webster, 2010b: Oscillations of the Intertropical Convergence Zone and the genesis of easterly waves. Part II: numerical verification. *Clim. Dyn.*, **34**, 605–613.

Wang, C., 2007: Variability of the Caribbean Low-Level Jet and its relations to climate. *Clim. Dyn.*, **29**, 411–422.

Wang, C., and S.-K. Lee, 2007: Atlantic warm pool, Caribbean low-level jet and their potential impact on Atlantic hurricanes. *Geophys. Res. Lett.*, **34**, L02 703.

Webster, P. J., and J. R. Holton, 1982: Cross-Equatorial Response to Middle-Latitude Forcing in a Zonally Varying Basic State. *J. Atmos. Sci.*, **39**, 722–733.

Wheeler, M., and G. N. Kiladis, 1999: Convectively Coupled Equatorial Waves: Analysis of Clouds and Temperature in the Wavenumber-Frequency Domain. *J. Atmos. Sci.*, **56**, 374–399.

Wheeler, M. C., and H. H. Hendon, 2004: An All-Season Real-Time Multivariate MJO Index: Development of an Index for Monitoring and Prediction. *Mon. Wea. Rev.*, **132**, 1917–1932.

Whitaker, J. W., and E. D. Maloney, 2018: Influence of the Madden-Julian Oscillation and Caribbean Low-Level Jet on East Pacific Easterly Wave Dynamics. *J. Atmos. Sci*, in press.

Wyrtki, K., 1981: An Estimate of Equatorial Upwelling in the Pacific. *J. Phys. Oceanogr.*, **11**, 1205–1214.

Xie, S.-P., H. Xu, W. S. Kessler, and M. Nonaka, 2005: Air-Sea Interaction over the Eastern Pacific Warm Pool: Gap Winds, Thermocline Dome, and Atmospheric Convection. *J. Climate*, **18**, 5–20.

Yanai, M., and R. H. Johnson, 1993: Impacts of Cumulus Convection on Thermodynamic Fields. *The Representation of Cumulus Convection in Numerical Models of the Atmosphere*, K. A. Emanuel, and D. J. Raymond, Eds., Vol. 46, Amer. Meteor. Soc., 39–62.

Zehnder, J. A., 1991: The Interaction of Planetary-Scale Tropical Easterly Waves with Topography: A Mechanism for the Initiation of Tropical Cyclones. *J. Atmos. Sci*, **48**, 1217–1230.

Zehnder, J. A., D. M. Powell, and D. L. Ropp, 1999: The Interaction of Easterly Waves, Orography, and the Intertropical Convergence Zone in the Genesis of Eastern Pacific Tropical Cyclones. *Mon. Wea. Rev.*, **127**, 1566–1585.

Zhang, C., 2005: Madden-Julian Oscillation. *Rev. Geophys.*, **43**, RG2003.

Zhang, G. J., 2009: Effects of entrainment on convective available potential energy and closure assumptions in convection parameterization. *J. Geophys. Res.*, **114 (D7)**, doi:10.1029/2008JD010976, D07109.